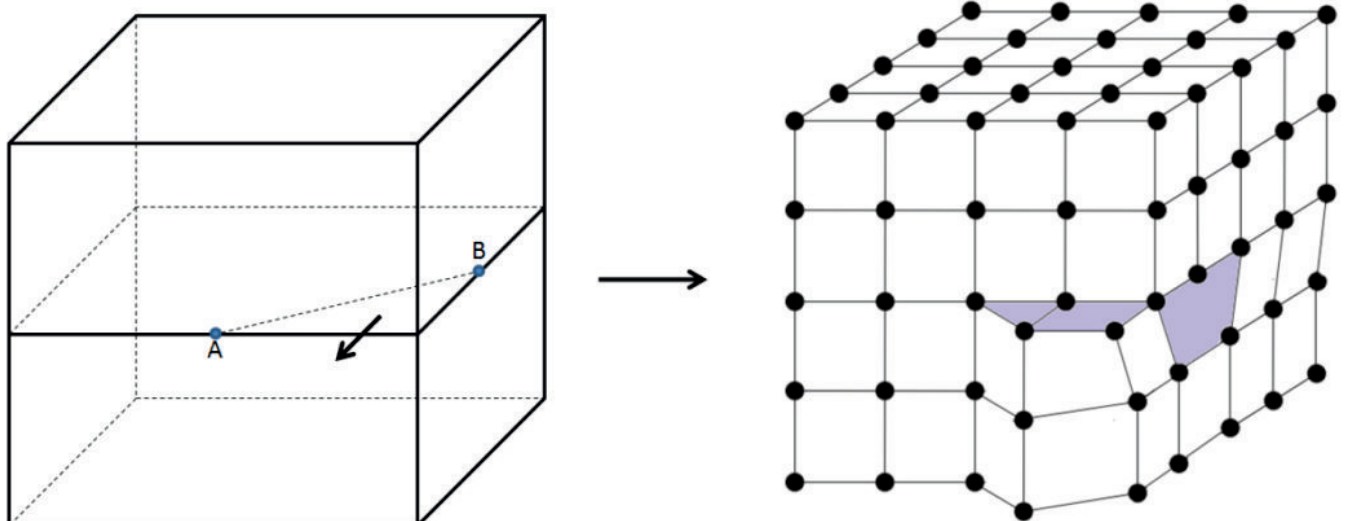**RU**B

Formation of dislocation structure in single crystals during plastic deformations

Binh Duong Nguyen

Dissertation

Formation of dislocation structure in single crystals during plastic deformations

Zur Erlangung des akademischen Grades

Dr.-Ing.

vorgelegt der

Fakultät für Bau- und Umweltingenieurwissenschaften

an der Ruhr-Universität Bochum

von

Binh Duong Nguyen,

geb. 22.01.1986 in Dak Lak, Vietnam

Bochum 2016

Abstract

Within continuum dislocation theory one-dimensional energy functional of a bent beam, made of a single crystal, is derived. By relaxing the continuously differentiable minimizer of this energy functional, we construct a sequence of piecewise smooth deflections and piecewise constant plastic distortions reducing the energy and exhibiting polygonization in the annealed state. In addition, the theory of plastic bending of single crystal beam taking into account continuously distributed dislocations is proposed. Applying the variational asymptotic method we reduce the energy functional of the beam to the one-dimensional energy functional which admits analytical solutions. The threshold value at the onset of plastic yielding as well as the dislocation density are found in terms of the applied bending moment. We consider also the polygonization of the bent beam after unloading and annealing and show that such state is energetically preferable. The number of polygons is estimated by comparing the surface energy of small angle tilt boundaries and the gradient terms in the bulk energy.

Moreover, the theory of formation of grain boundaries in ductile single crystals is proposed within the nonlinear continuum dislocation theory (CDT), where grain boundaries are interpreted as surfaces of weak discontinuity in placement but strong discontinuity in plastic slip. The set of governing equations and jump conditions are derived for the energy minimizers admitting such surfaces of discontinuity from the variational principle. By constructing energy minimizing sequences having piecewise constant plastic and elastic deformation in an example of ductile single crystals deforming in plane strain uniaxial compression, it is shown that the formation of lamellae structure with grain boundaries is energetically preferable. The number of lamellae is estimated by minimizing the energy of grain boundaries plus the energy of boundary layers.

Mündliche Prüfung: 22.06.2016

1. Gutachter: Prof. Dr. rer. nat. Khanh Chau Le

2. Gutachter: Prof. Dr. rer. nat. Klaus Hackl

3. Gutachter: Prof. Dr. rer. nat. Alexander Hartmaier

4. Gutachter: Prof. Dr.-Ing. Justin Geistefeldt

Acknowledgment

With full of gratitude I would like to thank the following persons and organisation who greatly assisted me in pursuing my doctorate.

First of all, I am deeply indebted to my advisor - Prof. Dr. rer. nat. Khanh Chau Le who not only provided insightful advice on my work but also allowed me to truly grow as a research scientist. Never would this dissertation be accomplished without his inspiration and tremendous effort put into training me.

Secondly, I highly appreciate Prof. Dr. rer. nat. Klaus Hackl for creating comfortable atmosphere and open environment to do research. I am also thankful to all colleagues in the Chair of Mechanics-Material Theory for their precious friendship which is definitely an important part of being a Ph.D. candidate at Ruhr-University Bochum.

In addition, I would like to acknowledge the German Science Foundation (DFG) through the research project LE 1216/4-2 for their financial support during my study. My research would have been impossible without their sponsorship.

Last but not least, I am grateful to my family for their love and care. I would like to take this opportunity to send my sincere thanks to my parent, especially my Mom whose whole life bore all difficulties to raise me up. Regrettably, she could not withstand cancer to witness this memorable moment of my life. This dissertation is dedicated to her.

Contents

Contents

List of Figures

List of Figures

1 Introduction

During processes of forming materials like cold working, hot working and annealing, metals and alloys undergo significant microstructural changes. Among such changes one should mention the formation and evolution of grain and subgrain boundaries (Hughes and Hansen [51], Kuhlmann-Wilsdorf and Hansen [58]), deformation twinning in low stacking fault metals and alloys (Christian and Mahajan [43], Tome et al. [73]), formation of macroscopic shear bands in polycrystals (Jia et al. [52]) and single crystals (Harren et al. [50], Uchic et al. [74]), polygonization (Cahn [15],Gilman [16]), texturing, recrystalization, deformation twinning, et cetera. The structural changes of metals and alloys at microlevel may influence the macroscopic properties of these materials directly, as the Taylor and Hall-Petch relations show (see, for instance, Hansen [49], Jiang and Weng [53]). As a consequence, new materials with exceptionally high strength could be created in this way. Therefore, the following question, interesting from the theoretical and important from the practical point of view, arises: what kind of theory can we develop to explain and predict such microstructural changes as well as the accompanying macroscopic responses of the materials? Unfortunately, so far there is no comprehensive answer to this question except for some particular cases. However, one thing is for sure: since the plastic slip as the product of collective movement of a huge number of dislocations and grain boundaries are the active participants in this structural rearrangement, any physically meaningful theory of formation and evolution of microstructure should capture their behavior in a proper way.

One of the main guiding principles in seeking an appropriate theory of formation of microstructure in metals and alloys has first been proposed by Hansen and Kuhlmann-Wilsdorf [48] in form of the so-called LEDS-hypothesis: the dislocation structures in the final state of deformation minimize the energy of crystals (see also Kuhlmann-Wilsdorf [57], Laird et al. [60]). However, it is still difficult to develop the theory of formation of dislocation structures based on this principle alone. The crucial step in this direction has been done by Ortiz and Repetto [67], and Ortiz et al. [68], who introduced a new ingredient to the energy minimization, namely the non-convexity of the energy. In their

papers the problem of non-convex energy minimization has been formulated and studied for ductile crystals within the finite crystal plasticity. By observing that the pseudoelastic energy densities of crystals undergoing geometrical softening or latent hardening are in fact non-convex, they showed that the laminate structures in which the piecewise constant plastic deformation caused by a single slip system and the piecewise constant elastic deformation in form of pure rotation serve as the energy minimizing sequences. Later on, Carstensen et al. [42] discovered the non-convexity of the energy densities even for crystals deforming in single slip without geometrical softening or latent hardening and thus, extended the non-convex energy minimization to the whole finite crystal plasticity. But crystal plasticity, as a phenomenological theory, operates with plastic slips while ignoring their source: dislocations. To achieve an agreement with experiments it has to introduce several phenomenological concepts like back stress or hardening as internal variables obeying additional constitutive equations which would otherwise be derivable as natural consequences of a more general continuum dislocation theory (see the series of recently papers Berdichevsky and Le [4], Le and Nguyen [8, 9], Le and Kaluza [20], Le and Kochmann [21, 22, 23], Le and Sembiring [26, 27, 28], Le and Nguyen [29], as well as the alternative approaches in Engels et al. [44], Lee et al. [63], Lim et al. [64], Mayeur and McDowell [65], Öztop et al. [66], which the framework of this theory has been laid down by Kondo [54], Nye [31], Bilby et al. [40], Kröner [56], Berdichevsky and Sedov [5], Le and Stumpf [11, 12], and Gurtin [39]. Let us mention also an approach proposed recently by Zhu et al. [79], Zhu and Xiang [80] in which continuum models of dislocation densities on low angle grain boundaries and the grain boundary energy (including also the long-range elastic energy when the grain boundary is not in equilibrium) are derived from the discrete dislocation dynamics. Such approach has the advantage of capturing details of the formation process of grain boundaries in which the grain boundaries are in general non-equilibrium. Ortiz and Repetto [67], at the end of their paper, did include the dislocations and their energy into the crystal plasticity to justify some heuristic estimates for the spacing of the dislocation walls and pointed out the way of generalization to the continuum dislocation theory. However, to the best of our knowledge, the whole set of governing equations as well as the boundary and jump conditions that must be satisfied at the grain boundaries have not yet been derived and studied thoughtfully from the continuum dislocation theory.

In this thesis, we will apply this CDT in two cases. Firstly, we use the linear version of the CDT for the problems of polygonization and bending (Chapter 4). Secondly, we use the nonlinear CDT for the shear banding problem (Chapter 5). After this short introduction we will explain some basic notions in dislocation theory in Chapter 2, and the continuum dislocation theory will be discussed details in Chapter 3.

In Chapter 4, the first part we will extend the qualitative modelling of polygonization based on the CDT Berdichevsky [2, 3] which was proposed only recently in Le and Nguyen [29] to the case of single crystal having one active slip system inclined at some angle to the beam axis and comparing with the experimental results reported in Gilman [16]. To match Gilman's experimental setup, we specify the displacements of one face of the beam rather than applying the bending moment to the ends of the beam. We then consider the exact two-dimensional variational problem of minimizing energy of the bent beam within the continuum dislocation theory. Applying the variational asymptotic procedure, we reduce the energy functional to the one-dimensional functional, whose smooth minimizer is found in closed analytical form. Based on this smooth solution we then construct a sequence of piecewise smooth deflections and piecewise constant plastic distortions having the same bending moment as that of the smooth minimizer. By including also energy contributions at jumps of the plastic distortion, proposed in accordance with the Read-Shockley formula for the low angle tilt boundaries Read and Shockley [32], we show that these discontinuous functions do reduce the total energy of the bent beam. We give also the estimation of the number of polygons and the average polygon distance.

The second part aims at constructing the asymptotically exact one-dimensional theory of bending of single crystal beams having one active slip system within CDT. We consider two cases: i) the dissipation due to the dislocation motion is assumed to be negligibly small so that the displacements as well as the plastic distortion can be determined from the energy minimization, ii) rate-independent dissipation is taken into account leading to the minimization of "relaxed" energies. In both cases the variational problems contain a small parameter and, consequently, they can be reduced to one-dimensional variational problems by applying the variational-asymptotic method Berdichevsky [1], Le [25]. The obtained one-dimensional variational problems admit analytical solutions representing the smooth minimizers. It is established that there exists a threshold value for the dislocation nucleation which depends on the thickness of the beam. This exhibits the typical size effect of the gradient theory. Based on this analytical solution the deflection of the beam, the dislocation density, and the moment-curvature curve are analyzed in terms of the bending moment for different loading/unloading processes. We then consider the polygonization of bent beam after unloading and annealing and prove that such state possessing non-smooth plastic distortion is energetically preferable (Le and Nguyen, 2011; Le and Nguyen, 2012).

In Chapter 5, we apply the developed theory to plane strain problem for single crystal deforming in single slip under the condition of uniaxial compression. Due to the non-convexity of the energy in certain ranges of the overall stretch, the construction of

the lamellae with piecewise constant plastic and elastic deformation leads to the energy minimizing sequences as the solutions of these non-convex variational problems. In case of plate under uniaxial compression the uniform states are not rank-one connected, so dislocations and grain boundaries should adapt to the elastic strains chosen from the homogeneous states in a smart way to satisfy the compatibility condition and, at the same time, to minimize the energy. It turns out that the whole set of jump conditions is needed to determine the orientation of grains (which are misoriented with respect to the slip direction), the plastic slips, and the elastic rotations.

2 Basic in dislocation theory

2.1 Physical background

It is well-known that metals, alloys and a great deal of non-metallic solids are crystalline, because the crystal structure of them is constructed by the periodically repeatable arrangement of the atoms in three dimensions (Hull and Bacon [61]). To describe the lattice structure, it is convenience to take one unit cell (parallelepiped), which is formed by sets of parallel lines as shown in Figure 2.1. It is characterized by three lattice vectors $\mathbf{v_1}, \mathbf{v_2}, \mathbf{v_3}$ which are orthogonal and have an equal magnitude in cubic crystals. The lattice structure will be formed periodically for all integers a_1, a_2, a_3 if it is translated by the combination $a_1\mathbf{v_1} + a_2\mathbf{v_2} + a_3\mathbf{v_3}$. In nature, there are around fourteen different types
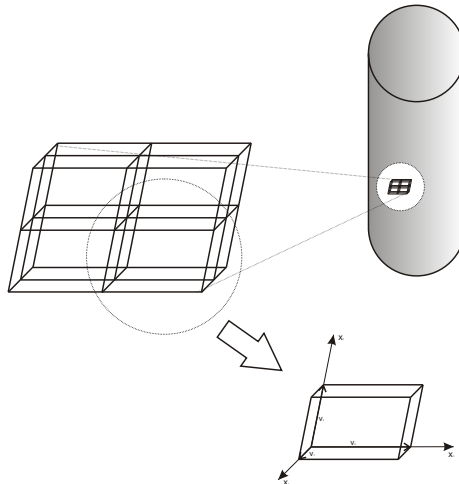
Figure 2.1: Unit cell in whole structure.

of crystal unit cell structures, however the primary crystal unit cell structures of metals are described as the body-centered cubic (bcc), face-centered cubic (fcc) and close-packed hexagonal (hcp). In body-centered cubic structure, its unit cell contains one atom at

each of the eight corners and one atom in the center (Fig.2.2a). The cornered atoms is also atoms of the remaining seven unit cells, thus they are shared among eight unit cell and in each unit cell there is just one per eight of a atom at each corner. The atoms are not allowed to pack together closely in bcc as in another structure. With a similar arrangement of atoms at eight corner, instead of having one atom at the center beside the cornered atoms, face-centered cubic structure has atoms at centered of all cubic faces (six faces)(Fig.2.2b). Each of these six atoms belong also to adjacent cells. Not like in bcc structure, the atoms here can pack closest together. There is also true of hcp crystal. Figure 2.2c displays the unit cell of hcp structure which consists twelve atoms at corner, two atoms in the center of the upper and lower faces and three atoms are arrange totally inside the cell as a triangle.

(a) Body-centered cubic.   (b) Face-centered cubic. (c) Close-packed hexago-
nal.
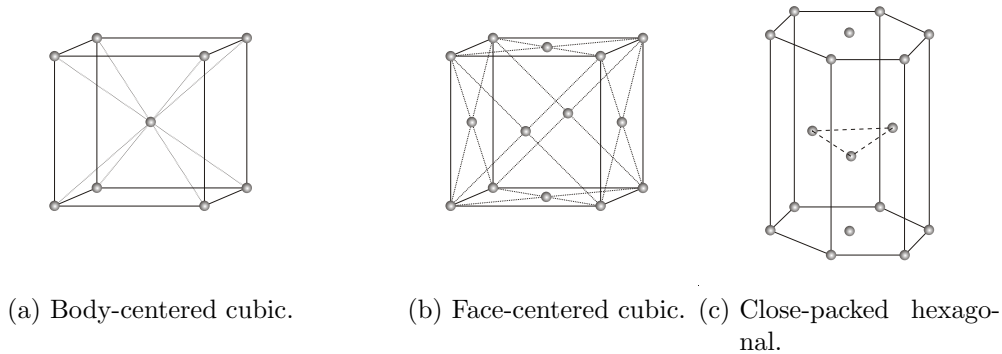
Figure 2.2: Crystal structure.

In material science, the motion of dislocations is divided into two basic notions: glide and climb. The movement of dislocations in the planes which contain dislocation line and Burgers' vector is called "glide", and the movement of dislocations normal to the Burgers' vector and out of the glide plane is called "climb". Slip planes is the planes which contains a lot of glide-dislocations, and normally it is the planes which one can observed experimentally the atomic density is the highest. In order to observe clearly the gliding ability of crystals, let us consider a single crystal bar being in a tensile test (shown in Figure 2.3). Its slip planes are inclined at some angle to the bar axis. In the test, a load (F) is applied in the vertical direction and it is measured together with the respective elongation Δl of the specimen. These two values are then converted into stress(σ) and strain(ϵ) by the relation,

$$\sigma = \frac{F}{A_0},$$
$$\epsilon = \frac{\Delta l}{l_0},$$

(2.1)
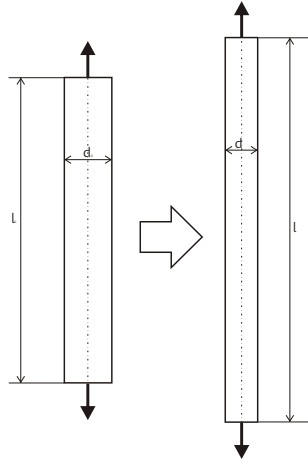
Figure 2.3: Tensile test.

where A_0, l_0 is the original cross-sectional area and length of the specimen. The curve displays the relationship between stress and strain is now can be seen by plotting all the values of them (shown in Figure 2.4). When stress is applied under such a critical value
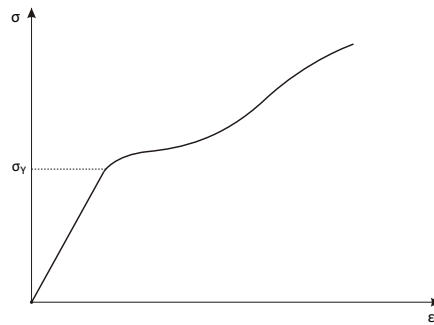
Figure 2.4: The stress-strain curve for metals.

which is called yield stress (σ_y), the deformation of the bar is perfectly elastic because if it is unloaded then it recovers the original state with the initial length. The values of stress in this region is always proportional to strain with a proportionality factor which is well-known as the modulus of elasticity or Young's modulus (E) and can be seen as the slope of the linear part of the stress-strain curve. Starting from the yield point, the bar begins to deform plastically if the stress is increased further. If looking closer to this

deformed bar, one can see continuously steps at the surface of it. These steps are the witnesses of the plastic slips on the active slip systems in which contains slip planes and slip directions correspondingly (shown in Figure 2.5).
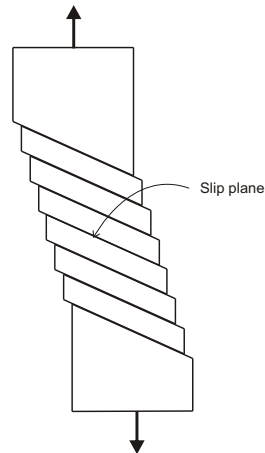
Figure 2.5: Schematic view of plastic slips.

In order to recognize and distinguish the planes and directions of these slip systems, Miller indices are used for this purpose because it show exactly where are these positions in crystallographic planes and directions. The Miller indices are defined by a set of three integers a_1, a_2, a_3 which are written in square brackets to indicate all directions parallel to the vector $a_1\mathbf{v_1} + a_2\mathbf{v_2} + a_3\mathbf{v_3}$. The smallest multiples of a_1, a_2, a_3 are chosen for the Miller indices. For instance, Miller indices for the directions s_1, s_2, s_3 in Figure 2.6 are $[\bar{1}01]$, $[01\bar{1}]$ and $[1\bar{1}0]$ respectively, where the bar over the index indicates the negative sign of the corresponding components. Consequently, in order to present the crystallograpic planes, the similar sets of integer are used and they are enclosed in parenthesis. For example, the Miller indices for the plane which is shown in Figure 2.6 is (111).

2.2 Critical resolved shear stress

In mechanical fields, in order to produce plastic deformation with polycrystalline metal specimens, the yield stress point must be exceeded. It is also true with single crystal metals to initiate the plastic deformation, which is known as slip of the atomic planes, the shear stress resolved on the slip plane and in the slip direction has to achieved the
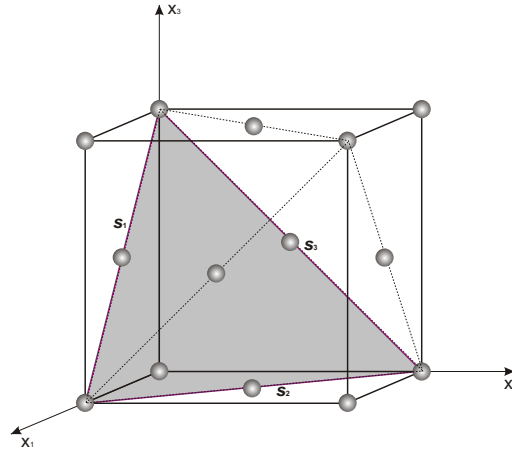
Figure 2.6: An example of slip directions (s_1, s_2, s_3) and slip plane in an unit cell of fcc crystals.

threshold value (or critical value). It is defined as critical resolved shear stress and how large this value is depends on the applied tensile stress and the orientation of the slip system. The equation of this relation can be derived as follow. Let consider a pillar with area of cross section (A) is applied tensile force (F) at upper and lower boundary (Figure 2.7).The tensile stress is calculated as, $\sigma = \frac{F}{A}$. ϕ is the angle between the normal of the slip plane and the stress axis and θ is the angle between the slip direction and the stress axis. The resolved shear stress is therefore given as

$$\tau = \frac{F_s}{A_s}, \tag{2.2}$$

where $F_s = F \cos \theta$ is the resolved force acting on the slip plane and $A_s = \frac{A}{\cos \phi}$ is the area of the slip plane. The equation is now can be written as,

$$\tau = \frac{F \cos \theta}{\frac{A}{\cos \phi}} = \sigma \cos \theta \cos \phi, \tag{2.3}$$

with $\cos \theta \cos \phi$ being the so-called Schmid factor (Schmid [1924]). The slip system which have the largest Schmid Factor is the active one. When $\theta = \phi = 45^0$ is occurred, the resolved shear stress can be seen as equals to one half of the tensile stress which is the maximum value that this shear stress can achieve, and when $\theta = \phi = 45^0$ the resolved shear stress equals to zero which means that there is no slip.
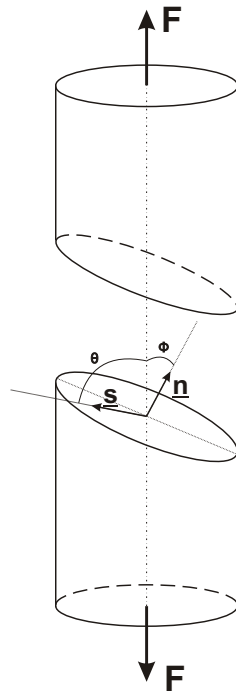
Figure 2.7: The determination of critical resolved shear stress equation.

2.3 Dislocation

Dislocation is an imperfection in crystals. Each dislocation is characterized by its line and Burgers' vector. A single dislocation can be created by cutting the crystal along any smooth surfaces. Then the atoms on one side of the cut are shifted in a direction parallel to the cut in one atom spacing. Finally, the atoms on both sides of the cut are rejoined again, and the crystal is elastically relaxed. Thus, with an exception near the dislocation line(line AB in the figures), the structure of the crystal is almost perfect. With different orientation of the shifting, we get different type of dislocations.

An edge dislocation shown in Fig. 3.2b is created when the atoms below the cut is shifted perpendicular to the dislocation line.

The migration of an edge dislocation through the crystal from left to right under an applied shear stress τ is illustrated in Fig. 2.9. This migration, from one position to the next, involves only a small rearrangement of the atomic bonds near the dislocation line.
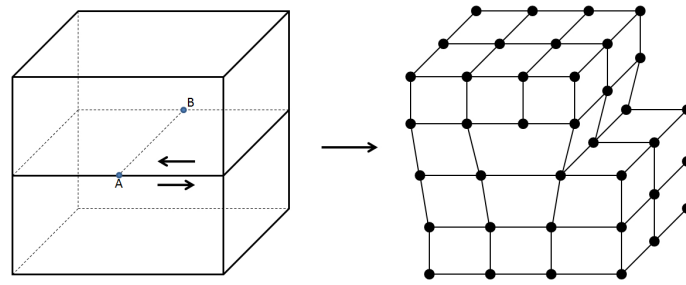
Figure 2.8: Edge dislocation.
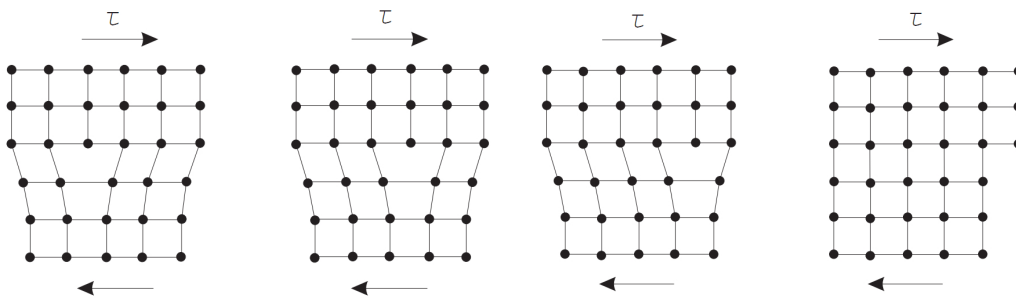
Figure 2.9: Migration of the edge dislocation.

A screw dislocation (Fig. 2.10) is created when the atoms below the cut is shifted parallel to the dislocation line.

A mixed dislocation (Fig. 2.11) is created when the atoms below the cut is shifted in a direction which is neither parallel nor perpendicular to the dislocation line.

2.3.1 Burgers' vector

The most important characteristic of a dislocation is given in terms of Burgers circuit. In Figure 2.12, the Burgers circuit is established around an edge dislocation. The left
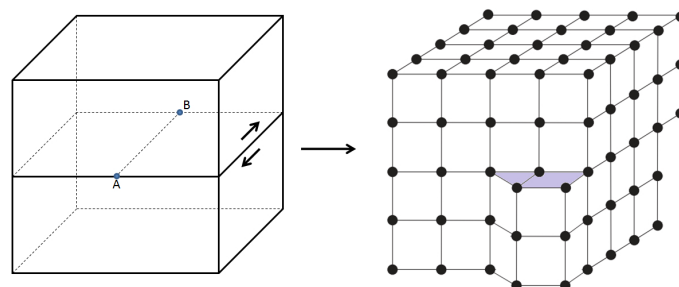
Figure 2.10: Screw dislocation.
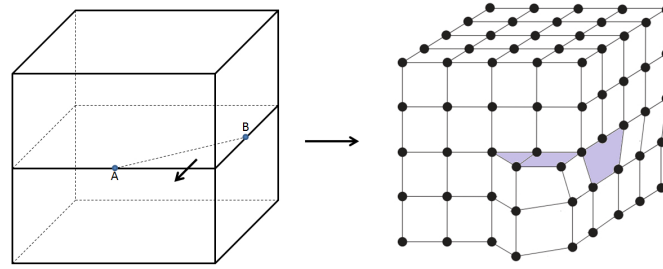
Figure 2.11: Mixed dislocation.

(a) Burgers circuit in dislocation-free crystal.

(b) Burgers circuit and Burgers vector in edge dislocation.
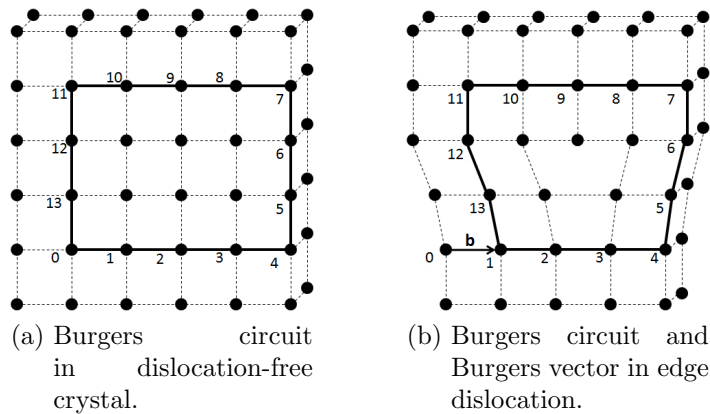
Figure 2.12: Burgers circuit around edge dislocation.

close circuit is drawn in the reference dislocation-free crystal, while the right one is drawn around an edge dislocation in the real crystal. The starting point and the end point correspond to the same atom in the left circuit. However in the right circuit, the starting point and the end point do not correspond to the same atom. There is a closure failure in this circuit, which defines Burgers vector. The sense of this vector depend on the sense of the dislocation line. We define the sense of the dislocation line by assigning a unit vector τ tangent to the dislocation line and taking the positive sense in the positive direction of τ. One can see that the Burgers vector of an edge dislocation is perpendicular to the dislocation line.
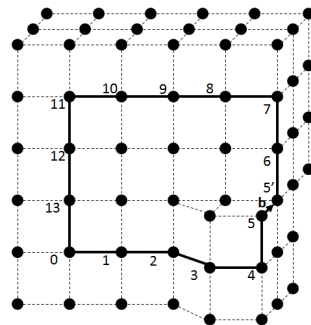
Figure 2.13: Burgers circuit and Burgers vector in screw dislocation.

On the contrary, in a screw dislocation, the Burgers vector is parallel to the dislocation line as shown in Figure 2.13.

2.3.2 Screw dislocation

It is true that stresses occur in the crystal containing dislocations although there are no external forces and tractions acting on it. By using the framework of linear elasticity as a foundation, we can determine these self-stresses through out the process of creating a single dislocation in crystal. As derived fully details in Le [6], there are only two independent non-zero components in the stress tensor, σ_{31} and σ_{32}, which are computed from stress function (Ψ) as,

$$\sigma_{31} = \Psi_{,2}, \quad \sigma_{32} = \Psi_{,1}, \tag{2.4}$$

where $\Psi = -\frac{\mu b}{2\pi} \ln |\mathbf{x}|$ is found by solving the differential equation,

$$\frac{1}{\mu}\nabla^2\Psi = -b\delta(x), \tag{2.5}$$

with b is the magnitude of the Burger's vector, $\delta(x)$ is the Dirac delta function and μ is the material constant. By differentiating the stress function we obtain,

$$\sigma_{31} = -\frac{\mu b}{2\pi}\frac{x_2}{r^2}, \quad \sigma_{32} = \frac{\mu b}{2\pi}\frac{x_1}{r^2}. \tag{2.6}$$

Applying the Hooke's law given us the elastic strains as,

$$\varepsilon_{31}^e = -\frac{b}{4\pi}\frac{x_2}{r^2}, \quad \varepsilon_{32}^e = \frac{b}{4\pi}\frac{x_1}{r^2}. \tag{2.7}$$

The total elastic energy per unit length of the dislocation line is obtained by taking the integral of the energy density of the crystal over the whole plane,

$$E = \int \phi d\mathbf{x}, \tag{2.8}$$

where $\phi = \frac{1}{2}\lambda(\varepsilon_{ii}^e)^2 + \mu\varepsilon_{ij}^e\varepsilon_{ij}^e = 2\mu[(\varepsilon_{31}^e)^2 + (\varepsilon_{32}^e)^2]$. The result come out as the total of the energy surrounding lattice and the dislocation core energy, respectively as,

$$E = \frac{\mu b^2}{4\pi}\ln\frac{a}{\pi\epsilon} + \mu b^2\tilde{e}, \tag{2.9}$$

where $\tilde{e} = 0.0327386$, a is the size of the square which is used to take the integral, ϵ is the effective size of the core.

2.3.3 Edge dislocation

The stresses in edge dislocations are more complicated than in screw dislocations, the non-zero components of the stress tensor are $\sigma_{11}, \sigma_{22}, \sigma_{33}, \sigma_{12} = \sigma_{21}$ which are also calculated from the stress function Ψ,

$$\sigma_{11} = \Psi_{,22}, \quad \sigma_{22} = \Psi_{,11}, \quad \sigma_{33} = \nu\nabla^2\Psi, \quad \sigma_{12} = \sigma_{21} = -\Psi_{,12}, \tag{2.10}$$

so that they can satisfied the equilibrium equations of the plane strain state due to the dislocation line along x_3-axis,

$$\sigma_{11,1} + \sigma_{12,2} = 0, \quad \sigma_{21,1} + \sigma_{22,2} = 0. \tag{2.11}$$

From Le [6], $\Psi = \frac{\mu b}{2\pi(1-\nu)} r \sin \upsilon \ln r = \frac{\mu b}{4\pi(1-\nu)} x_2 \ln(x_1^2 + x_2^2)$ is found from the fourth order differential equation,

$$\frac{1-\nu}{2\mu}\nabla^2\nabla^2\Psi = -b\delta_{,2}(\mathbf{x}). \tag{2.12}$$

From 2.11 we obtain,

$$
\begin{aligned}
\sigma_{11} &= -\frac{\mu b}{2\pi(1-\nu)}\frac{x_2(3x_1^2 + x_2^2)}{(x_1^2 + x_2^2)^2}, \\
\sigma_{22} &= \frac{\mu b}{2\pi(1-\nu)}\frac{x_2(x_1^2 - x_2^2)}{(x_1^2 + x_2^2)^2}, \\
\sigma_{12} = \sigma_{21} &= \frac{\mu b}{2\pi(1-\nu)}\frac{x_1(x_1^2 - x_2^2)}{(x_1^2 + x_2^2)^2}, \\
\sigma_{33} &= -\frac{\mu b\nu}{\pi(1-\nu)}\frac{x_2}{(x_1^2 + x_2^2)}.
\end{aligned}
\tag{2.13}
$$

The elastic strains are then calculated by applying Hooke's law yield,

$$
\begin{aligned}
\varepsilon_{11}^e &= -\frac{b}{4\pi(1-\nu)}\frac{x_2[(3-2\nu)x_1^2 + (1-2\nu)x_2^2]}{(x_1^2 + x_2^2)^2}, \\
\varepsilon_{22}^e &= \frac{b}{4\pi(1-\nu)}\frac{x_2[(1+2\nu)x_1^2 - (1-2\nu)x_2^2]}{(x_1^2 + x_2^2)^2}, \\
\varepsilon_{12}^e = \varepsilon_{21}^e &= \frac{b}{4\pi(1-\nu)}\frac{x_1(x_1^2 - x_2^2)}{(x_1^2 + x_2^2)^2}.
\end{aligned}
\tag{2.14}
$$

The total elastic energy per unit length of the dislocation line becomes,

$$E = \frac{\mu b^2}{4\pi(1-\nu)} \ln \frac{r}{r_0},$$
(2.15)

where r is the distance from the dislocation line to the boundary of the crystal and $r_0 = \frac{b}{\alpha}$ is the effective radius of the dislocation core ($\alpha = 4$).

2.4 Formation of microstructure

2.4.1 Cold working process

Cold working which is also called strength hardening or work hardening is a process of strengthening materials through the plastic deformation below the crystallization temperature, usually in room temperature. Because of the movement and generation of dislocations during this process, it make themselves get stuck and tangled, thus it is difficult for them to move then it makes the material become harder and stronger. However, it reduces the material ductility and induces residual stresses inside material. Some of the common cold working process are rolling (2.14 a), bending (2.14 b), drawing (2.14 c), etc....
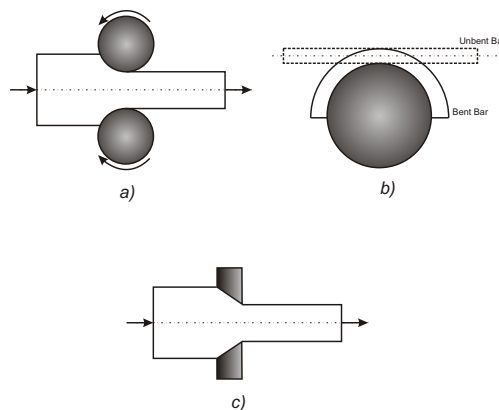
Figure 2.14: Cold working process.

2.4.2 Polygonization

2.4.2.1 Experiments

The experiments on polygonization of zinc monocrystals done by Gilmann can be presented in the following scheme.
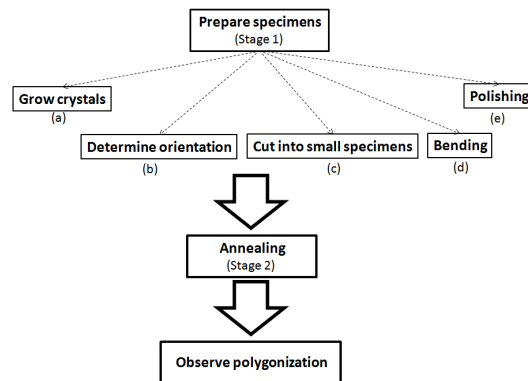
Figure 2.15: The stages of experiment.

In the following we describe each step in more details.

2.4.2.1.1 Preparation of the specimens

A single crystal must first be obtained by the crystal growth. Bridgman method was used for growing the crystals which was in round (5/32 in. I. D.) and square (6×6mm) precision Pyrex tubes. The crystals orientation was obtained by seeding method which control most of crystals having $\chi_0 = 35^0$, where χ_0 is the angle between the slip planes and the beam axis. The raw material was chosen from New Jersey Zinc Company with 99.999 percent of zinc.

In order to determine the orientation of the crystal, Greninger chart and back-reflection X-ray method, which is called Laue method, were used. The former, which is shown on Fig. 2.16 greatly facilitated the interpretation of the back reflection Laue pattern. The latter, which is shown on Fig. 2.17 is used for specifying the orientation of the crystal by meridian (longitude) and parallel coordinates (latitude). The angle of the longitude is varied by the rotation about the vertical axis(V-V), and the angle of the latitude is varied by the motion of the line along vertical circle.
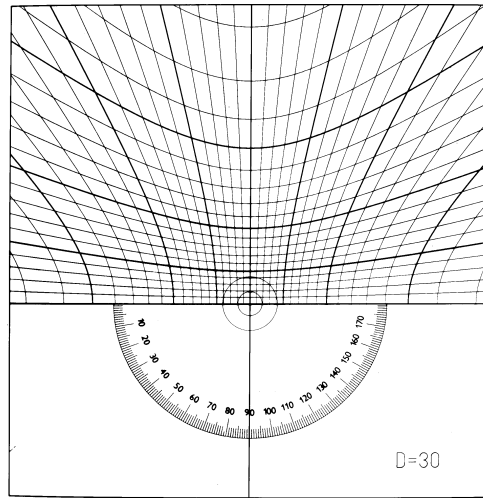
Figure 2.16: Greninger Chart (Hybler [19]). Reprinted by permission.
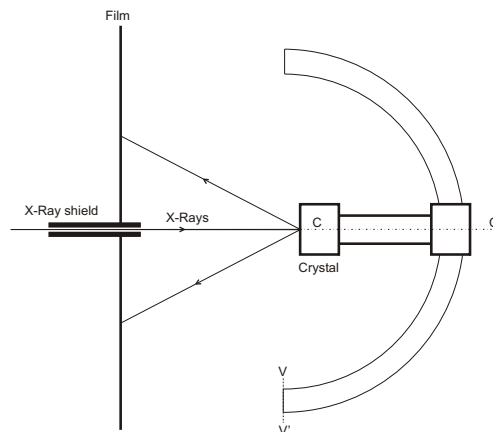
Figure 2.17: Laue back-reflection X-ray method.

After determining the orientation, the crystal was cut into small specimens whose size is about one and a quarter inch. Subsequently, on each specimen, for creating a sharp wedge to be flat on one side, one end was cleaved at a temperature negative 196 degrees of Celsius.

The next step in preparation process of the specimens is bending the crystal. A generating circle, which is called bending jig, is used for aligning the flat side of the crystal in order to fix the bending axis relative to the crystal axes. Afterward, at the ends of the crystal, a reverse bending moment was applied at low temperature, which is similiar to the temperature when creating sharp wedge (negative 196 degrees of Celsius), to cleaved along crystal bent cleavage surfaces.

The specimen was then polished due to macroscopic smoothness. Before immersing the crystal into chemical polish, it was cleaned in HCl. There were two solutions for choosing the chemincal polish for zinc, the first one yield fast action but difficult to control, therefore, the second solution was chosen. It was composed of 160g CrO_3, 20g $Na_2SO_4.10H_2O$ and 500cc H_2O. In order to get the highest result, the process in which the crystal was immersed and washed in chemical for 10 seconds, was repeated several times.

2.4.2.1.2 Annealing and observing polygonization

When the preparation process had finished, this polished bent crystal was annealed in furnaces at a temperature about 350 degree of Celsius. The furnace atmosphere is only air without any special chemical. At that temperature, the surfaces which were cleaved were not affected by appreciable oxide. In order to get the net annealing times for data table, the total time of the specimen in furnace was reduced due to the experience from the test with a typical specimen which required about three minutes to approach within 10 degrees of the annealing temperature.

There were two methods for observing results from the specimen: optical method and back reflection Laue technique. Both of them are used for determining the polygon angles when the polygonized state appeared. According to optical method, the polygon angles are calculated by taking the average spacings of the boundaries divided by the radius of curvature. This method used a fixed aperture of the lighting system to illuminated on a narrow band of the cleavage surfaces then measuring the widths of the illuminated bands on polished drill-rods to establish the calibration curve. Hence, the radius of curvature of the cleavage planes was found by using the graph of bandwidth versus drill-rod radius. The polygon angles were dectected through this method as small as 10^{-3} radian consistently. It was also dectected the similar results about 10^{-3} radian when using X-ray method (see Fig. 2.18).

2.4.3 Formation of grain and subgrain boundaries

In physical metallurgy, materials are composed not just only single crystal, on the other hand they are constructed by many crystallites (or grains) which have a variety of sizes and orientations (shown in Figure 2.19). The interface between grains is called grain boundaries. The grain boundary is commonly defined as the boundary between misoriented
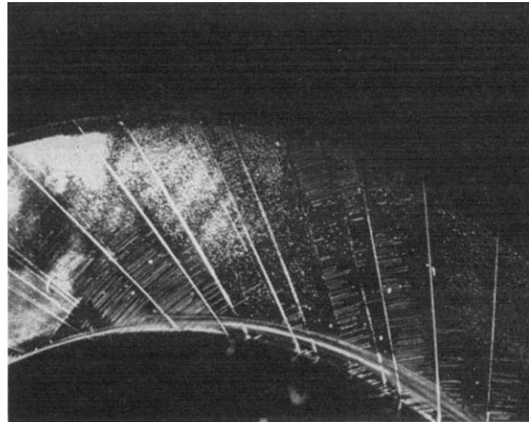
Figure 2.18: View along intersections of slip planes with polygon boundaries in a polygo-nized zinc crystal (Gilman [16]). Reprinted by permission.
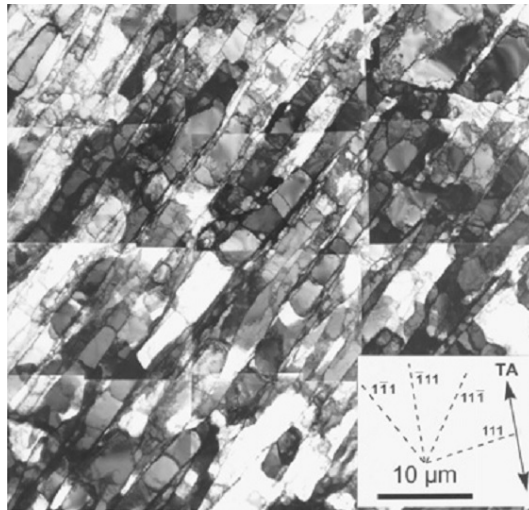
Figure 2.19: Transmission electron micrographs of polycrystalline pure aluminum (Hansen [17]). Reprinted by permission.

(and/or) misfitted crystallites as shown in Fig. 2.20. For single crystals such boundary can occur only due to the jump in the elastic deformation because the plastic deformation leaves the crystal lattice unchanged. However, as the multiplicative resolution of the deformation gradient applies, the logical possibility of jumps in the deformation gradient as well as in the plastic slip at such boundary should be admitted. At low temperature the grain boundaries are, as a rule, quite strong and do not weaken metals, therefore we may exclude the crack formation in these materials by assuming that the placement field exists and is continuous everywhere. In this case the grain boundary must be regarded as the surface of weak discontinuity in placement but strong discontinuity in plastic slip. These grain boundaries can be modeled as an arrays of dislocations. This idea was first proposed by Bragg and Burger in 1940. If the mis-orientation between two grains are less than 15 degree, so called *low angle grain boundaries* or *sub-grain boundaries* or *low misorientation*
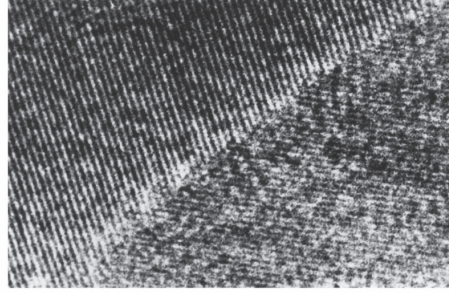
Figure 2.20: HREM micrograph of a typical grain boundary (Valiev [77]). Reprinted by permission.
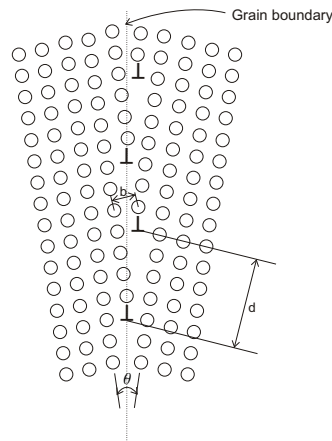
Figure 2.21: Dislocation model of low angle grain boundary.

tilt grain boundaries, it can be easily illustrated as in Figure 2.21. The relation between the misorientation angle (the angle of the tilt) θ and the distance between dislocation d can be express as,

$$\sin\frac{\theta}{2} = \frac{b}{2d}, \tag{2.16}$$

where b is the Burgers vector of a dislocation in the boundary. If the misorientation angle is small, it leads to $\sin\frac{\theta}{2} = \frac{\theta}{2}$, thus this relation becomes,

$$\theta = \frac{b}{d}. \tag{2.17}$$

2.4.4 Severe plastic deformation

Severe plastic deformation (SPD) is a general name for representing a group of methods which is applied for working with metals and alloys. It increases the strains state of materials dramatically by using high imposed pressure for making the materials deform plastic. Thus, the microstuctures are transformed into fine (with grains size $< 10\mu m$) and even extremely fine-grained structures (with grains size $< 1\mu m$). The most popular approaches of SPD are equal channel angular extrusion (ECAE) or equal channel angular pressing (ECAP), cyclic extrusion-compression, torsion-compression, multi-axis forging and accumulated roll bonding. All of these methods have the common characteristics that the materials are deformed under high pressure, therefore they are able to perform very large deformations while pressure prevents them from damage or cracks. We would like to discuss further in ECAP methods due to its significant advantages that does not reduce the cross sectional area during the processed operations, and with a pressure and load not so high it can produce such a large and uniform deformations.

ECAP is a process of pressing a billet (a piece of metal or alloy) which is lubricated through out two channel in a die as shown in Fig 2.22. This two channels cross-section
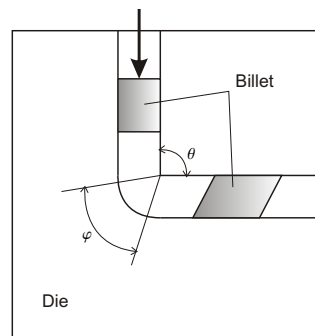
Figure 2.22: The ECAP process.

intersect at an angle θ and the the rounded corner with angle φ. Usually θ is chosen to be between 90^0 and 120^0 to prevent the billet from damages and cracks during repeated process and to maximize the results of each pass. In contrast with the significant effect of θ, the chosen of φ is less important, it is often chosen to be equal 0. Exceptionally in finite element modeling, it is chosen from 20^0 to 60^0 so that the material go smoothly through

out the channels to avoid the sharp corner problems in creating the FEM model. Because the cross section of the billet still remains the same after going through the channels, thus the process can be repeated until the billet strengthening gradually disappear. As a results a large amounts of plastic strains are imposed on the billet. The equivalent strain per each pass of the process, depends on the angles φ and θ, is given by Iwahashi, et al. [82] as,

$$\varepsilon_{eq} = \frac{1}{\sqrt{3}}[2\cot(\frac{\varphi}{2} + \frac{\theta}{2}) + \varphi\,cosec(\frac{\varphi}{2} + \frac{\theta}{2})]. \tag{2.18}$$

3 Continuum dislocation theory

3.1 Linearized continuum dislocation theory

3.1.1 Nye's dislocation density

The first attempt of taking into account the dislocations in the plastically bent beam was made by Nye [31] who expressed the curvature of a beam caused by dislocations in terms of the dislocation density tensor. The geometry for bending by single slip, which is used for the experiments, was first determined by West [18]. It is illustrated in Fig. 3.1, where the variety of symbols may be used to represent the parameters relations. According to West, the slip planes are defined through equations:

$$\begin{cases} x = a(\cos\psi + \psi\sin\psi) \\ y = a(\sin\psi - \psi\cos\psi) \end{cases} \tag{3.1}$$

where a is the radius of generating circle and equal to $R\sin\chi_0$.

The radius of curvature are calculated as

$$c = \sqrt{(L^2 - a^2)} \tag{3.2}$$

with $L = \sqrt{(x^2 + y^2)}$.

The local dislocation density (ρ) has been found by Nye which can be used for small strains. The local dislocation density is proportional to the Burgers' vector (b) with an assumption that $D << c$, where D is slip plane spacing, and reads,

$$\rho = \frac{1}{bc} \tag{3.3}$$

The average radius of curvature, which is used for obtaining the average dislocation den-

Figure 3.1: Geometry of slip planes in bent specimen (Gilman [16]). Reprinted by permission.

sity, is given by

$$\bar{c} = \frac{1}{t} \int_{r_2}^{r_1} \sqrt{(L^2 - a^2)} \mathrm{d}L \tag{3.4}$$

and can be roughly calculated from the value of R if $L \approx R$, thus,

$$c = (R^2 - R^2 \sin^2 \chi_0)^{\frac{1}{2}} = R \cos \chi_0 \approx \bar{c}. \tag{3.5}$$

Since the average radius of curvature (c) decreases for $R < L$ and increases for $R > L$, it can be seen that this approximation is fairly good provided $(r_1 - r_2)$ is small compared with R and χ_0 is not large.

Consideration of Fig. 3.1 will show that the slip planes become perpendicular to the surface of $r_2 = a$. According to discussion of West and Nye, this imposes a limitation on the minimum value that R can have for the deformation of a single slip system . However, this minimum is limited by another factor due to twinning. Hence, the factors, such as temperature and impurities, that affect the ratio of the twinning stress to the slip stress also cause the change of minimum of R.

For calculating the minimum value of R with a given crystal thickness t and orientation χ_0, Nye ignores the change in thickness of the crystal during bending. Because the

volume of the crystal do not change during bending process,

$$a^2 = R(R - t) \tag{3.6}$$

with $a = R \sin \chi_0$, so the minimum of R is obtained as,

$$R_{min} = \frac{t}{\cos^2 \chi_0} \tag{3.7}$$

From the equation, the crystal cannot be bent when $\chi_0 = 90^0$ and it is possible to bend the crystals when $\chi_0 = 0^0$ until $R = t$. It was found that crystals could be bent to small radius without tensile or compressive twinning when the orientation χ_0 is about 35^0.

According to Nye theory, in polygonization experiments on single hexagonal metal crystals, the polygon walls are planes while the glide planes are deformed into cylinders whose sections are the involutes of a single curve. In the general three dimensional case, by taking a Burgers circuit of a unit area normal to the unit vector **n** has Burgers vector **B** yields,

$$B_i = \alpha_{ij} n_j. \tag{3.8}$$

Nye had introduced here the coefficients α_{ij} as the dislocation density tensor for specifying the state of dislocations. With the assumption that the distribution of dislocations is continuous, there are several sets of dislocations in a deformed crystal with its local density ρ, dislocation line direction **l** and Burgers vector **b**. The dislocation density tensor is calculated as,

$$\alpha_{ij} = \rho b_i l_j. \tag{3.9}$$

Read [33] and Bilby et al [13] have extended this result to the case when the stress due to dislocations does not vanish. The macroscopic stress (average stress in a volume containing many dislocations) in a uniformly bent crystal is related to the dislocation density by a simple differential equation analogous to Poisson's equation. Differences between bending and tension tests give information about the dislocation mechanism of deformation. A material that has a flat stress-strain curve in tension may show a yield point in bending if the stress required to move dislocations is substantially less than the stress required to generate dislocations. Read has later derived for the special case

of simple bending a relation between the lattice curvature and stress gradient in a solid containing dislocations. It is shown that this relation follows at once from the fundamental relation in the theory of continuous distributions of dislocations. As a further example the relations between the stress gradient, dislocation density and lattice curvature in twisted cylindrical bars are given. It is also shown that the properties of linear dislocation arrays used by Read follow from the general expression for the dislocation tensor of a surface dislocation.

There is no doubt that these theories are not able to predict the distance between polygons. So, this is the motivation for us to consider the polygonization within continuum dislocation theory.

3.1.2 Linearized continuum dislocation theory

It is well-known that dislocations cause plastic deformation of single or polycrystals. The dislocation pile-up near obstacles increases the hardening of material (Fig. 3.2). When dislocations move to the grain or phase boundaries, the energy disspation of the crystal appears through the resistance against this motion. The understanding of the nucleation
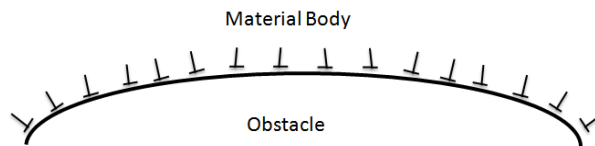
(a) Dislocation pile up at obstacle.
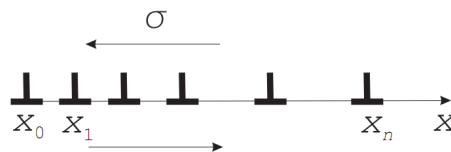
(b) An array of dislocations pile up under stress.

Figure 3.2: Dislocation pile-up.

and motion of dislocations is therefore crucial for explaining the plastic material properties. Continuum dislocation theory can be used to describe and simulate the complex dislocation network which contains an aggregate of a huge amount of dislocations. In what follows we present in some details this continuum dislocation theory.

Considering a crystal with one slip system. The total strains of the crystal are

the sum of the elastic strains and the plastic strains. The plastic strains are calculated through plastic distortion as below

$$\varepsilon_{ij}^{p} = \frac{1}{2}(\beta_{ij} + \beta_{ji}). \tag{3.10}$$

The elastic strains are then obtain by subtracting the plastic strains from the total strains,

$$\varepsilon_{ij}^{e} = \varepsilon_{ij} - \varepsilon_{ij}^{p} = \frac{1}{2}(u_{i,j} + u_{j,i}) - \varepsilon_{ij}^{p}, \tag{3.11}$$

with u_i being the components of the displacement vector. For one slip system the plastic distorsion is given by

$$\beta_{ij} = \beta(\mathbf{x})s_i m_j, \tag{3.12}$$

with s being the unit vector characterizing the slip direction, and m the normal vector to the slip plane.

In general, the continuous plastic distortion does not cause any volume change because $\beta_{ii} = 0$.

It is obvious that the plastic distortion is exactly the gradients of the plastic displacement fields as,

$$\beta_{ij} = u_{i,j}^{p}, \tag{3.13}$$

thus, we also have total distortion and elastic distortion,

$$\beta_{ij}^{T} = u_{i,j}^{T}, \qquad\qquad \beta_{ij}^{e} = u_{i,j}^{e}, \tag{3.14}$$

and

$$\beta_{ij}^{T} = \beta_{ij}^{e} + \beta_{ij} \tag{3.15}$$

which is compatible. By rewriting the above formula, let us introduce the changes of displacement over distances as,

$$du_j^T = \beta_{ij}^T dx_i, \tag{3.16}$$

$$du_j^e = \beta_{ij}^e dx_i, \tag{3.17}$$

$$du_j = \beta_{ij} dx_i, \tag{3.18}$$

where dx is the distance between two points. Integrating over an arbitrary loop c enclosing a surface A, these changes can be written using Stokes' theorem as,

$$\oint_c du_j^T = \oint_c \beta_{ij}^T dx_i = \int_A (\mathrm{curl}\beta^T)_{ij} n_i dA = 0, \tag{3.19}$$

$$\oint_c du_j^e = \oint_c \beta_{ij}^e dx_i = \int_A (\mathrm{curl}\beta^e)_{ij} n_i dA, \tag{3.20}$$

$$\oint_c du_j = \oint_c \beta_{ij} dx_i = \int_A (\mathrm{curl}\beta)_{ij} n_i dA. \tag{3.21}$$

From 3.15 and 3.22, we have,

$$\mathrm{curl}\beta^T = 0, \tag{3.22}$$

$$\mathrm{curl}\beta^e = -\mathrm{curl}\beta. \tag{3.23}$$

According to Burgers [83], the resultant Burgers' vector is calculated through elastic displacement as,

$$\mathcal{B}_i = -\oint_c du_j^e. \tag{3.24}$$

By substituting the relation between elastic and plastic distortion together with using 3.22 into 3.24 we obtain,

$$\mathcal{B}_i = \int_A (\mathrm{curl}\beta)_{ij} n_i dA = \int_A \epsilon_{jkl}\beta_{il,k} n_i dA. \tag{3.25}$$

In addition, from Nye theory, if one take an arbitrary infinitesimal surface da, $\alpha_{ij}n_j da$ give the resultant Burgers' vector of all dislocations whose dislocation lines cut this area

$$\mathcal{B}_i = \alpha_{ij} n_j da. \tag{3.26}$$

Equations 3.25 and 3.26 give, the important characteristic of dislocations, introduced by Nye [31], Bilby et al [13] and Kröner [14] , is the dislocation density tensor defined by

$$\alpha_{ij} = \epsilon_{jkl}\beta_{il,k}. \tag{3.27}$$

Here ϵ_{jkl} is the permutation symbol,

$$\epsilon_{jkl} = \begin{cases} 1 & \text{when } jkl \text{ are even permutations of 123,} \\ -1 & \text{when } jkl \text{ are odd permutations of 123,} \\ 0 & \text{when at least two of indices are equal.} \end{cases} \tag{3.28}$$

For a crystal deforming in single slip, the number of dislocations per unit area can be computed as:

$$\rho = \frac{|\mathcal{B}|}{bda} = \frac{|\alpha_{ij} n_j da|}{bda} = \frac{|\alpha_{ij} n_j|}{b} = \frac{1}{b}|\epsilon_{jkl}\beta_{,k}m_l n_j| \tag{3.29}$$

where b is the magnitude of Burgers' vector.

In continuum dislocation theory, the free energy density is the sum of the elastic energy density, which depends on the elastic strain ε_{ij}^e, and the energy density of microstructure, which depends on the dislocation density α_{ij}

$$\Phi = \frac{1}{2}\lambda(\varepsilon_{ii}^e)^2 + \mu\varepsilon_{ij}^e\varepsilon_{ij}^e + \phi_m(\alpha_{ij}). \tag{3.30}$$

Here $\phi_m(\alpha_{ij})$ corresponds to the energy density of the dislocation network, and for single crystal have only one slip system, this energy density becomes

$$\phi_m = \mu k \ln \frac{1}{1 - \frac{\rho}{\rho_s}} \tag{3.31}$$

with k being a material constant, μ the shear modulus, ρ_s the saturated dislocation density. The logarithmic energy stems from two facts: i) for small dislocation densities the energy of the dislocation network must be proportional to the dislocation density, and ii) there exists a saturated dislocation density which characterizes the closest packing of dislocations of equal signs admissible in the discrete crystal lattice. The logarithmic term ensures a linear increase of the energy for the small dislocation density ρ and tends to infinity as ρ approaches the saturated dislocation density ρ_s hence providing an energetic barrier against over-saturation.

Let V be a region occupied by the crystal in its initial state. The free energy of the crystal confined in the region V reads

$$E = \int_V \Phi(\varepsilon_{ij}^e, \rho)\, d\mathrm{x}. \tag{3.32}$$

Provided the energy dissipation can be neglected, the variational principle of the continuum dislocation theory states that the true displacement field and the plastic distortion in the final equilibrium state minimize this energy functional. As a consequence

$$\delta E = 0. \tag{3.33}$$

3.2 Nonlinear continuum dislocation theory

Nonlinear CDT starts from the basic kinematic resolution of the deformation gradient $\mathbf{F} = \partial \mathbf{y}/\partial \mathbf{x}$ into elastic and plastic parts [40]

$$\mathbf{F} = \mathbf{F}^e \cdot \mathbf{F}^p. \tag{3.34}$$

We attribute an active role to the plastic deformation: $\mathbf{F}^p$ is the deformation *creating* dislocations (either inside or at the boundary of the volume element) or *changing* their positions in the crystal without distorting the lattice parallelism (see Fig. 3.3). In contrary, the elastic deformation $\mathbf{F}^e$ deforms the crystal lattice having *frozen* dislocations [7]. Note that the lattice vectors remain unchanged when the plastic deformation is applied, while they change together with the shape vectors by the elastic deformation.
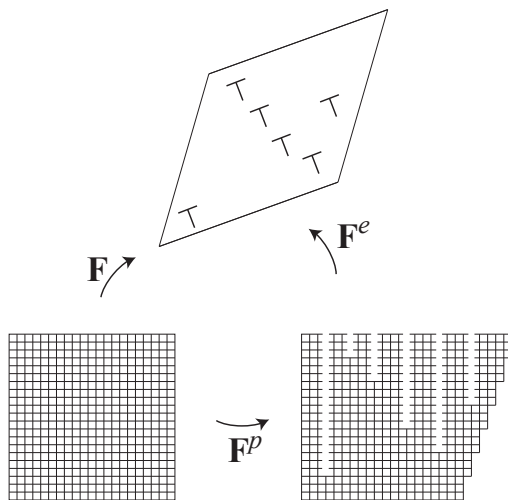
Figure 3.3: Multiplicative decomposition

For crystals deforming in single slip Ortiz and Repetto [67] introduced the resultant Burgers vector of excess dislocations, whose lines cross the area $\mathcal{A}$ in the reference configuration, in the following way

$$\mathbf{b}_r = \oint_{\mathcal{C}} \mathbf{F}^p \cdot d\mathbf{x}, \tag{3.35}$$

where $\mathcal{C}$ is the close contour surrounding $\mathcal{A}$. Le and Günther [7] have shown that, in the continuum limit, when the atomic distance goes to zero at the fixed sizes of the representative volume element and the fixed density of dislocations per area of unit cell, integral (3.35) gives the total closure failure induced by $\mathbf{F}^p$ which must be equal to the

resultant Burgers vector. It is natural to assume $\mathbf{F}^p$ continuously differentiable in this continuum limit, so, applying Stoke's theorem we get from (3.35)

$$\mathbf{b}_r = -\int_{\mathcal{A}} (\mathbf{F}^p \times \nabla) \cdot \mathbf{n} da,$$

where $\times$ denotes the vector product, ∇ is the nabla operator with respect to the coordinates $\mathbf{x}$ of the reference configuration, da the surface element, and $\mathbf{n}$ the unit vector normal to $\mathcal{A}$. This legitimates the introduction of the dislocation density tensor

$$\mathbf{T} = -\mathbf{F}^p \times \nabla. \tag{3.36}$$

For an infinitesimal area da with the unit normal vector $\mathbf{n}$, the resultant Burgers vector of all excess dislocations, whose dislocation lines cross this area is given by

$$\mathbf{b}_r = \mathbf{T} \cdot \mathbf{n} \, da.$$

This is quite similar to the Cauchy formula relating the traction with the stress tensor.

There is still one important question related to (3.36): can the dislocation density tensor defined in this way be experimentally measured in principle? Since this dislocation density tensor is referred to the reference configuration, the use of equation (3.36) is difficult in practice because the original reference configuration of the real sample is typically unknown or ambiguous. All that can be measured from the plastically deformed material, for example through high resolution electron backscatter diffraction EBSD (see [59] and the references therein), is the deformed lattice in the current configuration. To refer to the current configuration let us use the multiplicative resolution (3.34) of the compatible total deformation together with the relation $d\mathbf{y} = \mathbf{F} \cdot d\mathbf{x}$ to present integral (3.35) in the form

$$\mathbf{b}_r = \oint_c \mathbf{F}^{e-1} \cdot d\mathbf{y}, \tag{3.37}$$

where c is the corresponding close contour in the current configuration. This formula enables one to introduce the spatial dislocation density tensor

$$\mathbf{t} = -\mathbf{F}^{e-1} \times \nabla_{\mathbf{y}}, \tag{3.38}$$

where $\nabla_{\mathbf{y}}$ is the nabla operator with respect to the coordinates $\mathbf{y}$ of the current configuration. Definitions (3.37) and (3.38) seem more preferable since they do not depend on the reference configuration. Besides, formulas (3.37) and (3.38) remain also invariant with

respect to any superimposed homogeneous plastic deformation which does not change the dislocation content within the specimen. However, for crystals deforming in single slip and with the known reference configuration the use of the referential dislocation density tensor (3.36) in the constitutive equations is preferred.

According to Kröner [55], the elastic deformation $\mathbf{F}^e$ and the dislocation density tensor $\mathbf{T}$ characterize the current state of the crystal, so these two tensors are the state variables of the continuum dislocation theory. The reason why the plastic deformation $\mathbf{F}^p$ cannot be qualified for the state variable is that it depends on the cut surfaces and consequently on the whole history of creating dislocations (for instance, climb or glide dislocations are created quite differently). Likewise, the gradient of plastic strain tensor $\mathbf{C}^p$ cannot be used as the state variable by the same reason. In contrary, the dislocation density tensor depends only on the characteristics of dislocations in the current state (Burgers vector and positions of dislocation lines) and not on how they are created, so $\mathbf{T}$ is the proper state variable. Thus, if we consider isothermal processes of deformation, then the free energy per unit volume of crystal (assumed as macroscopically homogeneous) must be a function of $\mathbf{F}^e$ and $\mathbf{T}$

$$\psi = \psi(\mathbf{F}^e, \mathbf{T}).$$

Now, if we superimpose a rigid-body rotation $\mathbf{R}$ onto the actual deformation of the body, then the total and elastic deformation change according to

$$\mathbf{F}^* = \mathbf{R} \cdot \mathbf{F}, \quad \mathbf{F}^{e*} = \mathbf{R} \cdot \mathbf{F}^e.$$

At the same time, the plastic deformation $\mathbf{F}^p$, regarded as the linear map acting completely in the reference configuration, remains unchanged. As such superimposed rigid-body rotation does not change the elastic strain and the dislocation density, we expect that the energy remains unchanged. The standard argument (see, e.g., [46]) leads then to

$$\psi = \psi(\mathbf{C}^e, \mathbf{T}),$$

where $\mathbf{C}^e$ is the elastic strain defined by

$$\mathbf{C}^e = \mathbf{F}^{eT} \cdot \mathbf{F}^e.$$

For the single crystal having only one active slip system the plastic deformation has

the form

$$\mathbf{F}^p(\mathbf{x}) = \mathbf{I} + \beta(\mathbf{x})\mathbf{s} \otimes \mathbf{m},$$

where $\beta(\mathbf{x})$ is called the plastic slip. Then it is easy to see that

$$\mathbf{T} = -\mathbf{F}^p \times \nabla = \mathbf{s} \otimes (\nabla\beta \times \mathbf{m}).$$

If, in addition, all dislocation lines are straight lines parallel to the direction $\mathbf{l}$, then, taking the infinitesimal area da with the unit normal $\mathbf{l}$, we obtain the resultant Burgers vector of all excess dislocations whose dislocation lines cross da under right angle in the form

$$\mathbf{b}_r = \mathbf{s}[(\nabla\beta \times \mathbf{m}) \cdot \mathbf{l}]\, da.$$

Thus, this vector is parallel to the slip direction $\mathbf{s}$. The scalar dislocation density (or the number of excess dislocations per unit area) can then be determined as

$$\rho = \frac{1}{b}|(\nabla\beta \times \mathbf{m}) \cdot \mathbf{l}|. \tag{3.39}$$

In this case we will assume the free energy density in the following form

$$\psi = \psi(\mathbf{C}^e, \rho). \tag{3.40}$$

Let the undeformed single crystal occupy some region $\mathcal{V}$ of the three-dimensional euclidean space. The boundary of this region, $\partial\mathcal{V}$, is assumed to be the closure of union of two non-intersecting surfaces, ∂_k and ∂_τ. Let the displacement vector be a given smooth function of coordinates, and, consequently, the plastic slip β vanishes

$$\mathbf{y}(\mathbf{x}) = \mathbf{x} + \mathbf{u}(\mathbf{x}), \quad \beta(\mathbf{x}) = 0 \quad \text{at } \partial_k, \tag{3.41}$$

where $\mathbf{u}(\mathbf{x}) = \mathbf{y}(\mathbf{x}) - \mathbf{x}$ is the given displacement vector. At the remaining part ∂_τ the "dead" load $\boldsymbol{\tau}$ is specified. If no body force acts on this crystal, then its energy functional is defined as

$$I[\mathbf{y}(\mathbf{x}), \beta(\mathbf{x})] = \int_{\mathcal{V}} w(\mathbf{F}, \beta, \nabla\beta)\, dx - \int_{\partial_\tau} \boldsymbol{\tau} \cdot \mathbf{y}\, da, \tag{3.42}$$

where

$$w(\mathbf{F}, \beta, \nabla\beta) = \psi(\mathbf{C}^e, \rho), \tag{3.43}$$

and $dx = dx_1 dx_2 dx_3$ denotes the volume element. Provided the resistance to the dislocation motion is negligibly small and no surfaces of discontinuity occur inside crystals, then the following variational principle turns out to be valid for single crystals with one active slip system: the true placement vector $\check{\mathbf{y}}(\mathbf{x})$ and the true plastic slip $\check{\beta}(\mathbf{x})$ in the *final* equilibrium state of deformation minimize energy functional (3.42) among all continuously differentiable fields $\mathbf{y}(\mathbf{x})$ and $\beta(\mathbf{x})$ satisfying constraints (3.41).

If the resistance to the dislocation motion cannot be neglected, the energy minimization should be replaced by the following variational equation [70]

$$\delta I + \int_{\mathcal{V}} \frac{\partial D}{\partial \dot{\beta}} \delta \beta \, dx = 0. \tag{3.44}$$

The last term in this equation describes the energy dissipation due to the dislocation motion, where the dissipation function $D(\dot{\beta})$ is assumed to depend only on the rate of the plastic distortion. We shall consider the simplest rate-independent theory for which

$$D(\dot{\beta}) = K|\dot{\beta}|,$$

with K being the critical resolved shear stress. If the sign of $\dot{\beta}$ does not change during the evolution of β, the variational equation (3.44) reduces to minimizing the following "relaxed energy" functional

$$I_d[\mathbf{y}(\mathbf{x}), \beta(\mathbf{x})] = \int_{\mathcal{V}} [w(\mathbf{F}, \beta, \nabla\beta) + K\operatorname{sign}\dot{\beta}\,\beta]\,dx - \int_{\partial_\tau} \boldsymbol{\tau} \cdot \mathbf{y}\,da. \tag{3.45}$$

So, if no surfaces of discontinuity occur, the true placement and plastic slip fields in the *final* equilibrium state of deformation minimize the "relaxed" energy functional among all continuously differentiable admissible placements and plastic slips satisfying constraints (3.41). Finally, if $\dot{\beta} = 0$, then the plastic slip is frozen, while the displacements should be found by minimizing (3.42) with this frozen β. Note that this nonlinear CDT, in the limit of small displacements and small plastic slips, reduces to the linear CDT developed in [2] and in our numerous papers (see [4, 8, 9, 20, 21, 22, 23, 26, 27, 28, 29]).

3.3 Equilibrium conditions for crystals with grain boundaries

As we know from chapter 2 about grain boundaries, in order to be able to model the formation of the grain boundaries by CDT we must extend the variational principles formulated in the previous section to include the energy of the grain boundaries and to minimize the modified energy functional among functions $\mathbf{y}(\mathbf{x})$ and $\beta(\mathbf{x})$ admitting weak discontinuity in $\mathbf{y}(\mathbf{x})$ but strong discontinuity in $\beta(\mathbf{x})$ across some surface. For simplicity we analyze the case of single crystal having one active slip system and one grain boundary, where we let $\mathbf{F} = \partial \mathbf{y}/\partial \mathbf{x}$ and $\beta(\mathbf{x})$ be continuous everywhere except at some surface $\mathcal{S}$ on which these quantities suffer jumps. Denote by $\mathbf{F}^{\pm}$ and $\beta^{\pm}$ the limiting values of $\mathbf{F}$ and β on the two sides of $\mathcal{S}$ which divides the region $\mathcal{V}$ into $\mathcal{V}^+$ and $\mathcal{V}^-$ shown in Fig. 3.4. We assume that the boundary of $\mathcal{S}$ is a fixed curve lying at the boundary of the region $\mathcal{V}$.
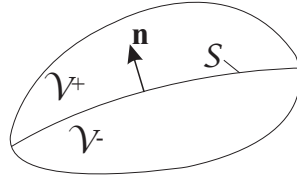
Figure 3.4: Region $\mathcal{V}$ with the discontinuity surface $\mathcal{S}$

Since the placement is continuous everywhere, Hadamard's compatibility condition must be fulfilled

$$\llbracket \mathbf{F} \rrbracket = \mathbf{q} \otimes \mathbf{n}, \tag{3.46}$$

where $\llbracket \mathbf{F} \rrbracket = \mathbf{F}^+ - \mathbf{F}^-$ denotes the jump, with $\mathbf{q}$ being the "polarization" vector measuring the amplitude of the jump, and $\mathbf{n}$ the unit normal on $\mathcal{S}$ pointing in the $+$ direction. Taking into account also the energy of the grain boundary, we redefine the energy functional as follows

$$I[\mathbf{y}(\mathbf{x}), \beta(\mathbf{x})] = \int_{\mathcal{V}\backslash\mathcal{S}} w(\mathbf{F}, \beta, \nabla\beta) \, dx + \int_{\mathcal{S}} \zeta \, da - \int_{\partial_\tau} \boldsymbol{\tau} \cdot \mathbf{y} \, da, \tag{3.47}$$

where ζ is the energy per unit area of the grain boundary. We assume ζ to be a constant (which is a good approximation except for small misorientation angles less than 15 degree). We formulate the following variational principle: among all admissible placements and plastic slips admitting weak discontinuity in $\mathbf{y}(\mathbf{x})$ but strong discontinuity in $\beta(\mathbf{x})$ across

some surface, the true placement and plastic slip in equilibrium minimizes functional (3.47) under constraints (3.41).

In order to derive the necessary conditions for the minimizer we must compare its energy with the energies of crystal evaluated at neighboring placements and plastic slips. Let us introduce a one-parameter family of neighboring placements $\mathbf{y}(\mathbf{x}, \epsilon)$ and plastic slips $\beta(\mathbf{x}, \epsilon)$ such that $\mathbf{y}(\mathbf{x}, 0) = \check{\mathbf{y}}(\mathbf{x})$ and $\beta(\mathbf{x}, 0) = \check{\beta}(\mathbf{x})$ (check denotes the energy minimizer in equilibrium). Since the surface of discontinuity is unknown and must also be subject to variation, we admit that these admissible fields have surfaces of discontinuity differing from the true surface $\check{\mathcal{S}}$ in equilibrium. We denote these surfaces by $\mathcal{S}_\epsilon$. Then the energy functional becomes

$$I[\mathbf{y}(\mathbf{x}, \epsilon), \beta(\mathbf{x}, \epsilon)] = \int_{\mathcal{V}_\epsilon^+} w(\mathbf{F}, \beta, \nabla\beta) \, dx + \int_{\mathcal{V}_\epsilon^-} w(\mathbf{F}, \beta, \nabla\beta) \, dx$$
$$+ \int_{\mathcal{S}_\epsilon} \zeta \, da - \int_{\partial_\tau} \boldsymbol{\tau} \cdot \mathbf{y} \, da. \tag{3.48}$$

The variation of the energy functional for this family of admissible placements and plastic slips can be defined as follows

$$\delta I = \left. \frac{d}{d\epsilon} I[\mathbf{y}(\mathbf{x}, \epsilon), \beta(\mathbf{x}, \epsilon)] \right|_{\epsilon=0}.$$

Since $I[\mathbf{y}(\mathbf{x}, \epsilon), \beta(\mathbf{x}, \epsilon)]$, as function of ϵ, has a minimum at $\epsilon = 0$, its first variation must vanish

$$\delta I = 0. \tag{3.49}$$

To draw consequences from (3.49) we must be able to compute the variation δI precisely. This is difficult, because the regions of integration $\mathcal{V}_\epsilon^\pm$ and surfaces of discontinuity $\mathcal{S}_\epsilon$ themselves depend on ϵ. This difficulty can be overcome by introducing a one-parameter family of smooth and one-to-one mappings $\mathbf{z}(\mathbf{x}, \epsilon)$ of $\mathcal{V}$ into itself such that (see, e.g., [6])

$$\check{\mathcal{V}}^+ \overset{\mathbf{z}}{\mapsto} \mathcal{V}_\epsilon^+, \quad \check{\mathcal{V}}^- \overset{\mathbf{z}}{\mapsto} \mathcal{V}_\epsilon^-, \quad \check{\mathcal{S}} \overset{\mathbf{z}}{\mapsto} \mathcal{S}_\epsilon,$$
$$\mathbf{z}(\mathbf{x}, \epsilon) = \mathbf{x}, \quad \text{when } \epsilon = 0 \text{ or when } \mathbf{x} \in \partial\mathcal{V}.$$

The purpose of such mappings is to transform the integrals in (3.48) to those taken over the regions $\check{\mathcal{V}}^\pm$ and surface $\check{\mathcal{S}}$ which are independent of ϵ. Since the regions of integration are independent of ϵ, the differentiation with respect to ϵ and the integration can be

interchanged. Employing now the index notation for clarity, we compute the variation of the first integral in (3.48)

$$
\delta \int_{\mathcal{V}_\epsilon^+} w(y_{i,a}, \beta, \beta_{,a})\, dx = \delta \int_{\check{\mathcal{V}}^+} w\left(\frac{\partial y_i}{\partial z_a}, \beta, \frac{\partial \beta}{\partial z_a}\right) \det z_{a,b}\, dx
$$
$$
= \int_{\check{\mathcal{V}}^+} \left[\delta w\left(\frac{\partial y_i}{\partial z_a}, \beta, \frac{\partial \beta}{\partial z_a}\right) + w\delta \det z_{a,b} \right] dx
$$
$$
= \int_{\check{\mathcal{V}}^+} \left(P_{ia}\delta\frac{\partial y_i}{\partial z_a} + \frac{\partial w}{\partial \beta}\delta\beta + \frac{\partial w}{\partial \beta_{,a}}\delta\frac{\partial \beta}{\partial z_a} + w\delta z_{a,a} \right) dx,
$$

where $\mathbf{P} = \partial w/\partial \mathbf{F}$ is the first Piola-Kirchhoff stress tensor. When deriving this formula the obvious identity $\delta \det z_{a,b} = \delta z_{a,a}$ is used. From now on δ under integral signs denotes partial derivatives with respect to ϵ at fixed $\mathbf{x}$, with the subsequent evaluation at $\epsilon = 0$. To compute the variations $\delta\partial y_i/\partial z_a$ and $\delta\partial\beta/\partial z_a$ we recall the identities

$$
\frac{\partial y_i}{\partial x_b} = \frac{\partial y_i}{\partial z_a}\frac{\partial z_a}{\partial x_b}, \quad \frac{\partial \beta}{\partial x_b} = \frac{\partial \beta}{\partial z_a}\frac{\partial z_a}{\partial x_b},
$$

which follow from the chain rule. Using the product rule we have

$$
\delta\frac{\partial y_i}{\partial z_a} = \delta y_{i,a} - y_{i,b}\delta z_{b,a}, \quad \delta\frac{\partial \beta}{\partial z_a} = \delta\beta_{,a} - \beta_{,b}\delta z_{b,a}.
$$

Substitution of these formulas into the variation of the first integral yields

$$
\delta \int_{\mathcal{V}_\epsilon^+} w(y_{i,a}, \beta, \beta_{,a})\, dx = \int_{\check{\mathcal{V}}^+} \left(P_{ia}\delta y_{i,a} + \frac{\partial w}{\partial \beta}\delta\beta + \frac{\partial w}{\partial \beta_{,a}}\delta\beta_{,a} + \mu_{ab}\delta z_{a,b} \right) dx.
$$

Here

$$
\mu_{ab} = -y_{i,a}P_{ib} - \beta_{,a}\frac{\partial w}{\partial \beta_{,b}} + w\delta_{ab}
$$

is the generalized Eshelby tensor, with δ_{ab} being the Kronecker delta. Similar formula holds true for the variation of the second integral in (3.48). For the variation of the two last surface integrals it is easy to show that

$$
\delta \int_{\mathcal{S}_\epsilon} \zeta\, da = -\int_{\check{\mathcal{S}}} 2\zeta\eta n_a\delta z_a\, da, \quad \delta \int_{\partial_\tau} \tau_i y_i\, da = \int_{\partial_\tau} \tau_i\delta y_i\, da,
$$

where η is the mean curvature of the surface $\check{\mathcal{S}}$. Integrating by parts the variation of the first two integrals with the help of Gauss' theorem and the use of constraints (3.41) and

combining the above formulas, we obtain finally

$$\delta I = \int_{\mathcal{V}\backslash\check{\mathcal{S}}} \{-P_{ia,a}\delta y_i + [w_\beta - (w_{\beta,a})_{,a}]\delta\beta - \mu_{ab,b}\delta z_a\}\, dx$$

$$- \int_{\check{\mathcal{S}}} \{[\![P_{ia}]\!]n_a\delta y_i + w_{\beta,a}^+ n_a\delta\beta^+ - w_{\beta,a}^- n_a\delta\beta^- + ([\![\mu_{ab}]\!]n_b + 2\zeta\eta n_a)\delta z_a\}\, da$$

$$+ \int_{\partial_\tau} [(P_{ia}n_a - \tau_i)\delta y_i + w_{\beta,a}n_a\delta\beta]\, da = 0. \quad (3.50)$$

Equation (3.50) implies that the minimizer must satisfy in $\mathcal{V}\backslash\check{\mathcal{S}}$ the equilibrium equations

$$\mathbf{P}\cdot\nabla = 0, \quad w_\beta - \nabla\cdot w_{\nabla\beta} = 0, \quad \boldsymbol{\mu}\cdot\nabla = 0, \qquad (3.51)$$

subjected to the kinematic boundary conditions (3.41) at ∂_k and the following natural boundary conditions at ∂_τ

$$\mathbf{P}\cdot\mathbf{n} = \boldsymbol{\tau}, \quad w_{\nabla\beta}\cdot\mathbf{n} = 0. \qquad (3.52)$$

We call $\mathbf{P}$ the first Piola-Kirchhoff stress tensor, $\tau_r = -w_\beta$ the resolved shear stress, and $\varsigma = \nabla\cdot w_{\nabla\beta}$ the back stress. The first equation of (3.51) is nothing else but the equilibrium of macro-forces acting on the crystal, while the second equation of (3.51) represents the equilibrium of micro-forces acting on dislocations. It turns out that the last equation of (3.51) does not contain new information and is automatically satisfied owing to the first two. Besides, since $\delta\mathbf{y}$, $\delta\beta^\pm$ and $\delta\mathbf{z}$ can be chosen arbitrarily on $\check{\mathcal{S}}$, the following jump conditions

$$[\![\mathbf{P}]\!]\cdot\mathbf{n} = 0, \quad w_{\nabla\beta}\cdot\mathbf{n} = 0, \quad [\![\boldsymbol{\mu}]\!]\cdot\mathbf{n} + 2\zeta\eta\mathbf{n} = 0 \qquad (3.53)$$

have also to be satisfied there. The second condition of (3.53) must be fulfilled on both sides of $\check{\mathcal{S}}$ which is the surface of strong discontinuity in $\beta(\mathbf{x})$. Among three boundary conditions (3.53)$_3$ only one is independent. Indeed, since $[\![\mathbf{F}]\!] = \mathbf{q}\otimes\mathbf{n}$, $[\![\mathbf{P}]\!]\cdot\mathbf{n} = 0$, and $w_{\nabla\beta}\cdot\mathbf{n} = 0$ on $\check{\mathcal{S}}$, we have

$$[\![\boldsymbol{\mu}]\!]\cdot\mathbf{n} + 2\zeta\eta\mathbf{n} = -[\![\mathbf{F}^T]\!]\cdot\mathbf{P}\cdot\mathbf{n} + [\![w]\!]\mathbf{n} + 2\zeta\eta\mathbf{n} = \mathbf{n}(-\mathbf{q}\cdot\mathbf{P}\cdot\mathbf{n} + [\![w]\!] + 2\zeta\eta),$$

where $\mathbf{P}$ can be taken on any side of $\check{\mathcal{S}}$. Multiplication of this vector equation with $\mathbf{n}$

yields the independent scalar equation

$$f = -\mathbf{q} \cdot \mathbf{P} \cdot \mathbf{n} + [\![w]\!] + 2\zeta\eta = 0. \tag{3.54}$$

The last equation can be interpreted as the thermodynamic condition of equilibrium, which states that the (thermodynamic) driving force acting on the grain boundary must vanish. The violation of this condition leads immediately to the motion of grain boundary through crystal under the action of nonzero driving force f.

The constitutive equations for $\mathbf{P} = w_{\mathbf{F}}$, w_β, and $-\nabla \cdot w_{\nabla\beta}$ can easily be obtained from the free energy density yielding the first Piola-Kirchhoff stress tensor

$$\mathbf{P} = 2\mathbf{F}^e \cdot \psi_{\mathbf{C}^e} \cdot \mathbf{F}^{p-T}. \tag{3.55}$$

For the resolved shear stress (Schmid stress) we get

$$\tau_r = -w_\beta = -\mathbf{s} \cdot \mathbf{F}^{eT} \cdot \mathbf{P} \cdot \mathbf{m}. \tag{3.56}$$

Finally, the back stress is equal to

$$\varsigma = \nabla \cdot w_{\nabla\beta} = \frac{1}{b}\text{sign}\left[(\nabla\beta \times \mathbf{m}) \cdot \mathbf{l}\right] \mathbf{l} \cdot \nabla(\psi_\rho) \times \mathbf{m}. \tag{3.57}$$

Substituting the constitutive equations (3.55)-(3.57) into (3.51)-(3.53) we get the closed system of equations and boundary conditions which, together with (3.46), enable one to determine $\check{\mathbf{y}}(\mathbf{x})$ and $\check{\beta}(\mathbf{x})$ as well as the surface of discontinuity $\check{\mathcal{S}}$.

4 Problems of polygonization and bending

In this chapter the linear continuum dislocation theory is applied into two problems of polygonization and bending respectively.

4.1 Polygonization

4.1.1 Bending of a beam

Consider a beam made up of a single crystal with one slip system (Fig. 4.1) and bent along a deformation jig whose radius (R) is much larger than the length (L) of the beam (Fig. 4.2).
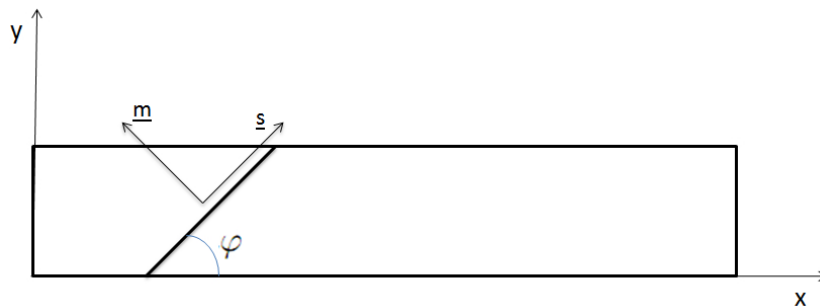
Figure 4.1: A beam with one slip system.

Under the assumption of plane-strain state, the displacements of this beam have two components, one in x-direction, and the other in y-direction:

$$u_x(x, y), \quad u_y(x, y) \tag{4.1}$$
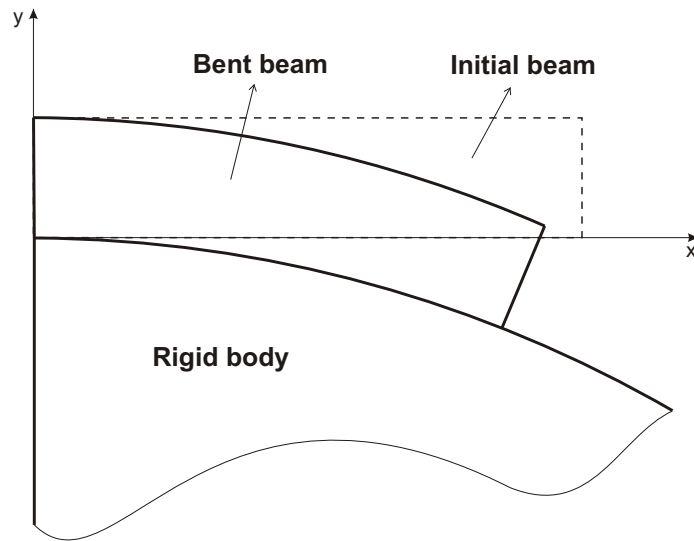
Figure 4.2: A beam is bent along a deformation jig.

Let the cross-section of the beam be a rectangle of length L and height h. Since only one slip system is active, the slip direction $\mathbf{s}$ and the normal vector to the slip plane $\mathbf{m}$, drawn in Figure 4.1, are given by:

$$\mathbf{s} = (\cos\varphi, \sin\varphi), \quad \mathbf{m} = (-\sin\varphi, \cos\varphi). \tag{4.2}$$

The components of plastic distorsion tensor $\beta_{ij} = \beta(x,y)s_i m_j$ which depend on both x and y are:

$$\implies \begin{cases} \beta_{xx} = -\beta\cos\varphi\sin\varphi, \\ \beta_{xy} = \beta\cos^2\varphi, \\ \beta_{yx} = -\beta\sin^2\varphi, \\ \beta_{yy} = \beta\cos\varphi\sin\varphi. \end{cases} \tag{4.3}$$

One can easily see that there is no volume change, because $\beta_{xx} + \beta_{yy} = 0$.

The in-plane components of the strain tensor

$$\varepsilon_{ij} = \frac{1}{2}(u_{i,j} + u_{j,i}) \tag{4.4}$$

are:

$$\begin{cases} \varepsilon_{xx} = u_{x,x}, \\ \varepsilon_{xy} = u_{y,y}, \\ \varepsilon_{yx} = \varepsilon_{yy} = \frac{1}{2}(u_{x,y} + u_{y,x}). \end{cases} \tag{4.5}$$

The components of the plastic strain tensor

$$\varepsilon^p_{ij} = \frac{1}{2}(\beta_{ij} + \beta_{ji}) \tag{4.6}$$

are:

$$\begin{cases} \varepsilon^p_{xx} = -\beta \cos\varphi \sin\varphi = -\frac{1}{2}\beta \sin(2\varphi), \\ \varepsilon^p_{yy} = \beta \cos\varphi \sin\varphi = \frac{1}{2}\beta \sin(2\varphi), \\ \varepsilon^p_{xy} = \varepsilon^p_{yx} = \frac{1}{2}\beta(\cos^2\varphi - \sin^2\varphi) = \frac{1}{2}\beta \cos(2\varphi). \end{cases} \tag{4.7}$$

With (4.5) and (4.7) we can compute the components of the elastic strain tensor according to

$$\varepsilon^e_{ij} = \varepsilon_{ij} - \varepsilon^p_{ij}. \tag{4.8}$$

Thus,

$$\begin{cases} \varepsilon^e_{xx} = u_{x,x} + \frac{1}{2}\beta \sin(2\varphi), \\ \varepsilon^e_{yy} = u_{y,y} - \frac{1}{2}\beta \sin(2\varphi), \\ \varepsilon^e_{xy} = \varepsilon^e_{yx} = \frac{1}{2}(u_{x,y} + u_{y,x}) - \frac{1}{2}\beta \cos(2\varphi). \end{cases} \tag{4.9}$$

The two non-zero components of the dislocation density tensor are:

$$
\begin{cases}
\begin{aligned}
\alpha_{xz} &= \epsilon_{zxy}\beta_{xy,x} + \epsilon_{zyx}\beta_{xx,y} \\
&= \beta_{xy,x} - \beta_{xx,y} \\
&= \beta_{,x}\cos^2\varphi - \beta_{,y}\cos\varphi\sin\varphi \\
&= (\beta_{,x}\cos\varphi - \beta_{,y}\sin\varphi)\cos\varphi, \\
\alpha_{yz} &= \epsilon_{zxy}\beta_{yy,x} + \epsilon_{zyx}\beta_{yx,y} \\
&= \beta_{yy,x} - \beta_{yx,y} \\
&= \beta_{,x}\cos\varphi\sin\varphi + \beta_{,y}\sin^2\varphi \\
&= (\beta_{,x}\cos\varphi + \beta_{,y}\sin\varphi)\sin\varphi.
\end{aligned}
\end{cases}
\tag{4.10}
$$

As seen from (3.26) the resultant Burgers vector of all dislocations whose dislocation lines cut da in our problem will be as below:

$$
\begin{cases}
\mathcal{B}_x = (\alpha_{xx}n_x + \alpha_{xy}n_y + \alpha_{xz}n_z)da = \alpha_{xz}n_z da, \\
\mathcal{B}_y = (\alpha_{yx}n_x + \alpha_{yy}n_y + \alpha_{yz}n_z)da = \alpha_{yz}n_z da, \\
\mathcal{B}_z = (\alpha_{zx}n_x + \alpha_{zy}n_y + \alpha_{zz}n_z)da = 0.
\end{cases}
\tag{4.11}
$$

With that Burgers' vector, we can now calculate the number of dislocations per unit area:

$$
\rho = \frac{|\mathcal{B}|}{bda} = \frac{1}{b}\left(\sqrt{\alpha_{xz}^2 + \alpha_{yz}^2}\right) = \frac{|\beta_{,x}\cos\varphi + \beta_{,y}\sin\varphi|}{b}.
\tag{4.12}
$$

Then, the energy density of the crystal reads

$$
\begin{aligned}
\Phi &= \frac{1}{2}\lambda(\varepsilon_{ii}^e)^2 + \mu\varepsilon_{ij}^e\varepsilon_{ij}^e + \mu k \ln\frac{1}{1-\frac{\rho}{\rho_s}} \\
&= \frac{1}{2}\lambda(\varepsilon_{xx}^e + \varepsilon_{yy}^e)^2 + \mu\left((\varepsilon_{xx}^e)^2 + (\varepsilon_{yy}^e)^2 + (\varepsilon_{xy}^e)^2 + (\varepsilon_{yx}^e)^2\right) + \mu k \ln\frac{1}{1-\frac{\rho}{\rho_s}}.
\end{aligned}
\tag{4.13}
$$

For small up to moderate dislocation densities the following asymptotic formula can be used

$$
\ln\frac{1}{1-\frac{\rho}{\rho_s}} = \frac{\rho}{\rho_s} + \frac{1}{2}\left(\frac{\rho}{\rho_s}\right)^2.
\tag{4.14}
$$

By substituting the above quantities into (4.13) we get the final formula for the energy

density

$$\Phi = \frac{1}{2}\lambda(u_{x,x} + u_{y,y})^2 + \mu(u_{x,x} + \frac{1}{2}\beta\sin 2\varphi)^2$$

$$+ \mu(u_{y,y} - \frac{1}{2}\beta\sin 2\varphi)^2 + \frac{1}{2}\mu(u_{x,y} + u_{y,x} - \beta\cos 2\varphi)^2$$

$$+ \mu k\frac{1}{b\rho_s}|\beta_{,x}\cos\varphi + \beta_{,y}\sin\varphi| + \frac{1}{2}\frac{\mu k}{b^2\rho_s^2}(\beta_{,x}\cos\varphi + \beta_{,y}\sin\varphi)^2. \tag{4.15}$$

Therefore, the energy functional which need to be minimized becomes

$$I[u_i, \beta] = a\int_0^L \int_0^h \Phi(\varepsilon_{ij}^e, \rho)\, dy dx$$

$$= a\int_0^L \int_0^h \left[\frac{1}{2}\lambda(u_{x,x} + u_{y,y})^2 + \mu(u_{x,x} + \frac{1}{2}\beta\sin 2\varphi)^2\right.$$

$$+ \mu(u_{y,y} - \frac{1}{2}\beta\sin 2\varphi)^2 + \frac{1}{2}\mu(u_{x,y} + u_{y,x} - \beta\cos 2\varphi)^2$$

$$\left. + \mu k\frac{1}{b\rho_s}|\beta_{,x}\cos\varphi + \beta_{,y}\sin\varphi| + \frac{1}{2}\frac{\mu k}{b^2\rho_s^2}(\beta_{,x}\cos\varphi + \beta_{,y}\sin\varphi)^2\right] dy dx. \tag{4.16}$$

4.1.2 Bending: Variational asymptotic method

4.1.2.1 Variational problem

For the method of bending described in Gilmann's experiment the displacements on one face of the beam are prescribed. Let an arbitrary point A on the lower face of the initial beam have the coordinate $x = R\theta$ and $y = 0$. After bending, the coordinates of this point are

$$\begin{cases} x' = R\sin\theta, \\ y' = -(R - R\cos\theta). \end{cases} \tag{4.17}$$

The displacements of points at the lower boundary are given by

$$\begin{cases} u_x(x,0) = x' - x, \\ u_y(x,0) = y' - y, \end{cases} \tag{4.18}$$
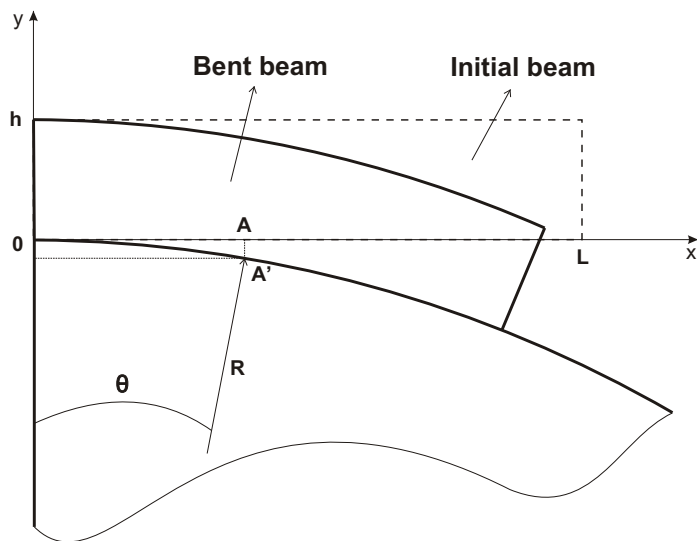
Figure 4.3: The displacements of the bent beam.

yielding

$$
\begin{cases}
u_x(x,0) = R\sin\dfrac{x}{R} - x, \\[2mm]
u_y(x,0) = R\cos\dfrac{x}{R} - R.
\end{cases}
\tag{4.19}
$$

where R is the radius of the generating circle. The upper and side boundaries of the beam are free from traction. The problem is to minimize the energy functional (4.16) under these constraints (4.19).

Functional (4.16) contains a small parameter h and can therefore be reduced in the limit $h \to 0$ to 1-D energy functional. The reduction is based on the variational asymptotic method Berdichevsky [1], Le [25]. For this purpose it is convenient to non-dimensionalize our variational problem. Let us introduce the following dimensionless variables and quantities

$$
\bar{u}_x = u_x b\rho_s,\, \bar{u}_y = u_y b\rho_s,\, \bar{x} = xb\rho_s,\, \bar{y} = yb\rho_s,\, \bar{R} = Rb\rho_s,\, \bar{L} = Lb\rho_s,\, \bar{h} = hb\rho_s.
\tag{4.20}
$$

Because the variable y changes on the interval $(0,h)$, the dimensionless coordinate $\bar{y}$ changes on the interval $(0,\bar{h})$. In terms of these variables the energy functional is expressed

as

$$I[\bar{u}_x, \bar{u}_y, \beta] = \frac{\mu a}{b^2 \rho_s^2} \int\limits_0^{\bar{L}} \int\limits_0^{\bar{h}} \left[\frac{1}{2} \frac{\lambda}{\mu} (\bar{u}_{x,\bar{x}} + \bar{u}_{y,\bar{y}})^2 + (\bar{u}_{x,\bar{x}} + \frac{1}{2} \beta \sin 2\varphi)^2 \right.$$
$$+ (\bar{u}_{y,\bar{y}} - \frac{1}{2} \beta \sin 2\varphi)^2 + \frac{1}{2} \mu (\bar{u}_{x,\bar{y}} + \bar{u}_{y,\bar{x}} - \beta \cos 2\varphi)^2$$
$$\left. + k|\beta_{,\bar{x}} \cos \varphi + \beta_{,\bar{y}} \sin \varphi| + \frac{1}{2} k (\beta_{,\bar{x}} \cos \varphi + \beta_{,\bar{y}} \sin \varphi)^2 \right] d\bar{y} d\bar{x}. \qquad (4.21)$$

With:

$$\bar{I} = \frac{b^2 \rho_s^2}{\mu a} I, \qquad (4.22)$$

the functional becomes

$$I[\bar{u}_x, \bar{u}_y, \beta] = \int\limits_0^{\bar{L}} \int\limits_0^{\bar{h}} \left[\frac{1}{2} \frac{\lambda}{\mu} (\bar{u}_{x,\bar{x}} + \bar{u}_{y,\bar{y}})^2 + (\bar{u}_{x,\bar{x}} + \frac{1}{2} \beta \sin 2\varphi)^2 \right.$$
$$+ (\bar{u}_{y,\bar{y}} - \frac{1}{2} \beta \sin 2\varphi)^2 + \frac{1}{2} \mu (\bar{u}_{x,\bar{y}} + \bar{u}_{y,\bar{x}} - \beta \cos 2\varphi)^2$$
$$\left. + k|\beta_{,\bar{x}} \cos \varphi + \beta_{,\bar{y}} \sin \varphi| + \frac{1}{2} k (\beta_{,\bar{x}} \cos \varphi + \beta_{,\bar{y}} \sin \varphi)^2 \right] d\bar{y} d\bar{x}. \qquad (4.23)$$

As we shall deal further only with the dimensionless quantities, the bars over them are dropped for short, and the energy functional reduces to

$$I = \int\limits_0^{L} \int\limits_0^{h} \left[\frac{1}{2} \gamma (u_{x,x} + u_{y,y})^2 + (u_{x,x} + \frac{1}{2} \beta \sin 2\varphi)^2 \right.$$
$$+ (u_{y,y} - \frac{1}{2} \beta \sin 2\varphi)^2 + \frac{1}{2} (u_{x,y} + u_{y,x} - \beta \cos 2\varphi)^2$$
$$\left. + k|\beta_{,x} \cos \varphi + \beta_{,y} \sin \varphi| + \frac{1}{2} k (\beta_{,x} \cos \varphi + \beta_{,y} \sin \varphi)^2 \right] dy dx, \qquad (4.24)$$

where $\gamma = \frac{\lambda}{\mu}$.

4.1.2.2 Variational asymptotic method

Because the height of the beam is small in comparison with the length $h << L$, one can use the variational-asymptotic method to analyze this variational problem. To make the

small parameter h enter the functional explicitly we introduce a new variable $\xi = \frac{y}{h}; \xi \in (0,1) \Rightarrow y = h\xi$.

With

$$
\begin{cases}
u_{x,y} & = \dfrac{1}{h} u_{x,\xi}, \\[2mm]
u_{y,y} & = \dfrac{1}{h} u_{y,\xi},
\end{cases}
\tag{4.25}
$$

the energy functional becomes

$$
\begin{aligned}
I = \int_0^L \int_0^1 & \left[\frac{1}{2}\gamma\left(u_{x,x} + \frac{1}{h}u_{y,\xi}\right)^2 + \left(u_{x,x} + \frac{1}{2}\beta\sin 2\varphi\right)^2 \right. \\
& + \left(\frac{1}{h}u_{y,\xi} - \frac{1}{2}\beta\sin 2\varphi\right)^2 + \frac{1}{2}\left(\frac{1}{h}u_{x,\xi} + u_{y,x} - \beta\cos 2\varphi\right)^2 \\
& \left. + k\left|\beta_{,x}\cos\varphi + \frac{1}{h}\beta_{,\xi}\sin\varphi\right| + \frac{1}{2}k\left(\beta_{,x}\cos\varphi + \frac{1}{h}\beta_{,\xi}\sin\varphi\right)^2 \right] h d\xi dx.
\end{aligned}
\tag{4.26}
$$

At the first step of the variational-asymptotic procedure, we keep only the asymptotically principal terms to obtain the functional

$$
\begin{aligned}
I_0 = \int_0^L \int_0^1 & \left[\frac{1}{2}\gamma\left(\frac{1}{h}u_{y,\xi}\right)^2 + \left(\frac{1}{2}\beta\sin 2\varphi\right)^2 + \left(\frac{1}{h}u_{y,\xi}\right)^2 + \frac{1}{2}\left(\frac{1}{h}u_{x,\xi}\right)^2 \right. \\
& \left. + k\left|\frac{1}{h}\beta_{,\xi}\sin\varphi\right| + \frac{1}{2}k\left(\frac{1}{h}\beta_{,\xi}\sin\varphi\right)^2 \right] h d\xi dx \geq 0.
\end{aligned}
\tag{4.27}
$$

It is obvious that this functional is positive defenite, therefore its minimum is zero and is achieved at

$$
\begin{aligned}
& \Rightarrow u_{x,\xi} = 0;\ u_{y,\xi} = 0;\ \beta_{,\xi} = 0, \\
& \Rightarrow u_x = u(x);\ u_y = v(x);\ \beta = \beta(x).
\end{aligned}
\tag{4.28}
$$

Taking the boundaries condition into account, we find

$$
\begin{cases}
u = R\sin\dfrac{x}{R} - x, \\[2mm]
v = R\cos\dfrac{x}{R} - R, \\[2mm]
\beta = 0.
\end{cases}
\tag{4.29}
$$

Thus, the displacements do not depend on ξ and the plastic distortion is identically zero

at the first step.

In the second step, we look for the the minimizer of the energy functional in the form

$$
\begin{cases}
u_x = R\sin\dfrac{x}{R} - x + u'_x, \\[2mm]
u_y = R\cos\dfrac{x}{R} - R + u'_y, \\[2mm]
\beta = \beta',
\end{cases}
\tag{4.30}
$$

where $u'_x(x,\xi)$, $u'_y(x,\xi)$, and $\beta'(x,\xi)$ are small in the asymptotic sense and besides, functions $u'_x(x,\xi)$, $u'_y(x,\xi)$, and $\beta'(x,\xi)$ must vanish at $\xi = 0$. We then substitute u_x, u_y and β into (4.23) to obtain:

$$
\begin{aligned}
I = \int_0^L \int_0^1 \Bigg[& \frac{1}{2}\gamma\Big(\cos\frac{x}{R} - 1 + u'_{x,x} + \frac{1}{h}u'_{y,\xi}\Big)^2 + \Big(\cos\frac{x}{R} - 1 + u'_{x,x} + \frac{1}{2}\beta'\sin 2\varphi\Big)^2 \\
& + \Big(\frac{1}{h}u'_{y,\xi} - \frac{1}{2}\beta'\sin 2\varphi\Big)^2 + \frac{1}{2}\Big(\frac{1}{h}u'_{x,\xi} - \sin\frac{x}{R} + u'_{y,x} - \beta'\cos 2\varphi\Big)^2 \\
& + k\Big|\beta'_{,x}\cos\varphi + \frac{1}{h}\beta'_{,\xi}\sin\varphi\Big| + \frac{1}{2}k\Big(\beta'_{,x}\cos\varphi + \frac{1}{h}\beta'_{,\xi}\sin\varphi\Big)^2 \Bigg] h\,d\xi dx.
\end{aligned}
\tag{4.31}
$$

By keeping the asymptotically leading terms which contain u'_x, u'_y, and β', we obtain:

$$
\begin{aligned}
I_1 = \int_0^L \int_0^1 \Bigg[& \frac{1}{2}\gamma\Big(\cos\frac{x}{R} - 1 + \frac{1}{h}u'_{y,\xi}\Big)^2 + \Big(\frac{1}{h}u'_{y,\xi}\Big)^2 + \frac{1}{2}\Big(\frac{1}{h}u'_{x,\xi} - \sin\frac{x}{R}\Big)^2 \\
& + k\Big|\frac{1}{h}\beta'_{,\xi}\sin\varphi\Big| + \frac{1}{2}k\Big(\frac{1}{h}\beta'_{,\xi}\sin\varphi\Big)^2 \Bigg] h\,d\xi dx.
\end{aligned}
\tag{4.32}
$$

This functional is again non-negative definite, hence, its minimizer is given by

$$
\Rightarrow u'_{x,\xi} = h\sin\frac{x}{R}; \ u'_{y,\xi} = \frac{\gamma}{\gamma+2}h(1 - \cos\frac{x}{R}); \ \beta' = 0.
\tag{4.33}
$$

By integrating over ξ using the boundary condition at $\xi = 0$ we obtain

$$
\begin{cases}
u'_x = h\xi\sin\dfrac{x}{R}, \\[2mm]
u'_y = \dfrac{\gamma}{\gamma+2}h\xi(1 - \cos\dfrac{x}{R}), \\[2mm]
\beta' = 0.
\end{cases}
\tag{4.34}
$$

At the third step of variational-asymptotic procedure, we look for the minimizer in the form:

$$\begin{cases} u_x = R\sin\dfrac{x}{R} - x + h\xi\sin\dfrac{x}{R} + u''_x, \\[2mm] u_y = R\cos\dfrac{x}{R} - R + \dfrac{\gamma}{\gamma+2}h\xi(1 - \cos\dfrac{x}{R}) + u''_y, \\[2mm] \beta = \beta''. \end{cases} \tag{4.35}$$

Substituting these into (4.23):

$$\begin{aligned} I = \int\limits_0^L \int\limits_0^1 & \left[\frac{1}{2}\gamma\left(\cos\frac{x}{R} - 1 + \frac{h}{R}\xi\cos\frac{x}{R} + u''_{x,x} + \frac{\gamma}{\gamma+2}(1 - \cos\frac{x}{R}) + \frac{1}{h}u''_{y,\xi}\right)^2 \right. \\ & + \left(\cos\frac{x}{R} - 1 + \frac{h}{R}\xi\cos\frac{x}{R} + u''_{x,x} + \frac{1}{2}\beta''\sin 2\varphi\right)^2 \\ & + \left(\frac{\gamma}{\gamma+2}(1 - \cos\frac{x}{R}) + \frac{1}{h}u''_{y,\xi} - \frac{1}{2}\beta''\sin 2\varphi\right)^2 \\ & + \frac{1}{2}\left(\sin\frac{x}{R} + \frac{1}{h}u''_{x,\xi} - \sin\frac{x}{R} + \frac{\gamma}{\gamma+2}\frac{h}{R}\xi\sin\frac{x}{R} + u''_{y,x} - \beta''\cos 2\varphi\right)^2 \\ & \left. + k\left|\beta''_{,x}\cos\varphi + \frac{1}{h}\beta''_{,\xi}\sin\varphi\right| + \frac{1}{2}k\left(\beta''_{,x}\cos\varphi + \frac{1}{h}\beta''_{,\xi}\sin\varphi\right)^2 \right] h\,d\xi\,dx. \end{aligned} \tag{4.36}$$

Now we keep the asymptotically leading terms containing u''_x, u''_y, and β''. Functional (4.21) becomes

$$\begin{aligned} I_2 = \int\limits_0^L \int\limits_0^1 & \left[\frac{1}{2}\gamma\left(\cos\frac{x}{R} - 1 + \frac{h}{R}\xi\cos\frac{x}{R} + \frac{\gamma}{\gamma+2}(1 - \cos\frac{x}{R}) + \frac{1}{h}u''_{y,\xi}\right)^2 \right. \\ & + \left(\cos\frac{x}{R} - 1 + \frac{h}{R}\xi\cos\frac{x}{R} + \frac{1}{2}\beta''\sin 2\varphi\right)^2 \\ & + \left(\frac{\gamma}{\gamma+2}(1 - \cos\frac{x}{R}) + \frac{1}{h}u''_{y,\xi} - \frac{1}{2}\beta''\sin 2\varphi\right)^2 \\ & + \frac{1}{2}\left(\frac{1}{h}u''_{x,\xi} + \frac{\gamma}{\gamma+2}\frac{h}{R}\xi\sin\frac{x}{R} - \beta''\cos 2\varphi\right)^2 \\ & \left. + k\left|\frac{1}{h}\beta''_{,\xi}\sin\varphi\right| + \frac{1}{2}k\left(\frac{1}{h}\beta''_{,\xi}\sin\varphi\right)^2 \right] h\,d\xi\,dx, \end{aligned} \tag{4.37}$$

or

$$I_2 = \int\limits_0^L \int\limits_0^1 \left[\frac{1}{2}\gamma\Big((1 - \frac{\gamma}{\gamma+2})(\cos\frac{x}{R} - 1) + \frac{h}{R}\xi\cos\frac{x}{R} + \frac{1}{h}u''_{y,\xi}\Big)^2 \right.$$
$$+ \Big(\cos\frac{x}{R} - 1 + \frac{h}{R}\xi\cos\frac{x}{R} + \frac{1}{2}\beta''\sin 2\varphi\Big)^2$$
$$+ \Big(\frac{\gamma}{\gamma+2}(1 - \cos\frac{x}{R}) + \frac{1}{h}u''_{y,\xi} - \frac{1}{2}\beta''\sin 2\varphi\Big)^2$$
$$+ \frac{1}{2}\Big(\frac{1}{h}u''_{x,\xi} + \frac{\gamma}{\gamma+2}\frac{h}{R}\xi\sin\frac{x}{R} - \beta''\cos 2\varphi\Big)^2$$
$$\left. + k\Big|\frac{1}{h}\beta''_{,\xi}\sin\varphi\Big| + \frac{1}{2}k\Big(\frac{1}{h}\beta''_{,\xi}\sin\varphi\Big)^2 \right] h\,d\xi\,dx. \tag{4.38}$$

In order to find the minimum of this functional, we now fix β'' and take the variation of the functional with respect to u''_x and u''_y:

$$\delta I_2 = \int\limits_0^L \int\limits_0^1 \left[\gamma\Big((1 - \frac{\gamma}{\gamma+2})(\cos\frac{x}{R} - 1) + \frac{h}{R}\xi\cos\frac{x}{R} + \frac{1}{h}u''_{y,\xi}\Big)\frac{1}{h}\delta u''_{y,\xi} \right.$$
$$+ 2\Big(\frac{\gamma}{\gamma+2}(1 - \cos\frac{x}{R}) + \frac{1}{h}u''_{y,\xi} - \frac{1}{2}\beta''\sin 2\varphi\Big)\frac{1}{h}\delta u''_{y,\xi}$$
$$\left. + \Big(\frac{1}{h}u''_{x,\xi} + \frac{\gamma}{\gamma+2}\frac{h}{R}\xi\sin\frac{x}{R} - \beta''\cos 2\varphi\Big)\frac{1}{h}\delta u''_{x,\xi} \right] h\,d\xi\,dx = 0. \tag{4.39}$$

After intergration by parts, taking into account that $\delta u''_x$ and $\delta u''_y$ are arbitrary for ξ in $(0,1)$ we obtain the differential equation

$$\begin{cases} \left[\gamma\Big((1 - \frac{\gamma}{\gamma+2})(\cos\frac{x}{R} - 1) + \frac{h}{R}\xi\cos\frac{x}{R} + \frac{1}{h}u''_{y,\xi}\Big)\right. \\ \qquad \left. + 2\Big(\frac{\gamma}{\gamma+2}(1 - \cos\frac{x}{R}) + \frac{1}{h}u''_{y,\xi} - \frac{1}{2}\beta''\sin 2\varphi\Big)\right]_{,\xi} = 0, \\ \Big(\frac{1}{h}u''_{x,\xi} + \frac{\gamma}{\gamma+2}\frac{h}{R}\xi\sin\frac{x}{R} - \beta''\cos 2\varphi\Big)_{,\xi} = 0. \end{cases} \tag{4.40}$$

Since $\delta u''_x$ and $\delta u''_y$ are arbitrary at the upper face of the beam we also get the boundary

condition at $\xi = 1$

$$\begin{cases} \gamma\Big((1 - \dfrac{\gamma}{\gamma+2})(\cos \dfrac{x}{R} - 1) + \dfrac{h}{R}\xi \cos \dfrac{x}{R} + \dfrac{1}{h}u''_{y,\xi}\Big) \\ \qquad + 2\Big(\dfrac{\gamma}{\gamma+2}(1 - \cos \dfrac{x}{R}) + \dfrac{1}{h}u''_{y,\xi} - \dfrac{1}{2}\beta'' \sin 2\varphi\Big) = 0, \\ \dfrac{1}{h}u''_{x,\xi} + \dfrac{\gamma}{\gamma+2}\dfrac{h}{R}\xi \sin \dfrac{x}{R} - \beta'' \cos 2\varphi = 0. \end{cases} \qquad (4.41)$$

It follows from these system of equations and boundary conditions that

$$\begin{cases} \gamma\Big((1 - \dfrac{\gamma}{\gamma+2})(\cos \dfrac{x}{R} - 1) + \dfrac{h}{R}\xi \cos \dfrac{x}{R} + \dfrac{1}{h}u''_{y,\xi}\Big) \\ \qquad + 2\Big(\dfrac{\gamma}{\gamma+2}(1 - \cos \dfrac{x}{R}) + \dfrac{1}{h}u''_{y,\xi} - \dfrac{1}{2}\beta'' \sin 2\varphi\Big) = 0, \\ \dfrac{1}{h}u''_{x,\xi} + \dfrac{\gamma}{\gamma+2}\dfrac{h}{R}\xi \sin \dfrac{x}{R} - \beta'' \cos 2\varphi = 0. \end{cases} \qquad (4.42)$$

Solving the above two equation we get for $u''_{x,\xi}$ and $u''_{y,\xi}$

$$\begin{cases} \dfrac{1}{h}u''_{y,\xi} = \dfrac{1}{\gamma+2}\beta'' \sin 2\varphi - \dfrac{\gamma}{\gamma+2}\dfrac{h}{R}\xi \cos \dfrac{x}{R}, \\ \dfrac{1}{h}u''_{x,\xi} = -\dfrac{\gamma}{\gamma+2}\dfrac{h}{R}\xi \sin \dfrac{x}{R} + \beta'' \cos 2\varphi. \end{cases} \qquad (4.43)$$

These equations can be used to find u''_x and u''_y once β'' is known. Substituting into (4.38) we have now the functional depend only on β'' as below

$$\begin{aligned} I_2 = \int_0^L \int_0^1 \Bigg[&\frac{1}{2}\gamma\Big((1 - \frac{\gamma}{\gamma+2})(\cos \frac{x}{R} - 1) + \frac{h}{R}\xi \cos \frac{x}{R} + \frac{1}{\gamma+2}\beta'' \sin 2\varphi \\ &- \frac{\gamma}{\gamma+2}\frac{h}{R}\xi \cos \frac{x}{R}\Big)^2 + \Big(\cos \frac{x}{R} - 1 + \frac{h}{R}\xi \cos \frac{x}{R} + \frac{1}{2}\beta'' \sin 2\varphi\Big)^2 \\ &+ \Big(\frac{\gamma}{\gamma+2}(1 - \cos \frac{x}{R}) + \frac{1}{\gamma+2}\beta'' \sin 2\varphi - \frac{\gamma}{\gamma+2}\frac{h}{R}\xi \cos \frac{x}{R} - \frac{1}{2}\beta'' \sin 2\varphi\Big)^2 \\ &+ \frac{1}{2}\Big(-\frac{\gamma}{\gamma+2}\frac{h}{R}\xi \sin \frac{x}{R} + \beta'' \cos 2\varphi + \frac{\gamma}{\gamma+2}\frac{h}{R}\xi \sin \frac{x}{R} - \beta'' \cos 2\varphi\Big)^2 \\ &+ k\Big|\frac{1}{h}\beta''_{,\xi} \sin \varphi\Big| + \frac{1}{2}k\Big(\frac{1}{h}\beta''_{,\xi} \sin \varphi\Big)^2 \Bigg] h d\xi dx. \end{aligned} \qquad (4.44)$$

Rearranging terms, we can simplify this functional

$$
\begin{aligned}
I_2 = \int\limits_0^L \int\limits_0^1 \Bigg[& \frac{1}{2}\gamma\left(\left(1 - \frac{\gamma}{\gamma+2}\right)\left((1 + \frac{h}{R}\xi)\cos\frac{x}{R} - 1\right) + \frac{1}{\gamma+2}\beta'' \sin 2\varphi \right)^2 \\
& + \left((1 + \frac{h}{R}\xi)\cos\frac{x}{R} - 1 + \frac{1}{2}\beta'' \sin 2\varphi \right)^2 \\
& + \left(\frac{\gamma}{\gamma+2}\left((1 + \frac{h}{R}\xi)\cos\frac{x}{R} - 1\right) + \left(\frac{1}{2} - \frac{1}{\gamma+2}\right)\beta'' \sin 2\varphi \right)^2 \\
& + k\left|\frac{1}{h}\beta''_{,\xi} \sin\varphi\right| + \frac{1}{2}k\left(\frac{1}{h}\beta''_{,\xi} \sin\varphi\right)^2 \Bigg] h\,d\xi dx.
\end{aligned}
\tag{4.45}
$$

We then change the variable ξ which is use as a temporary variable in variational asymptotic method back to the original variable y to get the functional as below:

$$
\begin{aligned}
I_2[\beta] = \int\limits_0^L \int\limits_0^h \Bigg[& \frac{1}{2}\gamma\left(\left(1 - \frac{\gamma}{\gamma+2}\right)\left((1 + \frac{y}{R})\cos\frac{x}{R} - 1\right) + \frac{1}{\gamma+2}\beta \sin 2\varphi \right)^2 \\
& + \left((1 + \frac{y}{R})\cos\frac{x}{R} - 1 + \frac{1}{2}\beta \sin 2\varphi \right)^2 \\
& + \left(\frac{\gamma}{\gamma+2}\left((1 + \frac{y}{R})\cos\frac{x}{R} - 1\right) + \left(\frac{1}{2} - \frac{1}{\gamma+2}\right)\beta \sin 2\varphi \right)^2 \\
& + k\left|\beta_{,y} \sin\varphi\right| + \frac{1}{2}k\left(\beta_{,y} \sin\varphi\right)^2 \Bigg] dy\,dx.
\end{aligned}
\tag{4.46}
$$

Since the upper boundary of the beam is traction-free and attract dislocations, the equilibrium is possible only if there is some dislocation free zone near this boundary. Therefore, at point x we assume that the dislocation free zone is $(l(x), h)$.

Now we seek the plastic distortion minimizing the energy functional in the form:

$$
\beta(x, y) = \begin{cases} \beta_1(x, y), & \text{for } y \in (0, l(x)), \\ \beta_0(x), & \text{for } y \in (l(x), h) \end{cases}
\tag{4.47}
$$

where $\beta_0(x)$ is a constant in y direction, $l(x)$ is an unknown length $(0 < l < h)$, and $\beta_1(x, l) = \beta_0(x)$. We have to find $\beta_1(x, y)$, $\beta_0(x)$ and $l(x)$.

With β from (4.47), the total energy functional becomes:

$$I_2[\beta] = \int_0^l \left[\frac{1}{2}\gamma \left((1 - \frac{\gamma}{\gamma+2})\left((1+\frac{y}{R})\cos\frac{x}{R} - 1\right) + \frac{1}{\gamma+2}\beta_1 \sin 2\varphi \right)^2 \right.$$

$$+ \left((1+\frac{y}{R})\cos\frac{x}{R} - 1 + \frac{1}{2}\beta_1 \sin 2\varphi \right)^2$$

$$+ \left(\frac{\gamma}{\gamma+2}\left((1+\frac{y}{R})\cos\frac{x}{R} - 1\right) + \left(\frac{1}{2} - \frac{1}{\gamma+2}\right)\beta_1 \sin 2\varphi \right)^2$$

$$\left. + k\left|\beta_{1,y} \sin\varphi\right| + \frac{1}{2}k\left(\beta_{1,y} \sin\varphi\right)^2 \right] dy$$

$$+ \int_l^h \left[\frac{1}{2}\gamma \left((1 - \frac{\gamma}{\gamma+2})\left((1+\frac{y}{R})\cos\frac{x}{R} - 1\right) + \frac{1}{\gamma+2}\beta_0 \sin 2\varphi \right)^2 \right.$$

$$+ \left((1+\frac{y}{R})\cos\frac{x}{R} - 1 + \frac{1}{2}\beta_0 \sin 2\varphi \right)^2$$

$$\left. + \left(\frac{\gamma}{\gamma+2}\left((1+\frac{y}{R})\cos\frac{x}{R} - 1\right) + \left(\frac{1}{2} - \frac{1}{\gamma+2}\right)\beta_0 \sin 2\varphi \right)^2 \right] dy. \tag{4.48}$$

With $(.) = \left((1+\frac{y}{R})\cos\frac{x}{R} - 1\right)$, we simplify this functional:

$$I_2[\beta] = \int_0^l \left[\frac{1}{2}\gamma \left((1 - \frac{\gamma}{\gamma+2})(.) + \frac{1}{\gamma+2}\beta_1 \sin 2\varphi \right)^2 + \left((.) + \frac{1}{2}\beta_1 \sin 2\varphi \right)^2 \right.$$

$$\left. + \left(\frac{\gamma}{\gamma+2}(.) + \left(\frac{1}{2} - \frac{1}{\gamma+2}\right)\beta_1 \sin 2\varphi \right)^2 + k\left|\beta_{1,y} \sin\varphi\right| + \frac{1}{2}k\left(\beta_{1,y} \sin\varphi\right)^2 \right] dy$$

$$+ \int_l^h \left[\frac{1}{2}\gamma \left((1 - \frac{\gamma}{\gamma+2})(.) + \frac{1}{\gamma+2}\beta_0 \sin 2\varphi \right)^2 + \left((.) + \frac{1}{2}\beta_0 \sin 2\varphi \right)^2 \right.$$

$$\left. + \left(\frac{\gamma}{\gamma+2}(.) + \left(\frac{1}{2} - \frac{1}{\gamma+2}\right)\beta_0 \sin 2\varphi \right)^2 \right] dy. \tag{4.49}$$

Let the second integral be A

$$A = \int_l^h \left[\frac{1}{2}\gamma\Big((1 - \frac{\gamma}{\gamma+2})(.) + \frac{1}{\gamma+2}\beta_0\sin 2\varphi\Big)^2 + \Big((.) + \frac{1}{2}\beta_0\sin 2\varphi\Big)^2 \right.$$
$$\left. + \Big(\frac{\gamma}{\gamma+2}(.) + (\frac{1}{2} - \frac{1}{\gamma+2})\beta_0\sin 2\varphi\Big)^2 \right] dy. \tag{4.50}$$

Simple calculations show that

$$\Rightarrow A = \int_l^h \left[\frac{1}{2}\gamma\Big((1 - \frac{\gamma}{\gamma+2})^2(.)^2 + \frac{2}{\gamma+2}(1 - \frac{\gamma}{\gamma+2})(.)\beta_0\sin 2\varphi + (\frac{1}{\gamma+2})^2\beta_0^2\sin^2 2\varphi\Big) \right.$$
$$+ \Big((.)^2 + (.)\beta_0\sin 2\varphi + \frac{1}{4}\beta_0^2\sin^2 2\varphi\Big)^2$$
$$\left. + \Big((\frac{\gamma}{\gamma+2})^2(.)^2 + (\frac{2\gamma}{\gamma+2})(\frac{1}{2} - \frac{1}{\gamma+2})(.)\beta_0\sin 2\varphi + (\frac{1}{2} - \frac{1}{\gamma+2})^2\beta_0^2\sin^2 2\varphi\Big)^2 \right] dy \tag{4.51}$$

$$\Rightarrow A = \int_l^h \left[\Big[\frac{1}{2}\gamma\Big(1 - \frac{\gamma}{\gamma+2}\Big)^2 + 1 + \Big(\frac{\gamma}{\gamma+2}\Big)^2\Big](.)^2 \right.$$
$$+ \Big[\Big(\frac{\gamma}{\gamma+2}\Big)\Big(1 - \frac{\gamma}{\gamma+2}\Big) + 1 + (\frac{2\gamma}{\gamma+2})\Big(\frac{1}{2} - \frac{1}{\gamma+2}\Big)\Big](.)\beta_0\sin 2\varphi$$
$$\left. + \frac{1}{2}\Big[\Big(\frac{\gamma}{(\gamma+2)^2}\Big) + \frac{1}{2} + 2\Big(\frac{1}{2} - \frac{1}{\gamma+2}\Big)^2\Big]\beta_0^2\sin^2 2\varphi \right] dy. \tag{4.52}$$

Taking into account the identities

$$\begin{cases} \frac{1}{2}\gamma\Big(1 - \frac{\gamma}{\gamma+2}\Big)^2 + 1 + \Big(\frac{\gamma}{\gamma+2}\Big)^2 = 2\Big(\frac{1+\gamma}{2+\gamma}\Big) \\ \Big(\frac{\gamma}{\gamma+2}\Big)\Big(1 - \frac{\gamma}{\gamma+2}\Big) + 1 + (\frac{2\gamma}{\gamma+2})\Big(\frac{1}{2} - \frac{1}{\gamma+2}\Big) = 2\Big(\frac{1+\gamma}{2+\gamma}\Big) \\ \Big(\frac{\gamma}{(\gamma+2)^2}\Big) + \frac{1}{2} + 2\Big(\frac{1}{2} - \frac{1}{\gamma+2}\Big)^2 = \Big(\frac{1+\gamma}{2+\gamma}\Big) \end{cases} \tag{4.53}$$

we obtain

$$A = \int_l^h \left[2\Big(\frac{1+\gamma}{2+\gamma}\Big)(.)^2 + 2\Big(\frac{1+\gamma}{2+\gamma}\Big)(.)\beta_0\sin 2\varphi + \frac{1}{2}\Big(\frac{1+\gamma}{2+\gamma}\Big)\beta_0^2\sin^2 2\varphi \right] dy. \tag{4.54}$$

Thus,

$$A = 2\Big(\frac{1+\gamma}{2+\gamma}\Big) \int\limits_l^h (.)^2 \, dy + 2\Big(\frac{1+\gamma}{2+\gamma}\Big)\beta_0(\sin 2\varphi) \int\limits_l^h (.)\, dy + \frac{1}{2}\Big(\frac{1+\gamma}{2+\gamma}\Big)\beta_0^2(\sin^2 2\varphi) \int\limits_l^h dy.$$

(4.55)

Substituting A into (4.49) and taking variation with respect to β_1, β_0 and l:

$$
\begin{aligned}
\delta I = \int\limits_0^l \bigg[& \gamma\Big(\big(1 - \frac{\gamma}{\gamma+2}\big)(.) + \frac{1}{\gamma+2}\beta_1 \sin 2\varphi\Big)\frac{1}{\gamma+2}\delta\beta_1 \sin 2\varphi \\
& + 2\Big((.) + \frac{1}{2}\beta_1 \sin 2\varphi\Big)\frac{1}{2}\delta\beta_1 \sin 2\varphi \\
& + 2\Big(\frac{\gamma}{\gamma+2}(.) + \big(\frac{1}{2} - \frac{1}{\gamma+2}\big)\beta_1 \sin 2\varphi\Big)\big(\frac{1}{2} - \frac{1}{\gamma+2}\big)\delta\beta_1 \sin 2\varphi \\
& + k\mathrm{sign}(\beta_{1,y})\delta\beta_{1,y}\Big|\sin\varphi\Big| + k\Big(\beta_{1,y}\sin\varphi\Big)\delta\beta_{1,y}\sin\varphi \bigg] dy \\
& + \bigg[\gamma\Big(\big(1 - \frac{\gamma}{\gamma+2}\big)(.) + \frac{1}{\gamma+2}\beta_1 \sin 2\varphi\Big)\frac{1}{\gamma+2}\delta\beta_1 \sin 2\varphi \\
& + 2\Big((.) + \frac{1}{2}\beta_1 \sin 2\varphi\Big)\frac{1}{2}\delta\beta_1 \sin 2\varphi \\
& + 2\Big(\frac{\gamma}{\gamma+2}(.) + \big(\frac{1}{2} - \frac{1}{\gamma+2}\big)\beta_1 \sin 2\varphi\Big)\big(\frac{1}{2} - \frac{1}{\gamma+2}\big)\delta\beta_1 \sin 2\varphi \\
& + k\mathrm{sign}(\beta_{1,y})\delta\beta_{1,y}\Big|\sin\varphi\Big| + k\Big(\beta_{1,y}\sin\varphi\Big)\delta\beta_{1,y}\sin\varphi \bigg]\bigg|_{y=l}\delta l \\
& - \bigg[\gamma\Big(\big(1 - \frac{\gamma}{\gamma+2}\big)(.) + \frac{1}{\gamma+2}\beta_1 \sin 2\varphi\Big)\frac{1}{\gamma+2}\delta\beta_1 \sin 2\varphi \\
& + 2\Big((.) + \frac{1}{2}\beta_1 \sin 2\varphi\Big)\frac{1}{2}\delta\beta_1 \sin 2\varphi \\
& + 2\Big(\frac{\gamma}{\gamma+2}(.) + \big(\frac{1}{2} - \frac{1}{\gamma+2}\big)\beta_1 \sin 2\varphi\Big)\big(\frac{1}{2} - \frac{1}{\gamma+2}\big)\delta\beta_1 \sin 2\varphi \bigg]\bigg|_{y=l}\delta l \\
& + 2\Big(\frac{1+\gamma}{2+\gamma}\Big)\delta\beta_0(\sin 2\varphi)\int\limits_l^h (.)\, dy + \Big(\frac{1+\gamma}{2+\gamma}\Big)\beta_0\delta\beta_0(\sin^2 2\varphi)(h - l) = 0.
\end{aligned}
$$

(4.56)

Integrating by parts and using the arbitrariness of $\delta\beta_1$ inside the interval $(0, l)$ we obtain

the differential equation

$$-k\beta_{1,yy}\sin^2\varphi + \left[\left(\frac{\gamma}{(\gamma+2)^2}\right) + \frac{1}{2} + 2\left(\frac{1}{2} - \frac{1}{\gamma+2}\right)^2\right]\beta_1\sin^2 2\varphi$$
$$+ \left[\left(\frac{\gamma}{\gamma+2}\right)\left(1 - \frac{\gamma}{\gamma+2}\right) + 1 + \left(\frac{2\gamma}{\gamma+2}\right)\left(\frac{1}{2} - \frac{1}{\gamma+2}\right)\right](\sin 2\varphi)\left(.\right) = 0,$$

$$(4.57)$$

where $\beta_1(x, y)$ is subjected to the boundary conditions:

$$\beta_1(x, l) = \beta_0(x), \quad \beta_1(x, 0) = 0. \tag{4.58}$$

The variation with respect to $l(x)$ gives an additional boundary condition at $y = l$

$$\beta_1'(x, l) = 0, \tag{4.59}$$

which means that the dislocation density must be continuous. Varying the energy functional with respect to $\beta_0(x)$ we obtain the transcendental equation which serves as the equation for determining $l(x)$:

$$k\,\text{sign}(\beta_{1,y})\sin\varphi + 2\left(\frac{1+\gamma}{2+\gamma}\right)(\sin 2\varphi)\int_l^h \left(.\right)dy + \left(\frac{1+\gamma}{2+\gamma}\right)\beta_0(\sin^2 2\varphi)(h - l) = 0,$$

$$(4.60)$$

where $\text{sign}(\beta_{1,y})$ is the limiting value as y approaches $l(x)$ from below.

We rewrite the governing equation

$$k\beta_{1,yy}\sin^2\varphi - \frac{1+\gamma}{2+\gamma}\beta_1\sin^2 2\varphi = 2\frac{1+\gamma}{2+\gamma}\left((1 + \frac{y}{R})\cos\frac{x}{R} - 1\right). \tag{4.61}$$

By neglecting the term $\frac{y}{R}$ which is small compared with 1,

$$\Rightarrow k\beta_{1,yy}\sin^2\varphi - \frac{1+\gamma}{2+\gamma}\beta_1\sin^2 2\varphi = 2\frac{1+\gamma}{2+\gamma}\left((1 + \underbrace{\frac{y}{R}}_{neglect})\cos\frac{x}{R} - 1\right), \tag{4.62}$$

the above equation becomes

$$k\beta_{1,yy}\sin^2\varphi - \frac{1+\gamma}{2+\gamma}\beta_1\sin^2 2\varphi = 2\frac{1+\gamma}{2+\gamma}\left(\cos\frac{x}{R} - 1\right). \tag{4.63}$$

4 Problems of polygonization and bending

By assigning some symbols,

$$\begin{cases} C_1 = k \sin^2 \varphi, \\ C_2 = \dfrac{1+\gamma}{2+\gamma} \sin^2 2\varphi, \\ C_3 = 2\dfrac{1+\gamma}{2+\gamma}\left(\cos \dfrac{x}{R} - 1\right)(\sin 2\varphi), \end{cases} \tag{4.64}$$

the differential equation can be rewritten as below:

$$C_1 \beta_{1,yy} - C_2 \beta_1 = C_3. \tag{4.65}$$

First of all, note that the characteristic equation

$$C_1 r^2 - C_2 = 0 \tag{4.66}$$

yields the solution

$$r = \pm\sqrt{\frac{C_2}{C_1}} = \pm\sqrt{\frac{2\kappa}{k}}\cos\varphi = \pm\eta. \tag{4.67}$$

Therefore, the general solution of the homogeneous equation reads

$$\beta_1^{CF} = A\cosh\eta y + B\sinh\eta y. \tag{4.68}$$

Next, we look for the particular solution of the inhomogeneous equation in the form

$$\beta_{1p} = Cy + D. \tag{4.69}$$

Substituting this solution Ansatz into the differential equation, we get the formula

$$-C_2 C y - C_2 D = C_3 \tag{4.70}$$

This implies

$$\begin{cases} C = 0, \\ D = -\dfrac{C_3}{C_2}. \end{cases} \tag{4.71}$$

Thus, substituting these into (4.67), the particular solution becomes

$$\beta_{1p} = -\frac{C_3}{C_2} = -\frac{2}{\sin 2\varphi}\left(\cos\frac{x}{R} - 1\right). \tag{4.72}$$

The solution of the differential equation (4.61) is the sum of these two

$$\beta_1 = \beta_1^{CF} + \beta_{1p} = A \cosh \eta y + B \sinh \eta y + \beta_{1p}. \tag{4.73}$$

The constant factors (A and B) from this formula should be found from the boundary conditions. With the first condition $\beta_1(0) = 0$, the coefficient A is computed as,

$$A + \beta_{1p} = 0 \Rightarrow A = -\beta_{1p}. \tag{4.74}$$

With condition $\beta_1'(l) = 0$, the remaining coefficient is obtained

$$\eta A \sinh \eta l + \eta B \cosh \eta l = 0 \Rightarrow B = -A \tanh \eta l \Rightarrow B = \beta_{1p} \tanh \eta l. \tag{4.75}$$

With these constants found, the final solution is given by

$$\begin{aligned}
\beta_1(x, y) &= \beta_{1p} - \beta_{1p}(\cosh \eta y - \tanh \eta l(x) \sinh \eta y) \\
&= \beta_{1p}\Big(1 - \cosh \eta y + \tanh \eta l(x) \sinh \eta y\Big),
\end{aligned} \tag{4.76}$$

for $0 < y < l$. The continuity for the plastic distortion implies that

$$\begin{aligned}
\beta_0 &= \beta_{1p}\Big(1 - \frac{1}{\cosh \eta l}\Big) \\
&= -\frac{2}{\sin 2\varphi}\Big(\cos \frac{x}{R} - 1\Big)\Big(1 - \cosh \eta l + \frac{\sinh^2 \eta l}{\cosh \eta l}\Big).
\end{aligned} \tag{4.77}$$

Now, the transcedental equation for determining $l(x)$ becomes:

$$k \sin \varphi + \kappa \left[\Big(\cos \frac{x}{R} - 1\Big) + \frac{1}{2}\beta_{1p}\Big(1 - \frac{1}{\cosh \eta l}\Big) \sin 2\varphi\right] \sin 2\varphi (h - l(x)) = 0, \tag{4.78}$$

where $\kappa = \frac{1}{1-\nu}$ with ν being Poisson ratio. For simpicity, we consider the case where $\text{sign}(\beta_{1,y}) = 1$.

It is easy to show that the real root $l(x) \in (0, h)$ of equation (4.75) exists only for $x > x_*$, where

$$x_* = R \arccos(1 - \frac{k}{2\kappa h \cos \varphi}).$$

For $x < x_*$ we must put $l(x) = 0$, i.e. in the interval $(0, x_*)$ there is no dislocation at all. Setting $x_* = L$, we get the critical threshold value of R for the dislocation nucleation in

the bent beam

$$R_{cr} = \frac{L}{\arccos(1 - \frac{k}{2\kappa h cos\varphi})}.$$

Thus, if the radius of the jig $R > R_{cr}$, then $l(x) = 0$ and $\beta = 0$ everywhere yielding the purely elastic deformation without dislocations. For $R < R_{cr}$ the dislocations are nucleated and pile-up against the lower boundary $y = 0$ with $x > x_*$ forming there the boundary layer.

To simulate the minimizer numerically, we choose $h = 1$, $L = 10$, $R = 5$, $\nu = 0.25$, $k = 10^{-4}$, and the angle $\varphi = \pi/5$. The plots of $l(x)$ and of $\beta_0(x)$ are shown in Figs. 4.11 and 4.12, respectively.
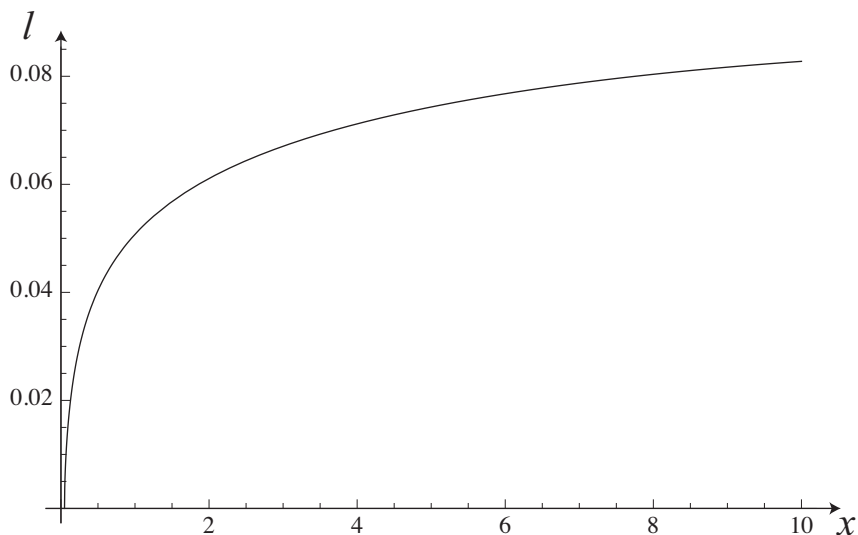
Figure 4.4: Function $l(x)$.

4.1.3 Polygonized state and comparison with Gilman's experiments

4.1.3.1 Polygonized state

As we know from the experiments, dislocations may climb in the transversal direction during annealing (see Fig. 4.6), and then glide along the direction parallel to the slip lines and be rearranged as shown in Fig. 5.1. In the final polygonized relaxed state the dislocations form low angle tilt boundaries between polygons which are perpendicular to the slip direction, while inside the polygons there are no dislocations. We want to show
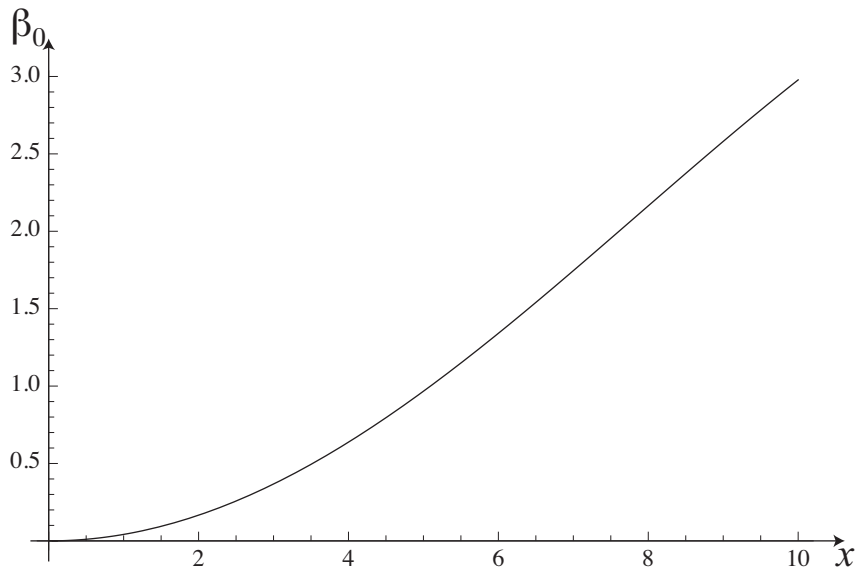
Figure 4.5: Function $\beta_0(x)$.

Climb-up line
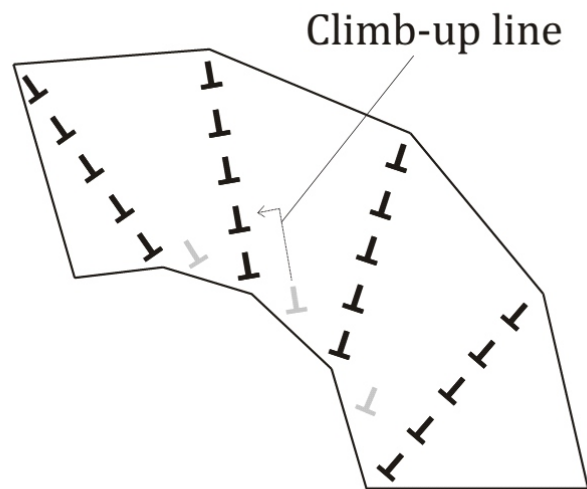
Figure 4.6: Dislocatons climbing and sliding: In the polygonized state dislocations form low angle tilt boundaries.

that this rearrangement of dislocations correspond to a sequence of piecewise constant $\check{\beta}(x, y)$ reducing energy of the beam compared with (4.41). Here and below check is used to denote the polygonized relaxed state after annealing. The jump of $\check{\beta}$ means the dislocations concentrated at the surface, therefore we ascribe to each jump point the

61

normalized Read-Shockley surface energy Read and Shockley [32]

$$\gamma(\llbracket \check{\beta} \rrbracket) = \gamma_* |\llbracket \check{\beta} \rrbracket| \ln \frac{e\beta_*}{|\llbracket \check{\beta} \rrbracket|}, \tag{4.79}$$

with $\llbracket \check{\beta} \rrbracket(x_i) = \check{\beta}(x_i + 0) - \check{\beta}(x_i - 0)$ denoting the jump of $\check{\beta}(x)$, $\gamma_* = \frac{b}{4\pi(1-\nu)}$, and β_* the saturated misorientation angle.
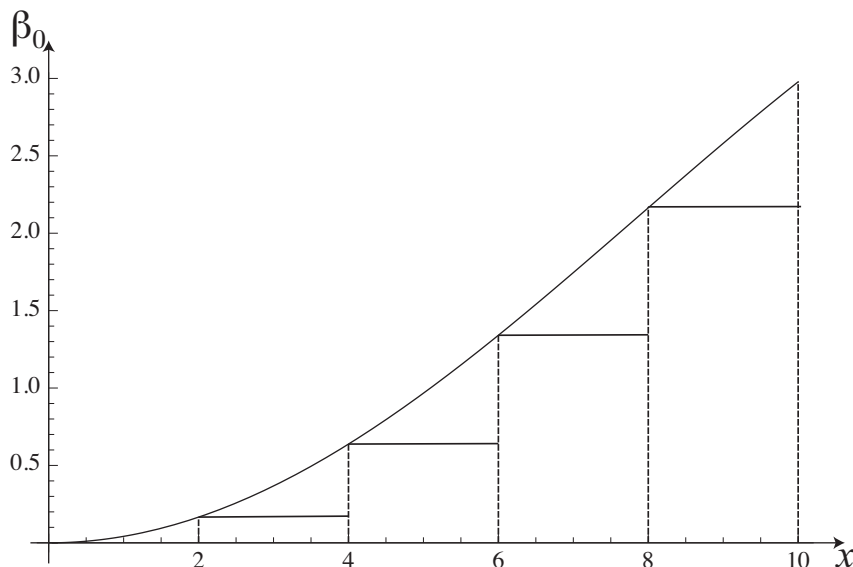
Figure 4.7: Piecewise constant function $\check{\beta}_0(x)$.

For this purpose we divide the interval (x_*, a) into N equal subintervals. We replace the smooth function $\beta_0(x)$ from formula (4.69) by a piecewise constant function $\check{\beta}_0(x)$ shown in Fig. 4.13 for $N = 5$ and define $\check{\beta}(x, y)$ as piecewise constant function which is equal to $\check{\beta}_i$ in the i-th polygon. Concerning the displacements $\check{u}_x(x, y)$ and $\check{u}_y(x, y)$ we define them according to

$$\check{u}_x(x, y) = R \sin(x/R) - x + h\xi \sin \frac{x}{R} + \check{u}_x''(x, y), \tag{4.80}$$

$$\check{u}_y(x, y) = R \cos(x/R) - R + \frac{\gamma}{\gamma + 2} h\xi \left(1 - \cos \frac{x}{R}\right) + \check{u}_y''(x, y),$$

where $\check{u}_x''(x, y)$ and $\check{u}_y''(x, y)$ should be found by integrating equations (4.35), with β'' being replaced by $\check{\beta}(x, y)$. Since $\check{\beta}(x)$ is piecewise constant, the displacements $\check{u}_x''(x, y)$ and $\check{u}_y''(x, y)$ are continuous and piecewise linear functions. However, their gradients describing the lattice rotation suffers jumps across the boundaries of the polygons. Thus, this sequence of deflections and plastic distortions exhibits polygonization of the bent beam.

Due to our choice of the plastic distortion and displacements, it is easy to show that the asymptotically main contributions to the energy of crystal in the final relaxed polygonized state are given by

$$E = \int_0^L \int_0^h \kappa (\cos \frac{x}{R} - 1 + \frac{1}{2}\check{\beta}\sin 2\varphi)^2 \, dxdy + \sum_{i=1}^N \gamma([\![\check{\beta}]\!](x_i))\frac{h}{\cos \varphi}. \tag{4.81}$$

As compared with the similar formula (4.46) we see that the gradient terms disappear due to the piecewise constant $\check{\beta}$, and instead of them, the surface energy of the low angle tilt boundaries are added. As N becomes large, the contribution of the first term in (4.81) approaches the corresponding contribution of the smooth minimizer in the state before polygonization apart from the small contributions in the elastic zone near $x = 0$ and in the boundary layer near the lower face. If the surface energy of the tilt boundaries is less than the contribution of the gradient terms from the smooth minimizer, the constructed plastic distortion $\check{\beta}(x,y)$ and displacements $\check{u}'_x(x,y)$ and $\check{u}'_y(x,y)$ do reduce energy of the relaxed state. The number of polygons can be estimated from above by requiring that the increase of the surface energy is less than the reduction in gradient terms giving

$$\sum_{i=1}^N \gamma([\![\check{\beta}]\!](x_i))\frac{h}{\cos \varphi} < \int_0^L \int_0^{l(x)} [k|\beta'_{,y}\sin \varphi| + \frac{1}{2}k(\beta'_{,y}\sin \varphi)^2] \, dxdy. \tag{4.82}$$

For the rough estimation at large N we may substitute

$$[\![\check{\beta}]\!] = \frac{\beta_{0m}}{N}, \beta_{0m} = \beta_0(L) = -\frac{2}{\sin 2\varphi}\Big(\cos \frac{L}{R} - 1\Big)\Big(1 - \frac{1}{\cosh \eta l(L)}\Big) \tag{4.83}$$

on the left hand side of (4.82). The calculation of the integral on the right hand side of (4.82) can be done by Gauss' numerical integration according to

$$\int_0^L \int_0^{l(x)} [f(x,y)] \, dxdy = \frac{L}{2}\sum_{i=1}^4 \frac{l(x)}{2}\sum_{j=1}^4 w_i w_j f\Big(\frac{L}{2}\xi_i + \frac{L}{2}, \frac{l(x)}{2}\xi_j + \frac{l(x)}{2}\Big) \tag{4.84}$$

where $f(x,y) = k|\beta'_{,y}\sin \varphi| + \frac{1}{2}k(\beta'_{,y}\sin \varphi)^2$, w_i and w_j are weighting factors, ξ_i and ξ_j are coordinate of Gauss' points.

4.1.3.2 Comparison with Gilman's experiments

For zinc the known material constants are given in the Table 5.1.
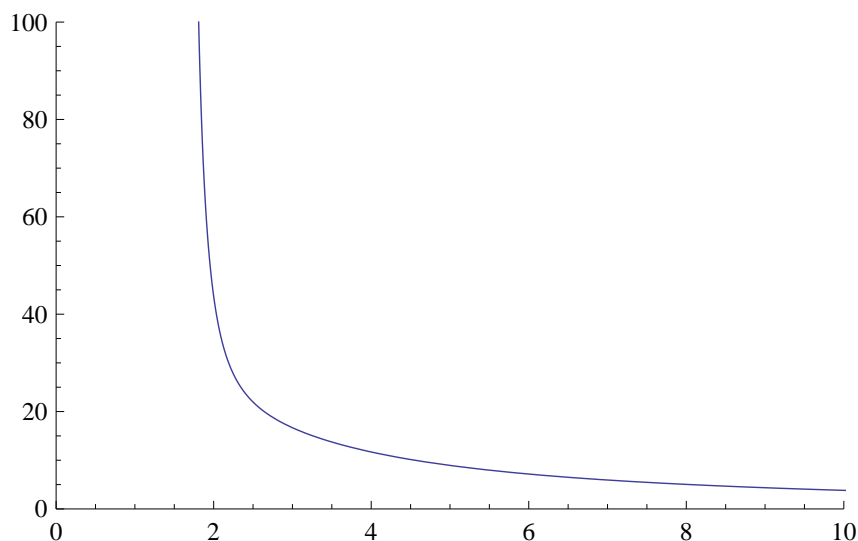
Figure 4.8: Plot of $\ln N$ as function of R.

Material	μ	ν	b
Zinc	43GPa	0.25	2.68×10^{-10}m

Table 4.1: The material constants of zinc

Actually the theory develop in this paper and our solution correspond to the case where we assume that the thickness is much smaller than the radius of the circle. The formula we found cannot actually be applied to the case of Gilman experiment where the radius is small but in many problem, the asymptotic formula have the range of applicability even in case the assumption is not quite true, therefore we have tried to compare although we know that the condition is not quite satisfied and the comparison still show good agreement. We take the sizes of the specimen and of the deformation jig as in his paper: $L = 10$mm, $h = 1.3$mm, $R = 1.17$mm.

Thus, there are only two material constants ρ_s and k which have to be identified. If we take $\rho_s = 1.454 \times 10^{14}$m^{-2} , $k = 1.56 \times 10^{-4}$, then the estimated average polygon distance (taken as the number of polygons divided by the length of the beam) is equal to around $2.7 \times 10^{-7}m$ which is in good agreement with the experimental result obtained in Gilman [16]. Note that the orders of ρ_s and k agree also with those proposed in [3] which is based on some thermodynamic reasoning. The plot of $\ln N$ as a function of R presented in Fig. 4.14 show the decrease of the estimated number of polygons with the increasing radius of the generating circle as expected.

4.2 Bending

4.2.1 Energy of single crystal beam containing dislocations

Figure 4.9: Single crystal beam bent by a moment M.

Consider a single crystal beam bent by a moment M. In the undeformed state the beam occupies the domain $\mathcal{V}$ of the three-dimensional euclidean space, with the cartesian coordinates $(x, y, z) \in (0, L) \times (-\frac{h}{2}, \frac{h}{2}) \times (0, a)$ where L, h, and a are the length, height, and wid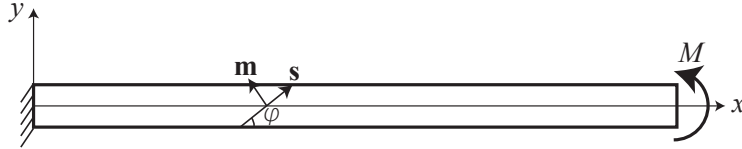th of the beam, respectively. We will assume that $h \ll a \ll L$ and that the beam is deformed under the plane strain condition. For definiteness, let the beam be clamped at $x = 0$ and subjected to a linearly distributed traction $-\tau y$ having the resultant moment M at $x = L$. Besides, the upper and lower boundaries of the beam at $y = \frac{h}{2}$ and $y = -\frac{h}{2}$ are traction free. If the applied moment is small, it is natural to expect that the beam deforms elastically and the stress distribution is linear over the thickness according to the elementary beam theory. However, if the applied moment exceeds some critical value, edge dislocations may appear to reduce energy of the bent beam. We assume that, at the onset of yielding and during the plastic deformations, the crystal admits only one active slip system whose slip planes are inclined at an angle φ to the plane $y = 0$ as shown in Fig. 4.9.

Under the plane strain state condition there are only two non-zero components of the displacements that do not depend on z, $u_x(x, y)$ and $u_y(x, y)$. Consequently, the non-zero components of the total strain tensor are

$$\varepsilon_{xx} = u_{x,x}, \quad \varepsilon_{yy} = u_{y,y}, \quad \varepsilon_{xy} = \varepsilon_{yx} = \frac{1}{2}(u_{x,y} + u_{y,x}).$$

Throughout the paper the comma before an index is used to denote the partial derivative with respect to the corresponding coordinate. Since only one slip system is active, the plastic distortion tensor is given by $\beta_{ij} = \beta(x, y)s_i m_j$, with $\mathbf{s} = (\cos \varphi, \sin \varphi, 0)$ denoting the slip direction and $\mathbf{m} = (-\sin \varphi, \cos \varphi, 0)$ being the unit vector normal to the slip

plane. Thus, the non-zero components of the plastic strain tensor, $\varepsilon_{ij}^p = \frac{1}{2}(\beta_{ij} + \beta_{ji})$, read

$$\varepsilon_{xx}^p = -\frac{1}{2}\beta \sin 2\varphi, \quad \varepsilon_{yy}^p = \frac{1}{2}\beta \sin 2\varphi, \quad \varepsilon_{xy}^p = \varepsilon_{yx}^p = \frac{1}{2}\beta \cos 2\varphi.$$

Accordingly, the non-zero components of the elastic strain tensor, $\varepsilon_{ij}^e = \varepsilon_{ij} - \varepsilon_{ij}^p$, are

$$\varepsilon_{xx}^e = u_{x,x} + \frac{1}{2}\beta \sin 2\varphi, \quad \varepsilon_{yy}^e = u_{y,y} - \frac{1}{2}\beta \sin 2\varphi,$$
$$\varepsilon_{xy}^e = \varepsilon_{yx}^e = \frac{1}{2}(u_{x,y} + u_{y,x} - \beta \cos 2\varphi).$$

The distribution of geometrically necessary edge dislocations associated with this active slip system is described by the dislocation density tensor (Nye, 1953), $\alpha_{ij} = \varepsilon_{jkl}\beta_{il,k}$, whose non-zero components read

$$\alpha_{xz} = \beta_{,x} \cos^2 \varphi + \beta_{,y} \cos \varphi \sin \varphi, \quad \alpha_{yz} = \beta_{,x} \cos \varphi \sin \varphi + \beta_{,y} \sin^2 \varphi.$$

These are the components of the resultant Burgers' vector of all excess edge dislocations whose dislocation lines cut the unit area perpendicular to the z-axis. Thus, the scalar dislocation density equals

$$\rho = \frac{1}{b}\sqrt{(\alpha_{xz})^2 + (\alpha_{yz})^2} = \frac{1}{b}|\beta_{,x} \cos \varphi + \beta_{,y} \sin \varphi|, \tag{4.85}$$

where b is the magnitude of the Burgers vector.

Under the assumptions made the bulk energy density per unit volume of the crystal with continuously distributed dislocations takes a simple form (Berdichevsky, 2006b)

$$U(\varepsilon_{ij}^e, \alpha_{ij}) = \frac{1}{2}\lambda(u_{x,x} + u_{y,y})^2 + \mu(u_{x,x} + \frac{1}{2}\beta \sin 2\varphi)^2 + \mu(u_{y,y} - \frac{1}{2}\beta \sin 2\varphi)^2$$
$$+ \frac{1}{2}\mu(u_{x,y} + u_{y,x} - \beta \cos 2\varphi)^2 + \mu k \ln \frac{1}{1 - \frac{\rho}{\rho_s}}, \tag{4.86}$$

with λ and μ the Lamé constants, ρ_s the saturated dislocation density, and k the material constant. The first four terms in (4.86) represents the elastic energy of the crystal lattice, while the last term corresponds to the energy of the dislocation network. The logarithmic nature of the energy of the dislocation network was extensively discussed in (Berdichevsky, 2006b). For small up to moderate dislocation densities this logarithmic term may be

approximated by the formula

$$\ln \frac{1}{1 - \frac{\rho}{\rho_s}} \cong \frac{\rho}{\rho_s} + \frac{1}{2} \frac{\rho^2}{\rho_s^2}.$$

We shall use further only this approximation.

With (4.85) and (4.86) the total energy functional of the bent beam becomes

$$
\begin{aligned}
I = a \int_0^L \int_{-\frac{h}{2}}^{\frac{h}{2}} [& \frac{1}{2}\lambda(u_{x,x} + u_{y,y})^2 + \mu(u_{x,x} + \frac{1}{2}\beta \sin 2\varphi)^2 + \mu(u_{y,y} - \frac{1}{2}\beta \sin 2\varphi)^2 \\
& + \frac{1}{2}\mu(u_{x,y} + u_{y,x} - \beta \cos 2\varphi)^2 + \mu k \frac{|\beta_{,x} \cos \varphi + \beta_{,y} \sin \varphi|}{b\rho_s} \\
& + \frac{1}{2}\mu k \frac{(\beta_{,x} \cos \varphi + \beta_{,y} \sin \varphi)^2}{b^2 \rho_s^2}] \, dxdy + a \int_{-\frac{h}{2}}^{\frac{h}{2}} \tau y u_x|_{x=L} \, dy. \quad (4.87)
\end{aligned}
$$

The last term in (4.87) is the work done by the linearly distributed traction $-\tau y$ acting at the boundary $x = L$. If the dissipation caused by the dislocation motion is negligible, then the true displacements u_x, u_y and plastic distortion β minimize energy functional (4.87) among all admissible displacements and plastic distortions satisfying the kinematic boundary condition. The bending moment $M = \tau a h^3 / 12$ is regarded as a control parameter, so one can study the evolution of the dislocation network in terms of M.

If the dissipation due to the dislocation motion cannot be neglected, the energy minimization should be replaced by the variational equation (Sedov, 1966)

$$\delta I + a \int_0^L \int_{-\frac{h}{2}}^{\frac{h}{2}} \frac{\partial D}{\partial \dot{\beta}} \delta \beta \, dxdy = 0. \tag{4.88}$$

The last term in this equation describes the energy dissipation due to the dislocation motion, where the dissipation function $D(\dot{\beta})$ is assumed to depend only on the rate of the plastic distortion. We shall consider the simplest rate-independent theory for which

$$D(\dot{\beta}) = K|\dot{\beta}|,$$

with K the critical resolved shear stress. Then, provided the sign of $\dot{\beta}$ does not change during the evolution of β, the variational equation (4.88) reduces to minimizing the fol-

lowing "relaxed energy" functionals

$$
I_d = a \int_0^L \int_{-\frac{h}{2}}^{\frac{h}{2}} [\frac{1}{2}\lambda(u_{x,x} + u_{y,y})^2 + \mu(u_{x,x} + \frac{1}{2}\beta\sin 2\varphi)^2 + \mu(u_{y,y} - \frac{1}{2}\beta\sin 2\varphi)^2
$$

$$
+ \frac{1}{2}\mu(u_{x,y} + u_{y,x} - \beta\cos 2\varphi)^2 + \mu k\frac{|\beta_{,x}\cos\varphi + \beta_{,y}\sin\varphi|}{b\rho_s}
$$

$$
+ \frac{1}{2}\mu k\frac{(\beta_{,x}\cos\varphi + \beta_{,y}\sin\varphi)^2}{b^2\rho_s^2} + K\mathrm{sign}(\dot\beta)\beta]\,dxdy + a\int_{-\frac{h}{2}}^{\frac{h}{2}} \tau y u_x|_{x=L}\,dy. \quad (4.89)
$$

Finally, if $\dot\beta = 0$, then the plastic distortion is frozen, while the displacements should be found by minimizing (4.87).

4.2.2 Energy minimization

We first analyze the minimization problem (4.87). It is convenient to introduce the following dimensionless variables and quantities

$$
\bar{x} = b\rho_s x, \quad \bar{y} = b\rho_s y, \quad \bar{h} = b\rho_s h, \quad \bar{L} = b\rho_s L, \quad \bar\tau = \frac{\tau}{\mu b\rho_s},
$$

$$
\bar{u}_x = b\rho_s u_x, \quad \bar{u}_y = b\rho_s u_y, \quad E = \frac{I(b\rho_s)^2}{\mu a}, \quad \gamma = \frac{\lambda}{\mu}, \quad (4.90)
$$

which simplify the minimization problem considerably. Now the energy functional can be rewritten in the dimensionless form as follows

$$
E = \int_0^L \int_{-\frac{h}{2}}^{\frac{h}{2}} [\frac{1}{2}\gamma(u_{x,x} + u_{y,y})^2 + (u_{x,x} + \frac{1}{2}\beta\sin 2\varphi)^2 + (u_{y,y} - \frac{1}{2}\beta\sin 2\varphi)^2
$$

$$
+ \frac{1}{2}(u_{x,y} + u_{y,x} - \beta\cos 2\varphi)^2 + k|\beta_{,x}\cos\varphi + \beta_{,y}\sin\varphi|
$$

$$
+ \frac{1}{2}k(\beta_{,x}\cos\varphi + \beta_{,y}\sin\varphi)^2]\,dxdy + \int_{-\frac{h}{2}}^{\frac{h}{2}} \tau y u_x|_{x=L}\,dy. \quad (4.91)
$$

The bar over the dimensionless quantities is dropped for short because we shall deal only with them.

As the energy functional (4.91) contains a small parameter h, it can be reduced to 1-D energy functional by the variational asymptotic method (see Berdichevsky, 1983; Le, 1999). For this purpose let us introduce the rescaled coordinate $\zeta = y/h$, $\zeta \in (-1/2, 1/2)$ so that the domain of ζ can be fixed in the passage to the limit $h \to 0$. Simultaneously,

the small parameter h enters the functional explicitly through the formulas

$$u_{i,y} = \frac{1}{h}u_{i,\zeta}, \quad \beta_{,y} = \frac{1}{h}\beta_{,\zeta}.$$

Since the boundary condition at $x = L$ does not influence the inner asymptotic distributions of the displacements and plastic distortion over the thickness, we first set $\tau = 0$ in (4.91) in order to apply the variational-asymptotic procedure. At its first step we keep the asymptotically principal terms in (4.91) to obtain

$$E_0 = h \int_0^L \int_{-1/2}^{1/2} [\frac{1}{2h^2}\gamma(u_{y,\zeta})^2 + \frac{1}{h^2}(u_{y,\zeta})^2 + \frac{1}{2h^2}(u_{x,\zeta})^2$$
$$+ \frac{k}{h}|\beta_{,\zeta}\sin\varphi| + \frac{1}{2h^2}k(\beta_{,\zeta}\sin\varphi)^2]\,dxd\zeta.$$

Functional E_0 is positive definite, so its minimum must be zero and is achieved at

$$u_{x,\zeta} = u_{y,\zeta} = \beta_{,\zeta} = 0.$$

For the bending states which we are interested in let us set at this step $u_x = 0$ and $\beta = 0$ to get

$$u_x = 0, \quad u_y = v(x), \quad \beta = 0.$$

At the second step, we fix $v(x)$ and seek the minimizer in the form

$$u_x = u'_x(x, \zeta), \quad u_y = v(x) + u'_y(x, \zeta), \quad \beta = \beta'(x, \zeta).$$

Substituting these formulas into (4.91) and then keeping the asymptotically leading terms, we obtain

$$E_1 = h \int_0^L \int_{-1/2}^{1/2} [\frac{1}{2h^2}\gamma(u'_{y,\zeta})^2 + \frac{1}{h^2}(u'_{y,\zeta})^2 + \frac{1}{2}(\frac{1}{h}u'_{x,\zeta} + v_{,x})^2$$
$$+ \frac{k}{h}|\beta'_{,\zeta}\sin\varphi| + \frac{1}{2h^2}k(\beta'_{,\zeta}\sin\varphi)^2]\,dxd\zeta.$$

Since functional E_1 is positive definite, its minimum is again zero and is achieved at

$$u'_{x,\zeta} = -hv_{,x}; \quad u'_{y,\zeta} = 0, \quad \beta'_{,\zeta} = 0.$$

Thus, at this step

$$u'_x = -h\zeta v_{,x}; \quad u'_y = 0, \quad \beta' = 0.$$

4 Problems of polygonization and bending

At the third step of the variational-asymptotic procedure, we look for the minimizer in the form

$$u_x = -h\zeta v_{,x} + u_x''(x, \zeta), \quad u_y = v(x) + u_y''(x, \zeta), \quad \beta = \beta''(x, \zeta). \tag{4.92}$$

Without restricting generality we may put the following constraints on the unknown functions

$$\langle u_y'' \rangle = 0, \quad \langle \beta'' \rangle = 0, \quad \text{where} \quad \langle . \rangle = \int_{-1/2}^{1/2} . \, d\zeta. \tag{4.93}$$

Constraint $\langle u_y'' \rangle = 0$ means that $v(x)$ is the mean deflection of the beam. Substituting (4.92) into (4.91), then keeping the leading terms to get

$$
\begin{aligned}
E_2 = \int_0^L \int_{-1/2}^{1/2} [\frac{1}{2}\gamma(-h\zeta v_{,xx} + \frac{1}{h}u_{y,\zeta}'')^2 + (-h\zeta v_{,xx} + \frac{1}{2}\beta'' \sin 2\varphi)^2 \\
+ (\frac{1}{h}u_{y,\zeta}'' - \frac{1}{2}\beta'' \sin 2\varphi)^2 + \frac{1}{2}(\frac{1}{h}u_{x,\zeta}'' - \beta'' \cos 2\varphi)^2 \\
+ \frac{k}{h}|\beta_{,\zeta}'' \sin\varphi| + \frac{1}{2h^2}k(\beta_{,\zeta}'' \sin\varphi)^2] \, dx d\zeta.
\end{aligned}
\tag{4.94}
$$

Functional (4.94) can be reduced to a functional depending only on β''. Indeed, fixing first β'' and varying this functional with respect to u_x'' and u_y'', then using the natural boundary conditions at $\zeta = \pm 1/2$, we obtain,

$$
\begin{cases}
\frac{1}{h}(\gamma + 2)u_{y,\zeta}'' = \gamma h\zeta v_{,xx} + \beta'' \sin 2\varphi, \\
\frac{1}{h}u_{x,\zeta}'' = \beta'' \cos 2\varphi,
\end{cases}
\tag{4.95}
$$

After finding u_x'' and u_y'' according to these equations, we substitute (4.95) into (4.94) and change ζ back to y. Since the functional does not contain $\beta_{,x}''$, the thickness problem reduces to minimizing the following functional with respect to $\beta''(x, y)$

$$E_3 = \int_{-\frac{h}{2}}^{\frac{h}{2}} [\frac{\kappa}{2}(-2v_{,xx}y + \beta'' \sin 2\varphi)^2 + k|\beta_{,y}'' \sin\varphi| + \frac{1}{2}k(\beta_{,y}'' \sin\varphi)^2] \, dy, \tag{4.96}$$

where $\kappa = \frac{1}{2(1-\nu)}$. In this variational problem variable x serves as a parameter.

From the elementary theory of elastic bending we know that the maximal and minimal resolved shear stresses are achieved at the free faces of the beam and hence dislocations should be nucleated from there. However, dislocations cannot stay very near to the free faces due to the image forces attracting them to the boundaries. Thus, two dislocation-

free zones near the free faces exist in equilibrium. Besides, due to the symmetry reasoning function $\beta(x, y)$ must be odd with respect to y: $\beta''(x, y) = -\beta''(x, -y)$. This leads to the following Ansatz for the minimizer of (4.96)

$$\beta''(x, y) = \begin{cases} \beta_0(x) & \text{for } y \in (-\frac{h}{2}, -\frac{l(x)}{2}), \\ \beta_1(x, y) & \text{for } y \in (-\frac{l(x)}{2}, 0), \\ -\beta''(x, -y) & \text{for } y \in (0, \frac{h}{2}), \end{cases} \tag{4.97}$$

where $\beta_0(x)$ and $l(x)$ are unknown functions, $0 \leq l(x) \leq h$, $\beta_1(x, -\frac{l(x)}{2}) = \beta_0$, and $\beta_1(x, 0) = 0$. We have to find $\beta_1(x, y)$, $\beta_0(x)$, and $l(x)$. Functional (4.96) becomes

$$E_3 = 2 \int_{-\frac{l}{2}}^{0} \left[\frac{\kappa}{2}(-2v_{,xx}y + \beta_1 \sin 2\varphi)^2 + k|\beta_{1,y} \sin \varphi| + \frac{1}{2}k(\beta_{1,y} \sin \varphi)^2\right] dy$$
$$+ 2 \int_{-\frac{h}{2}}^{-\frac{l}{2}} \frac{\kappa}{2}(-2v_{,xx}y + \beta_0 \sin 2\varphi)^2 \, dy. \tag{4.98}$$

Varying this functional with respect to β_1, we obtain the following equation

$$-k\beta_{1,yy} \sin^2 \varphi + \kappa\beta_1 \sin^2 2\varphi = 2\kappa yv_{,xx} \sin 2\varphi. \tag{4.99}$$

The variation of (4.98) with respect to l leads to the boundary condition

$$\beta_{1,y}(x, -\frac{l(x)}{2}) = 0, \tag{4.100}$$

guaranteeing the continuity of the dislocation density. Besides, the continuity of plastic distortion

$$\beta_1(x, 0) = 0, \quad \beta_1(x, -\frac{l(x)}{2}) = \beta_0 \tag{4.101}$$

must also be fulfilled. Finally, the variation of (4.98) with respect to β_0 yields the boundary condition at $y = -l/2$

$$\kappa v_{,xx} \frac{1}{4}(h^2 - l^2) \sin 2\varphi + \kappa\beta_0 \frac{1}{2}(h - l) \sin^2 2\varphi - k \operatorname{sign}(\beta_{1,y}) \sin \varphi = 0. \tag{4.102}$$

The solution to (4.99), (4.100), and (4.101)$_1$ reads

$$\beta_1(x, y) = \frac{v_{,xx}}{\sin 2\varphi} \frac{1}{\eta}(2\eta y - \frac{2}{\cosh \frac{\eta l}{2}} \sinh \eta y), \tag{4.103}$$

where

$$\eta = 2\sqrt{\frac{\kappa}{k}}\cos\varphi.$$

Using the boundary condition $(4.101)_2$ we find $\beta_0(x)$

$$\beta_0(x) = \frac{v_{,xx}}{\sin 2\varphi}\frac{1}{\eta}(-\eta l + 2\tanh\frac{\eta l}{2}).$$

Substituting this formula into the last boundary condition (4.102) we obtain

$$\kappa v_{,xx}\frac{1}{4}(h^2 - l^2)\sin 2\varphi + \kappa v_{,xx}\frac{1}{\eta}(-\eta l + 2\tanh\frac{\eta l}{2})\frac{1}{2}(h - l)\sin 2\varphi$$

$$- k\,\text{sign}(\beta_{1,y})\sin\varphi = 0. \quad (4.104)$$

The first consequence of this equation can already be obtained. Let us restrict ourselves to the case $\varphi \in (0, \pi/2)$. If the length l is small, then the sign of $v_{,xx}$ coincides with the sign of $\beta_{1,y}$ evaluated right from the point $y = -l/2$. For definiteness let $\beta_{1,y}(-l/2 + 0) > 0$ so that $v_{,xx} > 0$. Note that, if the curvature of the beam is constant, then $l(x)$ does not depend on x and remains constant over the whole length of the beam. In this case (4.104) can be regarded as the equation for $v_{,xx}$ once l is known. By integrating (4.95) and taking the above constraints into account, we obtain the solution for u_x'' and u_y'' in the form

$$\begin{cases} u_x'' = \int_0^y \beta(x, \xi)\,d\xi\cos 2\varphi, \\ u_y'' = \frac{\gamma}{\gamma+2}\frac{1}{2}(y^2 - \frac{h^2}{12})v_{,xx} + \frac{1}{\gamma+2}(\int_0^y \beta(x, \xi)\,d\xi - \chi)\sin 2\varphi, \end{cases} \quad (4.105)$$

where $\chi = \langle\int_0^y \beta(x, \xi)\,d\xi\rangle$.

Having found the solution of the thickness problem, let us now substitute

$$\begin{cases} u_x = -v_{,x}y + \int_0^y \beta(x, \xi)\,d\xi\cos 2\varphi, \\ u_y = v(x) + \frac{\gamma}{\gamma+2}\frac{1}{2}(y^2 - \frac{h^2}{12})v_{,xx} + \frac{1}{\gamma+2}(\int_0^y \beta(x, \xi)\,d\xi - \chi)\sin 2\varphi, \end{cases} \quad (4.106)$$

together with β from (4.97) and (4.103) into the energy functional (4.91). Keeping the asymptotically principal terms and integrating over the thickness we obtain the functional

$$I[v(x)] = \int_0^L \Phi(v_{,xx})\,dx - Mv_{,x}|_{x=L}, \quad (4.107)$$

where the bending energy density reads

$$\Phi(\omega) = c_1 \omega^2 + c_2 \omega. \tag{4.108}$$

In these formulas we use ω to denote the curvature $v_{,xx}$, $M = \tau h^3/12$ is the resultant moment, and

$$
\begin{aligned}
c_1 &= 2 \int_{-\frac{h}{2}}^{-\frac{l}{2}} \frac{\kappa}{2}(q_0 - 2y)^2 \, dy + 2 \int_{-\frac{l}{2}}^{0} [\frac{\kappa}{2}(q - 2y)^2 + \frac{k}{8\cos^2 \varphi}(q_{,y})^2] \, dy, \\
c_2 &= 2 \int_{-\frac{l}{2}}^{0} k q_{,y} \frac{\sin \varphi}{\sin 2\varphi} \, dy = -\frac{k}{\cos \varphi} q_0 = -\frac{k}{\eta \cos \varphi}(-\eta l + 2\tanh \frac{\eta l}{2}),
\end{aligned}
\tag{4.109}
$$

with

$$q(y) = \frac{1}{\eta}(2\eta y - \frac{2}{\cosh \frac{\eta l}{2}} \sinh \eta y),$$

and $q_0 = q(-l/2)$. Note that, as the coefficients c_1 and c_2 depends on the curvature ω through l, the energy density is not quadratic with respect to ω. Besides, if $q(y) = 0$, then $c_1 = \kappa h^3/6$ and $c_2 = 0$, so the obtained functional reduces to the classical 1-D functional of the elastic beam as expected (Le, 1999).

Varying the functional (4.107) with respect to the deflection v, we obtain the differential equation of bending

$$m_{,xx} = 0, \quad m = \frac{\partial \Phi}{\partial \omega}, \tag{4.110}$$

subject to the boundary conditions

$$
\begin{cases}
v(0) = 0, \quad v_{,x}(0) = 0, \\
m(L) - M = 0, \quad m_{,x}(L) = 0.
\end{cases}
\tag{4.111}
$$

Equation (4.110), together with the conditions $(4.111)_2$, implies that

$$m(\omega) = 2c_1 \omega + \frac{dc_1}{d\omega}\omega^2 + c_2 + \frac{dc_2}{d\omega}\omega = M. \tag{4.112}$$

Since the bending moment m is independent of x, the curvature must also be constant over the length of the beam. Together with (4.104), this equation determines the moment-curvature curve during the plastic deformations. To plot this curve let us compute the

derivatives of c_1 and c_2 with respect to ω

$$\frac{dc_1}{d\omega} = \frac{dc_1}{dl}\frac{dl}{d\omega}, \quad \frac{dc_2}{d\omega} = \frac{dc_2}{dl}\frac{dl}{d\omega}.$$

From (4.104) we find that

$$\frac{d\omega}{dl} = \frac{4k\eta\tanh\frac{l\eta}{2}\left(\eta(h-l)\tanh\frac{l\eta}{2}+2\right)}{\kappa\cos\varphi(h-l)^2\left(\eta(h-l)+4\tanh\frac{l\eta}{2}\right)^2}.$$

This formula, together with (4.109), enables one to determine $dc_1/d\omega$ and $dc_2/d\omega$, required for plotting the moment-curvature curve.

The threshold value of curvature at which dislocations begin to nucleate is calculated by letting l go to zero in (4.104) which yields

$$\omega_{en} = \frac{2k}{\kappa h^2\cos\varphi}.$$

The threshold value of moment can be computed from (4.112). Taking into account that, at $l = 0$, $c_1 = \kappa h^3/6$, $c_2 = 0$, while $dc_1/d\omega = dc_2/d\omega = 0$, we find

$$M_{en} = \frac{2kh}{3\cos\varphi}.$$

Thus, if $M < M_{en}$, then $\beta = 0$, so no dislocation are nucleated and we have purely elastic solution. The plastic yielding begins at $M = M_{en}$.

Combining the purely elastic solution with the solution containing dislocations, we present the moment-curvature relation in the following form

$$M = \begin{cases} \frac{\kappa h^3}{3}\omega & \text{when } M < M_{en}, \\ 2c_1\omega + c_2 + \frac{dc_1}{d\omega}\omega^2 + \frac{dc_2}{d\omega}\omega & \text{when } M > M_{en}. \end{cases} \tag{4.113}$$

Knowing the curvature ω from M, we integrate the equation $v_{,xx} = \omega$ and use the boundary conditions $(4.111)_1$ to obtain the deflection of the beam

$$v(x) = \frac{1}{2}\omega x^2. \tag{4.114}$$

4.2.3 Numerical simulations

In order to simulate the minimizer numerically, we choose $h = 0.1$, $L = 10$, $\nu = 0.25$, $k = 10^{-4}$. Fig. 4.10 shows the plot of energetic threshold of the bending moment M_{en} as function of the angle φ. It can be seen that the threshold moment becomes infinite as φ goes to $\pi/2$ and has a local minimum at $\varphi = 0$.
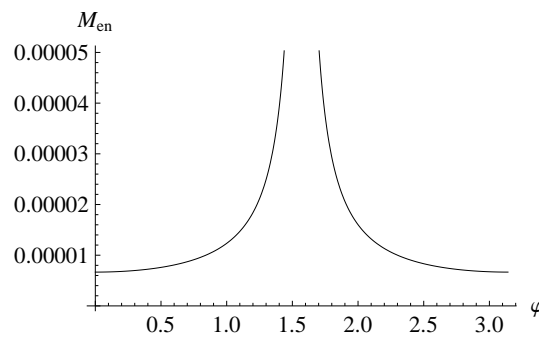
Figure 4.10: Function $M_{en}(\varphi)$.

For $M > M_{en}$ the plastic distortion becomes non-zero. Fig. 4.11 show the plots of plastic distortion $\beta(y)$ for $M = 0.00015$ at two different orientations of slip systems. The plastic strain vanishes on the middle line of the beam as expected and reaches its maximum and minimum at the free faces.
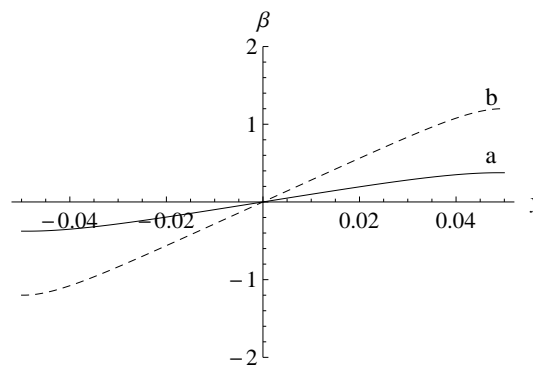
Figure 4.11: Function $\beta(y)$ for $M = 0.00015$ and a) $\varphi = \frac{\pi}{3}$, b) $\varphi = \frac{\pi}{6}$.

On Fig. 4.12, where the dislocation density $\rho(y)$ is plotted for $M = 0.00015$ and for two different angles it is seen that the excess dislocations of the same sign are concentrated in the middle of the beam thickness, with maximum dislocation density achieved at $y = 0$. Although no obstacle exists on the middle line, the repulsive forces between dislocations of the same sign prevent them from colliding. Thus, the high concentration of dislocations

Figure 4.12: Dislocation density for $M = 0.00015$ and a) $\varphi = \frac{\pi}{3}$, b) $\varphi = \frac{\pi}{6}$.

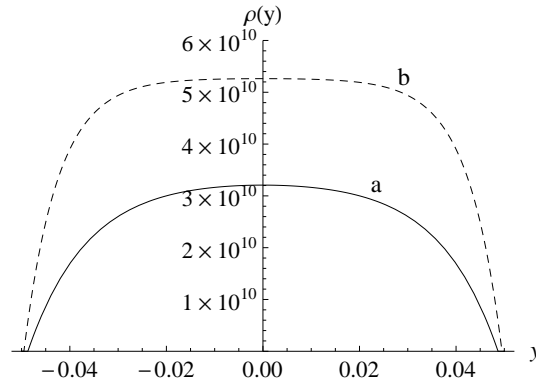can be regarded as the dislocation pile-up against the middle line. The dislocation free zones are $y \in (-h/2, -l/2)$ and $y \in (l/2, h/2)$.
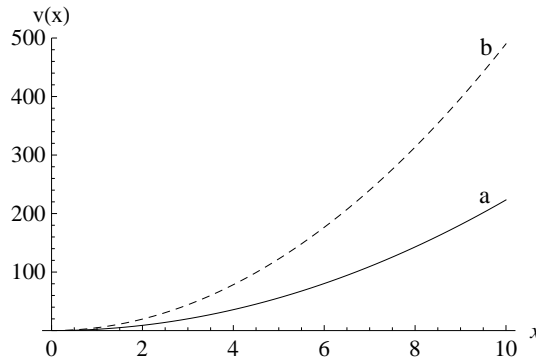
Figure 4.13: Deflection of the beam.

The deflection of the beam, $v(x)$, is shown in Fig. 4.13 for $M = 0.00015$ and a) $\varphi = \frac{\pi}{3}$, b) $\varphi = \frac{\pi}{6}$. Since the curvature of the beam is constant, the thickness of the dislocation zone l does not depend on x.

On Fig. 4.14 we show the moment-curvature curve for $\varphi = \pi/3$ and $\varphi = \frac{\pi}{6}$. Up to the threshold moment M_{en} (corresponding to point A on this figure) the moment-curvature curve is a straight line corresponding to the linear elastic beam theory. Then the curve becomes non-linear and increasing as M increases and l increases from zero to $h/2$. This nonlinear portion describes the work hardening due to the dislocation pile-up against the middle line of the beam. If the bending moment is increased from zero up to the moment M_B corresponding to B (the loading case) we follow the moment-curvature curve from O through A to B. Now, if we unload the beam by decreasing the bending moment from M_B to zero, we come back by the same path BAO, and at the end of the unloading path no residual curvature of the beam is observed.

Figure 4.14: Moment-curvature curve for: a) $\varphi = \frac{\pi}{3}$, b) $\varphi = \frac{\pi}{6}$.

4.2.4 Non-zero dissipation

If the dissipation cannot be neglected, the problems reduce to minimizing the relaxed energy functionals (4.89). The sign of its last term in the energy density depends on whether $\dot{\beta} > 0$ or $\dot{\b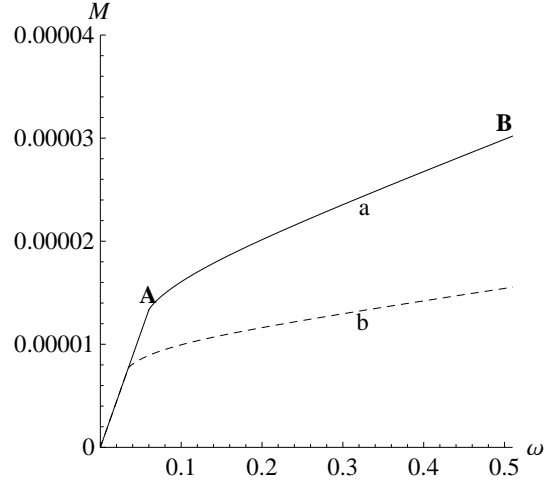eta} < 0$. However, for the beam bending it is easy to see that both cases occur simultaneously during the plastic deformations. Indeed, from the elementary beam theory (and also from the previous simulations) we know that, as the bending moment is increased (loading), $\dot{\beta} > 0$ for $y > 0$ and $\dot{\beta} < 0$ for $y < 0$. In contrary, if the bending moment is decreased (unloading or loading in the opposite direction), β is either frozen or $\dot{\beta} > 0$ for $y < 0$ and $\dot{\beta} < 0$ for $y > 0$. Since these functionals differs from each other in the loading and unloading case, the case study must be done separately.

Consider first the loading case for which the term $\text{sign}(\dot{\beta})K\beta$ in (4.89) must be replaced by $\text{sign}\, y\, K\beta$. It is convenient to introduce the dimensionless quantities (4.90) as in Section 3 and rewrite the energy functionals (4.89) in the dimensionless form

$$
E_d = \int_0^L \int_{-\frac{h}{2}}^{\frac{h}{2}} [\frac{1}{2}\gamma(u_{x,x} + u_{y,y})^2 + (u_{x,x} + \frac{1}{2}\beta \sin 2\varphi)^2 + (u_{y,y} - \frac{1}{2}\beta \sin 2\varphi)^2
$$

$$
+ \frac{1}{2}(u_{x,y} + u_{y,x} - \beta \cos 2\varphi)^2 + k|\beta_{,x} \cos \varphi + \beta_{,y} \sin \varphi|
$$

$$
+ \frac{1}{2}k(\beta_{,x} \cos \varphi + \beta_{,y} \sin \varphi)^2 + \epsilon \, \text{sign}\, y\, \beta] \, dxdy + \int_{-\frac{h}{2}}^{\frac{h}{2}} \tau y u_x|_{x=L} \, dy, \quad (4.115)
$$

where $\epsilon = K/\mu$. As compared to the previous functional (4.91) the additional term $\epsilon \, \text{sign}\, y\, \beta$ does not belong to the asymptotically principal terms. Therefore, up to the

second step of the variational-asymptotic procedure this term does not have any influence on the inner asymptotic expansion. At the third step we look for the minimizer in the form (4.92) such that the constraints (4.93) are obeyed. Fixing β'' and minimizing the relaxed energy with respect to u''_x and u''_y, we find them in the form (4.95). Then, the functional reduces to

$$E_d = \int_{\frac{-h}{2}}^{\frac{h}{2}} [\frac{\kappa}{2}(-2v_{,xx}y + \beta'' \sin 2\varphi)^2 + \epsilon \operatorname{sign} y\beta'' + k|\beta''_{,y} \sin \varphi| + \frac{1}{2}k(\beta''_{,y} \sin \varphi)^2] \, dy.$$

Now, the term $\epsilon \operatorname{sign} y\beta''$ should be kept because it is of the same order as the cross term $-\kappa 2v_{,xx}y\beta'' \sin 2\varphi$. Up to an unessential constant we may rewrite this functional as

$$E_d = \int_{\frac{-h}{2}}^{\frac{h}{2}} [\frac{\kappa}{2}(-2v_{,xx}y + \frac{\epsilon \operatorname{sign} y}{\kappa \sin 2\varphi} + \beta'' \sin 2\varphi)^2 + k|\beta''_{,y} \sin \varphi| + \frac{1}{2}k(\beta''_{,y} \sin \varphi)^2] \, dy. \quad (4.116)$$

Similar to the case of energy minimization we use the Ansatz (4.97) for the minimizer. Then the functional (4.116) becomes

$$E_d = 2\int_{-\frac{l}{2}}^{0} [\frac{\kappa}{2}(-2v_{,xx}y - \frac{\epsilon}{\kappa \sin 2\varphi} + \beta_1 \sin 2\varphi)^2 + k|\beta_{1,y} \sin \varphi|$$
$$+ \frac{1}{2}k(\beta_{1,y} \sin \varphi)^2] \, dy + 2\int_{-\frac{h}{2}}^{-\frac{l}{2}} \frac{\kappa}{2}(-2v_{,xx}y - \frac{\epsilon}{\kappa \sin 2\varphi} + \beta_0 \sin 2\varphi)^2 \, dy. \quad (4.117)$$

Here the oddness of β'' is used. Varying this functional with respect to β_1, we obtain the following equation

$$-k\beta_{1,yy} \sin^2 \varphi + \kappa\beta_1 \sin^2 2\varphi = 2\kappa yv_{,xx} \sin 2\varphi + \epsilon. \quad (4.118)$$

The variation of (4.117) with respect to l leads to the boundary condition

$$\beta_{1,y}(x, -\frac{l(x)}{2}) = 0, \quad (4.119)$$

which should be posed together with the continuity of β

$$\beta_1(x, 0) = 0, \quad \beta_1(x, -\frac{l(x)}{2}) = \beta_0 \quad (4.120)$$

Finally, the variation of (4.117) with respect to β_0 yields the boundary condition at

$y = -l/2$

$$\kappa v_{,xx} \frac{1}{4}(h^2 - l^2)\sin 2\varphi + (\frac{\kappa \beta_0}{2}\sin^2 2\varphi - \frac{\epsilon}{2})(h - l) - k\,\text{sign}(\beta_{1,y})\sin\varphi = 0. \quad (4.121)$$

The solution to (4.118), (4.119) and $(4.120)_1$ reads

$$\beta_1(y) = \frac{v_{,xx}}{\eta \sin 2\varphi}(2\eta y - \frac{2\sinh \eta y}{\cosh \frac{\eta l}{2}}) + \frac{\epsilon}{\kappa \sin^2 2\varphi}(1 - \cosh \eta y - \tanh \frac{\eta l}{2}\sinh \eta y). \quad (4.122)$$

Computing $\beta_1(y)$ at $y = -l/2$ we get

$$\beta_0 = \frac{v_{,xx}}{\eta \sin 2\varphi}(-\eta l + 2\tanh \frac{\eta l}{2}) + \frac{\epsilon}{\kappa \sin^2 2\varphi}(1 - \frac{1}{\cosh \frac{\eta l}{2}}).$$

Substitution of this formula into (4.121) yields

$$\kappa v_{,xx} \frac{1}{4}(h^2 - l^2)\sin 2\varphi + \kappa v_{,xx}\frac{1}{\eta}(-\eta l + 2\tanh \frac{\eta l}{2})\frac{1}{2}(h - l)\sin 2\varphi$$

$$- \frac{\epsilon}{2}\frac{1}{\cosh \frac{\eta l}{2}}(h - l) - k\,\text{sign}(\beta_{1,y})\sin\varphi = 0. \quad (4.123)$$

Knowing β, we can now determine the displacement field in accordance with (4.105). Then, substituting this field together with $\beta(y)$ from (4.97) and (4.122) into the energy functional (4.116), keeping the asymptotically principal terms and integrating over the thickness we obtain the 1-D functional given by

$$I = \int_0^L \Phi(v_{,xx})^2\,dx - Mv_{,x}|_{x=L}. \quad (4.124)$$

where

$$\Phi(\omega) = c_1\omega^2 + c_2\omega. \quad (4.125)$$

The coefficient c_1 and c_2 are given by

$$\begin{cases} c_1 = & 2\int_{-\frac{l}{2}}^0 [\frac{\kappa}{2}(q(y) - 2y)^2 + \frac{k}{8\cos^2\varphi}(q_{,y})^2]\,dy + 2\int_{-\frac{h}{2}}^{-\frac{l}{2}} \frac{\kappa}{2}(q_0 - 2y)^2\,dy, \\ c_2 = & 2\int_{-\frac{l}{2}}^0 [\frac{k}{2\cos\varphi}q_{,y} + \frac{\epsilon}{\kappa \sin 2\varphi}(\frac{k}{4\cos^2\varphi}q_{,y}p_{,y} + \kappa(p(y) - 1)(q(y) - 2y))]\,dy \\ & +2\int_{-\frac{h}{2}}^{-\frac{l}{2}}[\frac{\epsilon}{\sin 2\varphi}(p_0 - 1)(q_0 - 2y)]\,dy, \end{cases}$$

with

$$q(y) = \frac{1}{\eta}(2\eta y - 2\frac{\sinh \eta y}{\cosh \frac{\eta l}{2}}), \quad p(y) = 1 - \cosh \eta y - \tanh \frac{\eta l}{2} \sinh \eta y,$$

and $q_0 = q(-l/2)$, $p_0 = p(-l/2)$. Note that the coefficients c_1 and c_2 depends on the curvature ω, so the energy density is not quadratic with respect to ω.

Varying the functional (4.124) with respect to the deflection v, we obtain the differential equation of bending (4.110) subject to the boundary conditions (4.111). This implies the moment-curvature relation (4.112) as in Section 4. Consequently, the moment-curvature relation remains valid if c_1 and c_2 from above are substituted. It turns out that the straight line $M = \kappa h^3 \frac{\omega}{3}$ corresponding to the purely elastic solution does not intersect the moment-curvature curve corresponding to the solution with dislocations at $l = 0$ for the case with non-zero dissipation. The threshold value for the curvature must therefore be calculated by solving the system of equations

$$\omega(l_d) = \omega_d, \quad m(l_d) = \kappa h^3 \frac{\omega_d}{3}, \tag{4.126}$$

where l_d and ω_d are regarded as unknowns. Using (4.112) we can find also the threshold value for the bending moment M_d. Computing the curvature from the given moment, we can find the deflection in accordance with equation (4.114).

Let the beam be bent slowly and successively by the increasing moment reaching the maximal value $M_* > M_d$ such that at the end of the loading process the plastic distortion becomes β_*. Consider now the unloading process in which we reduce the bending moment back to zero. Assuming that dislocations are frozen during this unloading process with $\beta = \beta_*$ and $\dot{\beta} = 0$, we find the displacements of the beam by minimizing the energy functional

$$E = \int_0^L \int_{-\frac{h}{2}}^{\frac{h}{2}} [\frac{1}{2}\gamma(u_{x,x} + u_{y,y})^2 + (u_{x,x} + \frac{1}{2}\beta_* \sin 2\varphi)^2 + (u_{y,y} - \frac{1}{2}\beta_* \sin 2\varphi)^2$$

$$+ \frac{1}{2}(u_{x,y} + u_{y,x} - \beta_* \cos 2\varphi)^2 + k|\beta_{*,x} \cos \varphi + \beta_{*,y} \sin \varphi|$$

$$+ \frac{1}{2}k(\beta_{*,x} \cos \varphi + \beta_{*,y} \sin \varphi)^2] \, dxdy + \int_{-\frac{h}{2}}^{\frac{h}{2}} \tau y u_x|_{x=L} \, dy. \tag{4.127}$$

where, now, β_* is fixed and does not subject to the variation. Doing the variational-asymptotic analysis similar to the case presented in Sections 3 and 5, we obtain on the

third step the following displacement field

$$\begin{cases} u_x = -v_{,x}y + \int_0^y \beta_*(x,\xi)\,d\xi \cos 2\varphi, \\ u_y = v(x) + \frac{\gamma}{\gamma+2}\frac{1}{2}(y^2 - \frac{h^2}{12})v_{,xx} + \frac{1}{\gamma+2}(\int_0^y \beta_*(x,\xi)\,d\xi - \chi_*)\sin 2\varphi, \end{cases} \tag{4.128}$$

where $\chi_* = \langle \int_0^y \beta_*(x,\xi)\,d\xi \rangle$. Substituting this displacement field into functional (4.127) and keeping the asymptotically principal terms, we obtain

$$E_3 = \int_0^L \int_{-\frac{h}{2}}^{\frac{h}{2}} [\frac{\kappa}{2}(-2v_{,xx}y + \beta_* \sin 2\varphi)^2 + k|\beta_{*,y} \sin \varphi| + \frac{1}{2}k(\beta_{*,y} \sin \varphi)^2]\,dxdy$$

$$- \int_{-\frac{h}{2}}^{\frac{h}{2}} \tau y^2 v_{,x}|_{x=L}\,dy, \quad (4.129)$$

Integrating over the thickness and neglecting the terms containing known function β_*, we obtain 1-D functional (4.124) with the bending energy density (4.125), but now

$$c_1 = \kappa h^3/6, \quad c_2 = 2\int_{-\frac{l}{2}}^0 \kappa\omega_* q_*(y)(-2y)\,dy + 2\int_{-\frac{h}{2}}^{-\frac{l}{2}} \kappa\omega_* q_{0*}(-2y)\,dy, \tag{4.130}$$

where ω_* is the curvature corresponding to M_* and

$$q_*(y) = \frac{1}{\eta}(2\eta y - \frac{2}{\cosh \frac{\eta l_*}{2}} \sinh \eta y), \quad q_{0*} = q_*(-l/2).$$

Thus, during this unloading process the moment-curvature relation takes the form

$$m = 2c_1\omega + c_2 = M,$$

so that, at the end of the unloading when $M = 0$, the residual curvature is

$$\omega_r = -\frac{c_2}{c_1}.$$

Note that, although the bending moment after unloading is zero, the elastic strain is not, so there is still some eigenstress in the beam at the end of this process. The energy of the beam after unloading is given by the asymptotic formula

$$E_u = \int_0^L \int_{-\frac{h}{2}}^{\frac{h}{2}} [\frac{\kappa}{2}(-2\omega_r y + \beta_* \sin 2\varphi)^2 + k|\beta_{*,y} \sin \varphi| + \frac{1}{2}k(\beta_{*,y} \sin \varphi)^2]\,dxdy. \tag{4.131}$$

Here the first term describes the elastic energy due to the eigenstress, while the remaining terms correspond to the energy of the frozen dislocations. Mention also that this unloading

process can also be combined with the energy minimization.

The case of loading in the opposite direction with $\dot{\beta} > 0$ for $y < 0$ and $\dot{\beta} < 0$ for $y > 0$ reduces to the minimization of functional (4.115), in which the term $\epsilon \operatorname{sign} y \, \beta$ should be changed to $-\epsilon \operatorname{sign} y \, \beta$. This case can be studied in a similar manner.

4.2.5 Numerical simulation

In order to simulate the minimizer numerically, we choose $h = 0.1$, $L = 10$, $\nu = 0.25$, $k = 10^{-4}$, $K = 5 \times 10^6 \text{Pa}$ and $\mu = 26 \times 10^9 \text{Pa}$. In order to find the dissipative threshold for the bending moment we need to solve equations 4.126 with respect to ω_d and l_d. Then $M_d = \kappa h^3 \frac{\omega_d}{3}$. Numerical simulations give for instance $\omega_d = 0.07226$, $l_d = 0.0221 \Rightarrow M_d = 0.0000160588$ for $\varphi = \frac{\pi}{3}$ and $\omega_d = 0.04489$, $l_d = 0.0213 \Rightarrow M_d = 0.997654 \times 10^{-5}$ for $\varphi = \frac{\pi}{6}$. Thus, if we increase M steadily, then at the onset of plastic yielding the plastic slip and the total number of dislocations turn out to be finite. This could be explained physically in the following way: in the presence of nonzero dissipation dislocations should accumulate enough to give the crystal
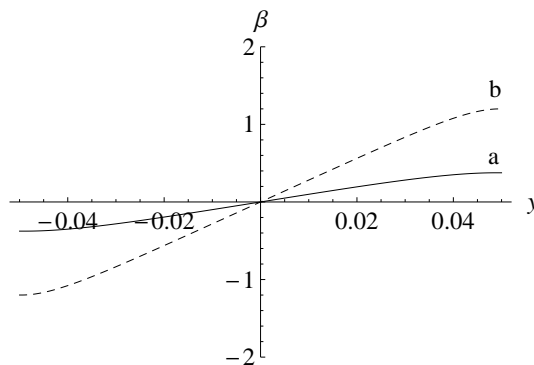
Figure 4.15: Function $\beta(y)$ for $M = 0.00015$ and a) $\varphi = \frac{\pi}{3}$, b) $\varphi = \frac{\pi}{6}$.

For $M > M_d$ the plastic distortion becomes non-zero. Fig. 4.15 show the plots of plastic distortion $\beta(y)$ for $M = 0.00015$ at two different orientations of slip systems. The plastic strain is zero on the middle line of the beam and reaches its maximum and minimum at the free faces. On Fig. 4.16, where the dislocation density $\rho(y)$ is plotted for $M = 0.00015$ and for two different angles, we see that the excess dislocations of the same sign are concentrated in the middle of the beam thickness, with maximum dislocation density achieved at $y = 0$. Although no obstacle exists on the middle line, the repulsive force between dislocations of the same sign prevent them from colliding. Thus, the high
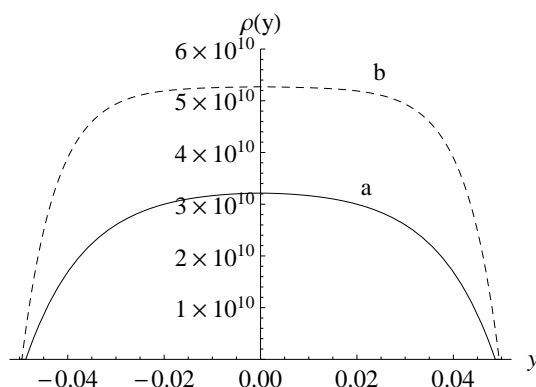
Figure 4.16: Dislocation density for $M = 0.00015$ and a) $\varphi = \frac{\pi}{3}$, b) $\varphi = \frac{\pi}{6}$.
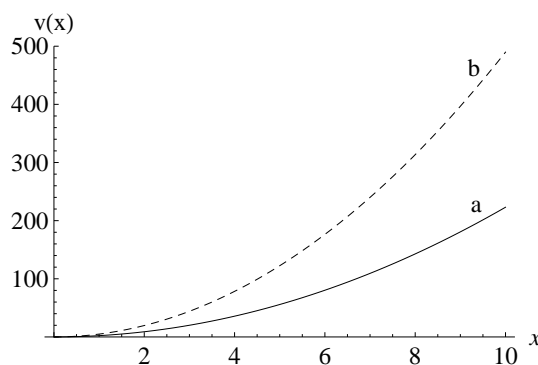
Figure 4.17: Deflection of the beam.

concentration of dislocations can be regarded as the dislocation pile-up against the middle line. The dislocation free zones are $y \in (-h/2, -l/2)$ and $y \in (l/2, h/2)$.

The deflection of the beam, $v(x)$, is shown in Fig. 4.17 for $M = 0.00015$ and a) $\varphi = \frac{\pi}{3}$, b) $\varphi = \frac{\pi}{6}$. Since the curvature of the beam is constant, the thickness of the dislocation zone l does not depend on x.

On Fig. 4.18 we show the moment-curvature curve for $\varphi = \pi/3$ and $\varphi = \frac{\pi}{6}$. Up to the threshold moment M_d (corresponding to point A on this figure) the moment-curvature curve is a straight line corresponding to the linear elastic beam theory. Then the curve becomes non-linear and increasing as M increases and l increases from zero to $h/2$. This nonlinear portion describes the work hardening due to the dislocation pile-up against the middle line of the beam. If the bending moment is increased from zero up to the moment M_B corresponding to B (the loading case) we follow the moment-curvature curve from O through A to B. If the beam is then unloaded, the moment-curvature curve becomes a straight line BC with the same slope like that of OA as shown in Fig. 4.19.
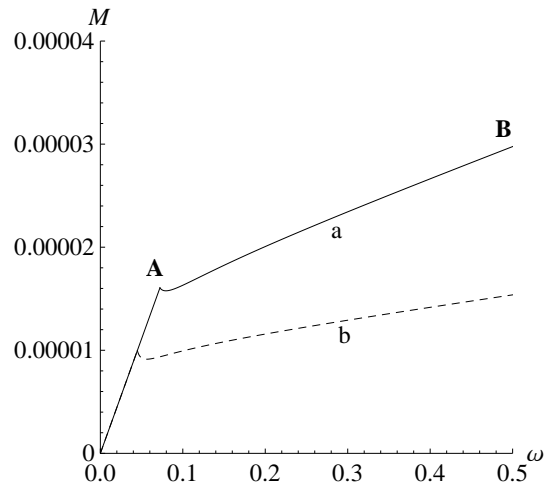
Figure 4.18: Moment-curvature curve for: a) $\varphi = \frac{\pi}{3}$, b) $\varphi = \frac{\pi}{6}$.
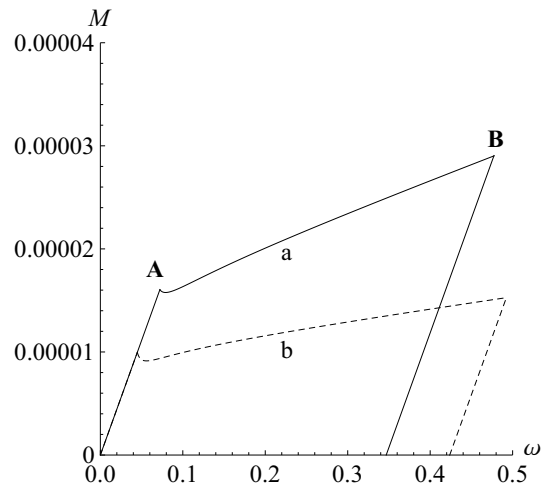
Figure 4.19: Moment-curvature curve during loading and unloading for: a) $\varphi = \frac{\pi}{3}$, b) $\varphi = \frac{\pi}{6}$.

4.2.6 Energy reducing sequence for polygonized state

Assume that the beam is bent by the increasing moment up to the value $M_* > M_d$ and then unloaded by decreasing the moment to zero. At the end of these processes the dislocations produced at loading are frozen such that energy of the beam is given by formula (4.131). Then the beam is subject to annealing which means that it is placed in a thermal bad with fixed but rather high temperature (ca. 400-500° Celsius) for sufficiently long time. Under this condition the mobility of vacancies become high enough to make dislocations climb and then glide so that at the end of annealing the polygonized state of the beam is realized as shown schematically on Fig. 4.20. Each polygon is a single crystal

oriented slightly differently with respect to its neighbors and the boundaries between them are low angle tilt boundaries. The dislocations align themselves into ordered arrays at these boundaries, and there are practically no dislocations inside the polygons. As compared to the unloaded state the rearrangement in displacements is quite small: the polygons undergo rigid-body rotation so that the elastic strain inside them vanishes. The deflection of the beam is nearly the same as that after unloading.

Figure 4.20: A polygonized bent beam.

We want to show that the rearrangement of dislocations and displacements leading to the polygonized relaxed state correspond to a sequence of piecewise constant $\check{\beta}(x, y)$ and the piecewise linear displacement field $\check{u}_x(x,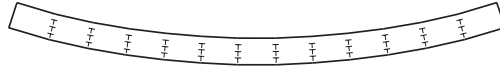 y)$ and $\check{u}_y(x, y)$ reducing energy of the beam compared with (**??**). For simplicity let us consider the case $\varphi = 0$ Let the interval $(0, L)$ be divided into N equal subintervals so that the domain $(0, L) \times (-h/2, h/2)$ is decomposed into N polygons. The boundaries between polygons are perpendicular to the beam axis. Consider first the rotation angle of the beam, $\vartheta(x) = v_{,x}$, which, after unloading, was a linear function $\vartheta_r = \omega_r x$. Let us replace this rotation angle by a piecewise constant function $\check{\vartheta}(x)$ such that $\check{\vartheta}(x) = \omega_r \frac{L}{N} i$ in the i-th interval. The deflection $\check{v}$ is then defined as a piecewise linear function whose slope is constant and equal to $\check{\vartheta}(x) = \omega_r \frac{L}{N} i$ in each polygon. It is easy to see that, as N goes to infinity, this function goes to $\frac{1}{2}\omega_r x^2$ which was the deflection of the beam after unloading. The plastic distortion $\check{\beta}(x)$ is defined to be a piecewise constant function which is equal to $\delta \frac{L}{N} i$ in the i-th polygon. Concerning the displacements $\check{u}_x(x, y)$ and $\check{u}_y(x, y)$ we take them as piecewise linear according to

$$
\begin{cases}
\check{u}_x = -\check{\vartheta}(x)y + \check{\beta}(x)y, \\
\check{u}_y = \check{v}(x)
\end{cases}
\tag{4.132}
$$

Note that the plastic distortion as well as the rotation angle of the beam are discontinuous across the boundaries of the polygons. To guarantee the continuity of displacement across the boundaries of polygons, we must choose δ such that

$$
\delta = \omega_r.
$$

With this choice the component of displacement $\check{u}_x$ vanishes. It is then easy to check that the elastic strain is identically zero. Likewise, the bulk dislocation density must be zero

because $\check{\beta}$ is constant inside each polygon.

The jump of $\check{\beta}$ means the dislocations concentrated at the surface, therefore we ascribe to each jump point the normalized Read-Shockley surface energy (Read and Shockley, 1950)

$$\gamma(\delta\frac{L}{N}) = \gamma_* |\delta L/N| \ln \frac{e\Delta\alpha_*}{\delta L/N}, \tag{4.133}$$

with $\gamma_* = \frac{b}{4\pi(1-\nu)}$, and α_* the saturated misorientation angle.

Substitute the displacements and plastic distortion into the energy functional together with the surface energy term and taking into account that the elastic strain as well as the bulk dislocation density vanish, we obtain the following expression for the energy after dislocation and displacement rearrangement

$$E_p = \sum_{i=1}^{N} \gamma(\delta\frac{L}{N})h. \tag{4.134}$$

Since the first term in (4.131) is positive, the energy (4.134) is less than that of (4.131) if the increase of the surface energy is less than the reduction in gradient terms. Thus, the number of polygons can be estimated by requiring that

$$\sum_{i=1}^{N} \gamma(\delta\frac{L}{N})h < 2 \int_0^L \int_{\frac{-l}{2}}^0 [k|\beta_{*,y} \sin\varphi| + \frac{1}{2}k(\beta_{*,y} \sin\varphi)^2]\, dxdy. \tag{4.135}$$
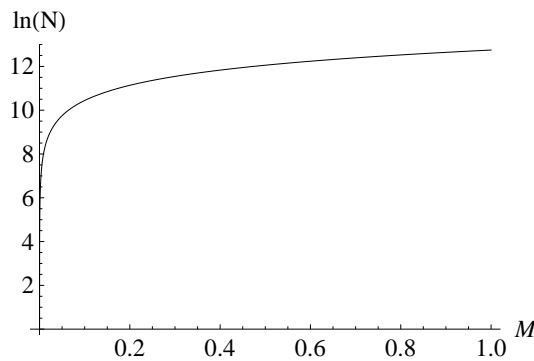

Figure 4.21: Plot of $\ln N$ as function of M.

The plot of the upper bound of $\ln N$ as a function of M is presented in Fig. 4.21 where we took $L = 10$m, $h = 0.1$m, $b = 2.68 \times 10^{-10}$m, $\rho_s = 1.454 \times 10^{14}$m^{-2}, $k = 1.56 \times 10^{-4}$,

$\nu = 0.25$. One can see the increase of the estimated number of polygons with the increasing moment.

5 Formation of dislocation microstructure

In this Chapter the nonlinear continuum dislocation theory is applied into the two-dimensional problems of uniaxial compression. From this, shear bands can be observed through out the process of constructing lamellaers.

5.1 Plane strain deformation

The purpose of this Section is to further specify the general theory developed in Sections 2 and 3 of Chapter 3 for the plane strain deformation for the later applications in two-dimensional problems of uniaxial compression. Consider a single crystal which is initially dislocation-free. Assume that this crystal occupies in its undeformed state a cuboid of width L, height H, and depth D so that in the chosen rectangular coordinate system $0 \leq x_1 \leq L$, $0 \leq x_2 \leq H$, and $0 \leq x_3 \leq D$. We realize the plane-strain deformation by placing this crystal in a "hard" device with the prescribed displacements at some part of its boundaries that do not depend on the x_3-coordinate. We assume that the depth of the crystal D is large enough compared with L and H to guarantee the plane strain state for which $y_3 = x_3$ everywhere. Due to this reason we may drop the third component of vectors and tensors for convenience and regard the equation

$$\mathbf{y} = \mathbf{y}(\mathbf{x})$$

as two-dimensional. Likewise, all vectors and tensors obtained from it (as the deformation gradient, the strain tensor et cetera) are two-dimensional. If the parameter characterizing the given position of the boundary is such that the resulting displacements there are sufficiently small, then it is natural to expect that the crystal deforms elastically and the plastic slip must be zero everywhere. If this parameter exceeds some critical threshold,

then edge dislocations may appear. We admit only the slip directions (or the directions of the Burgers vectors) inclined at an angle φ to the x_1-axis and the dislocation lines parallel to the x_3-axis. Thus, the only active slip system is characterized by the pair of unit (2-D) vectors

$$\mathbf{s}^T = (\cos\varphi, \sin\varphi), \quad \mathbf{m}^T = (-\sin\varphi, \cos\varphi),$$

where $\mathbf{s}$ indicates the slip direction and $\mathbf{m}$ is the normal to the slip plane. Besides, the plastic slip β, under the plane strain state condition, may depend only on x_1 and x_2. Then, taking the infinitesimal area da in the (x_1, x_2)-plane, we obtain the resultant Burgers vector of all excess dislocations whose dislocation lines cross da at right angle in the form

$$\mathbf{b}_r = \mathbf{s}(\beta_{,1}\cos\varphi + \beta_{,2}\sin\varphi)da.$$

Thus, this vector is parallel to the slip direction $\mathbf{s}$ indicating that we are dealing with the edge dislocations only. The scalar dislocation density (or the number of excess dislocations per unit area) can then be determined as

$$\rho = \frac{1}{b}|\beta_{,1}\cos\varphi + \beta_{,2}\sin\varphi|.$$

Let us propose the free energy per unit volume of the undeformed crystal in the form

$$\psi(\mathbf{E}^e, \rho) = \frac{1}{2}\lambda(\operatorname{tr}\mathbf{E}^e)^2 + \mu\operatorname{tr}(\mathbf{E}^e \cdot \mathbf{E}^e) - \mu\chi(\ln J)^3 + \mu cb^2\rho. \tag{5.1}$$

Here $\mathbf{E}^e = \frac{1}{2}(\mathbf{C}^e - \mathbf{I})$ is the elastic strain tensor, $J = \det\mathbf{F}^e = \det\mathbf{F}$ (because $\det\mathbf{F}^p = 1$), λ and μ are the Lamé constants, χ and c are positive constants (c is of order 0.3 while χ is a small parameter). The first three terms in (5.1) represent the elastic energy of the crystal due to the macroscopic elastic deformation that assumes the standard quadratic form of the elastic strain if the latter becomes small. Without the third term the energy required to compress the whole material into the single point is finite, so the material behavior would not be adequately reflected in this limit. The adding of this correction term into the energy is the simplest way to remove this deficiency, maintaining at the same time the correct material behavior at small strains for metals. One can show that this term is small for principal stretches close to 1 if χ is small. The alternative way is to propose the free energy as a quadratic form in terms of the Hencky strain measure although the model is computationally more elaborate (see, for instance, Brünig [41], Xiao

et al. [81]). The last term in (5.1) corresponds to the energy of the dislocation network for small dislocation densities Berdichevsky [2], Ortiz and Repetto [67].

With this free energy density we can now compute the first Piola-Kichhoff stress tensor

$$\mathbf{P} = 2\mathbf{F}^e \cdot \psi_{\mathbf{C}^e} \cdot \mathbf{F}^{p-T} = \mathbf{F}^e \cdot [\lambda(\operatorname{tr}\mathbf{E}^e)\mathbf{I} + 2\mu\mathbf{E}^e - 3\mu\chi(\ln J)^2\mathbf{C}^{e-1}] \cdot \mathbf{F}^{p-T}. \tag{5.2}$$

The Schmid stress becomes

$$\tau_r = -w_\beta = -\mathbf{s} \cdot \mathbf{C}^e \cdot [\lambda(\operatorname{tr}\mathbf{E}^e)\mathbf{I} + 2\mu\mathbf{E}^e - 3\mu\chi(\ln J)^2\mathbf{C}^{e-1}] \cdot \mathbf{F}^{p-T} \cdot \mathbf{m}. \tag{5.3}$$

Finally, the back stress in this model is given by

$$\varsigma = \nabla \cdot w_{\nabla\beta} = \mu cb\nabla \cdot [\operatorname{sign}(\nabla\beta \cdot \mathbf{s})\mathbf{s}], \tag{5.4}$$

so it is identically zero unless the dislocation density is zero. In the latter case the back stress must be understood in terms of the sub-derivative of the non-differentiable function (see Section 5.2).

5.2 Uniaxial compression

Consider a single crystal plate having an original height L, a depth D, and a thickness H (see the cross section of the plate in the (x_1, x_2)-plane in Fig. 5.1). Let this plate be placed in a hard device such that the lower boundary at $x_1 = 0$ is clamped, while the upper boundary at $x_1 = L$ experiences the vertical displacement $-(1 - \gamma)L$. We will assume L large enough compared with H to neglect the influence of the plate edges on the far fields (but not too large to avoid the buckling). The problem is to find placement $\mathbf{y}(\mathbf{x})$ and plastic slip $\beta(\mathbf{x})$ for a given overall stretch $\gamma \in (0, 1)$. The latter is regarded as a control parameter in this plane strain problem.

Let us consider the case with zero dissipation and study the energy of the plate at the uniform total deformations such that

$$\mathbf{F} = \begin{pmatrix} \gamma & 0 \\ 0 & \kappa \end{pmatrix},$$

with γ and κ being the principal stretches in vertical and transversal directions, respec-
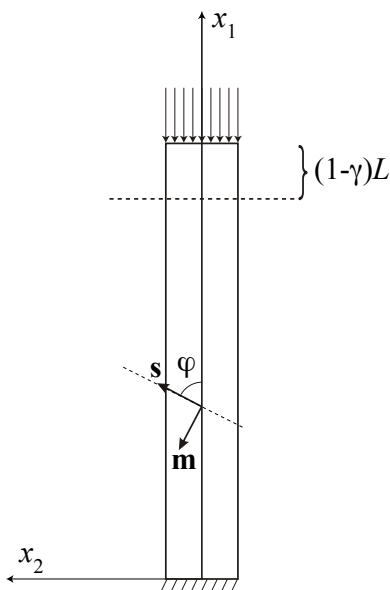
Figure 5.1: Cross section of a single crystal plate under plane strain compression.

tively. Thus, $J = \det \mathbf{F} = \gamma\kappa$. Obviously, these uniform total deformations do not satisfy the boundary conditions at the upper and lower edges of the plate exactly. However, since $H \ll L$, the regions where the deformation deviates from being uniform near the edges of the plate are small and can be neglected. We also assume that, when the plastic slip occurs, the plastic deformation is uniform

$$\mathbf{F}^p = \mathbf{I} + \beta \mathbf{s} \otimes \mathbf{m},$$

with β being also a constant (again, far from the plate edges). In this case the elastic deformation turns out to be uniform as well and is given by

$$\mathbf{F}^e = \mathbf{F}\mathbf{F}^{p-1} = \begin{pmatrix} \gamma(1 + \beta\cos\varphi\sin\varphi) & -\beta\gamma\cos^2\varphi \\ \beta\kappa\sin^2\varphi & \kappa(1 - \beta\cos\varphi\sin\varphi) \end{pmatrix}. \tag{5.5}$$

Since the plastic deformation is uniform, the dislocation density inside the plate vanishes. Substituting these uniform elastic and plastic deformations into the energy functional, we see that the energy of dislocations vanishes. Thus, we obtain the energy of crystal evaluated at uniform deformations in the form

$$I_u = |\mathcal{V}|[\frac{1}{2}\lambda(\operatorname{tr}\mathbf{E}^e)^2 + \mu\operatorname{tr}(\mathbf{E}^e \cdot \mathbf{E}^e) - \mu\chi(\ln J)^3]. \tag{5.6}$$

It is convenient to deal with the energy normalized by $\mu|\mathcal{V}|$. The latter is a function of

three variables γ, κ, and β which, for $\lambda = 0$, reads

$$E(\gamma, \kappa, \beta) = \frac{1}{4}[(\beta^2 \gamma^2 \cos^4 \varphi + \kappa^2 (\beta \sin \varphi \cos \varphi - 1)^2 - 1)^2$$
$$+ 2(\beta \kappa^2 \sin^2 \varphi (1 - \beta \sin \varphi \cos \varphi) - \beta \gamma^2 \cos^2 \varphi (\beta \sin \varphi \cos \varphi + 1))^2 \tag{5.7}$$
$$+ (\beta^2 \kappa^2 \sin^4 \varphi + (\beta \gamma \sin \varphi \cos \varphi + \gamma)^2 - 1)^2 - 4\chi \ln^3(\gamma \kappa)].$$

We want first to minimize the above energy with respect to κ and β. Theoretically, this can be done by equating the derivatives of E with respect to κ and β to zero, then solving the resulting transcendental equations to determine κ and β in terms of γ, and finally, substituting back into E and evaluating it to get the condensed energy $e(\gamma)$. Since the obtained transcendental equations are difficult to solve, the more effective way of computing $e(\gamma)$ is to minimize the energy (5.7) with respect to κ and β numerically. The result of this numerical minimization (provided for $\varphi = \frac{\pi}{2.5}(72°)$ and $\chi = 0.007$) is shown in Fig. 5.2, where it is seen that $e(\gamma)$ is non-convex in the interval between γ_A and γ_B. The convex hull is obtained if the curve $e(\gamma)$ between A and B is replaced by the straight line connecting the points A and B and serving as the common tangent to the curve at A and B.
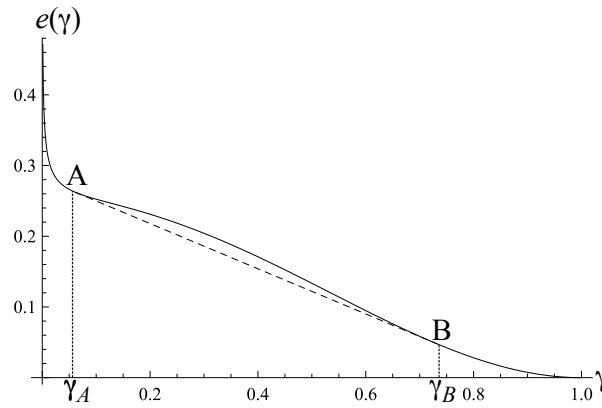
Figure 5.2: Non-convex condensed energy $e(\gamma)$ with $\varphi = \frac{\pi}{2.5}$.

The finding of the interval (γ_A, γ_B) where the condensed energy is non-convex can easily be done in terms of the derivative $e'(\gamma)$ using Maxwell rule of equal area (see the plot of $e'(\gamma)$ in Fig. 5.3). However, since $e(\gamma)$ is obtained from the numerical minimization, a certain extrapolation and smoothing of $e(\gamma)$ is required for the numerical evaluation of $e'(\gamma)$. The numerical algorithm, presented below, leads to the numerical values of $\gamma_A = 0.0617$ and $\gamma_B = 0.7285$ for the chosen angle and other parameters.

Numerical algorithm:

5 Formation of dislocation microstructure

1. Set up an initial value for γ_0, an increment *step* for each loop, and a tolerance *tol*.

2. Compute $e'(\gamma_0)$. Find γ_1 and γ_2 such that $\gamma_2 > \gamma_1 > \gamma_0$ and $e'(\gamma_1) = e'(\gamma_2) = e'(\gamma_0)$.

3. Compute the areas A_1 and A_2 between the curve $e'(\gamma)$ and the horizontal straight line connecting three points A, C, and B as shown in Fig. 5.3.

4. Compare the values of A_1 and A_2. If the absolute value of $A_1 - A_2$ is less than *tol* then go to 5. Otherwise, assign $\gamma_0 = \gamma_0 + step$, go to 2.

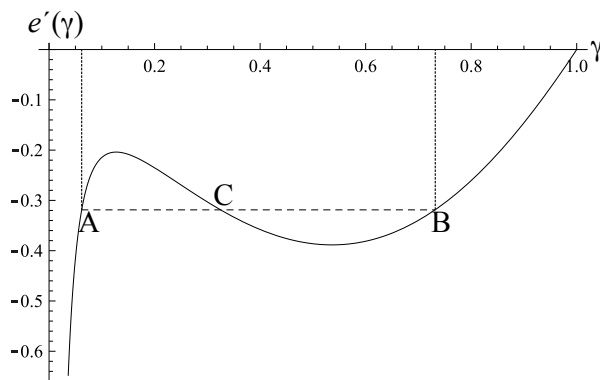5. Assign $\gamma_A = \gamma_0$ and $\gamma_B = \gamma_2$. Exit.

Figure 5.3: The derivative $e'(\gamma)$ and Maxwell's construction.

Although the uniform total and plastic deformations found above satisfy the equilibrium equations, they do not correspond to the energy minimizer in the range $\gamma \in (\gamma_A, \gamma_B)$ due to the non-convexity of the energy in this range. To achieve the lowest possible energy, let us construct the energy minimizing sequence of placements and plastic slips such that the energy evaluated on them approaches the convex hull for the condensed energy

$$e^c(\gamma) = \begin{cases} e(\gamma) \text{ for } 0 < \gamma < \gamma_A \text{ and } \gamma_B < \gamma < 1, \\ e(\gamma_A) + \frac{\gamma - \gamma_A}{\gamma_B - \gamma_A}[e(\gamma_B) - e(\gamma_A)] \text{ for } \gamma_A \le \gamma \le \gamma_B, \end{cases} \tag{5.8}$$

which is lower than the energy of the uniform deformation in the range $\gamma \in (\gamma_A, \gamma_B)$ (see Fig. 5.2). For this purpose let us divide the plate into a sequence of bands of two types which we denote by $+$ and $-$ (see Fig. 5.4). The volume fraction of bands $+$ is s, while that of $-$ is $1 - s$. We choose the elastic stretch tensor to be piecewise constant in the bands $+$ and $-$ according to

$$\mathbf{U}^{e+} = \sqrt{\mathbf{F}_A^{eT} \cdot \mathbf{F}_A^e}, \quad \mathbf{U}^{e-} = \sqrt{\mathbf{F}_B^{eT} \cdot \mathbf{F}_B^e},$$
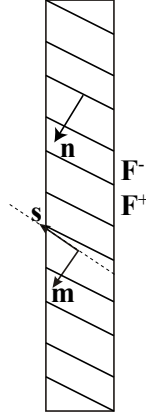
94

Figure 5.4: Shear bands in the plate.

where $\mathbf{F}^e_A$ and $\mathbf{F}^e_B$ are the elastic deformations obtained from (5.5) when $(\gamma_A, \kappa_A, \beta_A)$ and $(\gamma_B, \kappa_B, \beta_B)$ found at the states A and B are substituted, respectively. This choice guarantees that the energy in those bands coincides with the energy in the state A and B, respectively. The elastic rotation is also piecewise constant such that

$$\mathbf{R}^{e+} = \begin{pmatrix} \cos\theta^+ & -\sin\theta^+ \\ \sin\theta^+ & \cos\theta^+ \end{pmatrix}, \quad \mathbf{R}^{e-} = \begin{pmatrix} \cos\theta^- & -\sin\theta^- \\ \sin\theta^- & \cos\theta^- \end{pmatrix},$$

but the rotation angles θ^+ and θ^- are left undetermined. We will find them from the jump conditions at the grain boundary. The elastic deformation, computed from the polar decomposition, becomes then also piecewise constant: $\mathbf{F}^{e\pm} = \mathbf{R}^{e\pm} \cdot \mathbf{U}^{e\pm}$. The plastic deformation is chosen to be piecewise constant too

$$\mathbf{F}^{p\pm} = I + \beta^\pm \mathbf{s} \otimes \mathbf{m}$$

with $\beta^\pm$ being still unknowns. With the multiplicative resolution we then find the total deformations $\mathbf{F}^\pm = \mathbf{F}^{e\pm} \cdot \mathbf{F}^{p\pm}$ that contains four unknowns θ^+, θ^-, β^+, β^-. To guarantee the existence of the placement field, the Hadarmard's compatibility condition

$$[\![\mathbf{F}]\!] = \mathbf{q} \otimes \mathbf{n}, \tag{5.9}$$

have to be fulfilled, where $\mathbf{q}$ and $\mathbf{n}$ are unknown vectors. Besides, the condition of force equilibrium,

$$[\![\mathbf{P}]\!] \cdot \mathbf{n} = 0, \tag{5.10}$$

thermodynamic equilibrium (for the plane grain boundary with $\eta = 0$)

$$-\mathbf{q} \cdot \mathbf{P} \cdot \mathbf{n} + [\![w]\!] = 0, \tag{5.11}$$

as well as the identity

$$\mathbf{n} \cdot \mathbf{n} = 1 \tag{5.12}$$

must also be satisfied. Thus, there are altogether eight equations to determine eight unknowns θ^+, θ^-, β^+, β^-, $\mathbf{n}^T = (n_1, n_2)$, and $\mathbf{q}^T = (q_1, q_2)$.

The system (5.9)-(5.12) can be solved as follows. We first eliminate one unknown by taking $\mathbf{n}^T = (-\sin\alpha, \cos\alpha)$ that satisfies the identity (5.12). Then we solve four equations of compatibility (5.9) as linear equations with respect to β^+, β^-, q_1, q_2 to find them as functions of three angles α, θ^+, θ^-. Substituting these functions into (5.10) and (5.11) we get three scalar equations containing three unknowns angles that can be written as

$$f_i(\mathbf{r}) = 0, \quad i = 1, 2, 3, \tag{5.13}$$

with $\mathbf{r}$ the three-dimensional unknown vector. The robust numerical algorithm to find the solution of (5.13) is to minimize the function

$$g(\mathbf{r}) = \sum_{i=1}^{3} f_i^2(\mathbf{r}).$$

The result of this numerical minimization done in *Matlab* is

$$\alpha = 1.242, \ \beta^+ = 67.402, \ \beta^- = 67.755, \ \theta^+ = -1.526, \ \theta^- = -0.705.$$

From this result we see that the misorientation angle between the shear band boundary and the slip direction is $\vartheta = -0.84°$ which is really small as observed in Uchic et al. [74].[1] Computing the change in heights of the bands in the vertical direction due to $\mathbf{F}^\pm$, we find the volume fraction of bands +

$$s = \frac{\gamma - \gamma_A}{\gamma_B - \gamma_A}.$$

---

[1]Dimiduk informed the authors in his private communication about this small misorientation between the shear bands and the slip direction.

The resolved shear stresses in these bands, normalized by the shear modulus μ, are

$$\tau_r^+ = 7.252 \times 10^{-8}, \quad \tau_r^- = 1.620 \times 10^{-6},$$

so they are small but not equal to zero. The equilibrium of micro forces, in case of zero dislocation density inside the layers, must be understood in the following sense (see Berdichevsky and Le [4])

$$|\tau_r| \leq \frac{2cb\sin\vartheta}{h}$$

where h is the thickness of the bands. The right-hand side can be interpreted as the back stress in this case. This puts some constraints on the thickness of the bands.

It is not difficult to extend these results to the case with non-zero dissipation. To be able to compare with experiments conducted in Uchic et al. [74] the proposed theory must be extended to three dimensions which is still in progress and will be reported elsewhere.

6 Conclusions

In this thesis the continuum dislocation theory has been used and developed for modeling of microstructures. Both linear and nonlinear theory are applied into specific approaches. In the first approach we have shown that there exists a sequence of piecewise constant plastic distortions reducing the energy of the relaxed state of the bent beam and exhibiting the polygonization. We mention that the theory developed above does not provide any information about the kinetics of polygonization, which may be quite complicated due to the temperature-dependent dislocation climb and due to the interaction between dislocations and vacancies. Thus, for the kinetics of polygonization the knowledge about dissipation due to the dislocation climb becomes unavoidable.

Moreover, the one-dimensional theory of bending of a single crystal beam taking into account continuously distributed dislocations has been developed. The threshold bending moment exhibiting the size effect has been found for the case without and with dissipation. We have found also the dislocation density and the moment-curvature curves at loading and unloading. Furthermore, we have shown that there exists a sequence of piecewise constant plastic distortions and piecewise linear displacements reducing the energy of the annealed and relaxed state of the bent beam and exhibiting the polygonization. We mention that the theory developed above does not provide any information about the kinetics of polygonization, which may be quite complicated due to the temperature-dependent dislocation climb and due to the interaction between dislocations and vacancies.

The second approach have we developed the nonlinear CDT for crystals with dislocations and with grain boundaries regarded as the surfaces of weak discontinuity in placement but strong discontinuity in plastic slip. The whole set of equilibrium equations, boundary conditions and jump conditions are derived from the energy minimization problem. We have shown on the examples of crystals deforming in simple shear or in uniaxial compression that the formation of grains with piecewise constant plastic slip and elastic deformation satisfies all equilibrium conditions and provides the energy minimizing sequences to these non-convex variational problems. In case the homogeneous states are

not rank-one connected, the whole set of jump conditions is needed to find the elastic rotation and the plastic slip leading to the energy minimizing sequences. Let us mention that the modification of the surface energy density depending on the misorientation angle in accordance with Read-Schockley's energy would make the theory more suitable for low angle tilt boundaries.

In future works, we would like to applied these theories into more general cases which can explain and understand clearly the formation of microstructures.

Bibliography

[1] Berdichevsky V.L. (1983) Variational principles of continuum mechanics, Nauka, Moskva.

[2] Berdichevsky V.L. (2006a). Continuum theory of dislocations revisited. Continuum Mech. Thermodyn. 18, 195–222.

[3] Berdichevsky V.L. (2006b). On thermodynamics of crystal plasticity. Scripta Materialia 54, 711–716.

[4] Berdichevsky V.L., Le K.C. (2007). Dislocation nucleation and work hardening in anti-planed constrained shear. Continuum Mech. Thermodyn. 18, 455–467.

[5] Berdichevsky, V. L. and Sedov, L. I. (1967). Dynamic theory of continuously distributed dislocations. its relation to plasticity theory. J. Appl. Math. Mech. (PMM), 31:989–1006.

[6] Le, K. C. (2010). Introduction to Micromechanics. Nova Science.

[7] Le, K.C., Günther, C., (2014). Nonlinear continuum dislocation theory revisited. Int. J. Plasticity 53, 164–178.

[8] Le, K.C., Nguyen, B.D., (2012). Polygonization: Theory and comparison with experiments. Int. J. Engng Sci. 59, 211–218.

[9] Le, K.C., Nguyen, B.D., (2013). On bending of single crystal beam with continuously distributed dislocations. Int. J. Plasticity 48, 152–167.

[10] Koster, M., Le, K.C., Nguyen, B.D., (2015). Formation of grain boundaries in ductile single crystals at finite plastic deformations. Int. J. Plasticity 69, 134–151.

[11] Le, K. C. and Stumpf, H. (1996a). A model of elastoplastic bodies with continuously

distributed dislocations. Int. J. Plasticity, 12:611–627.

[12] Le, K. C. and Stumpf, H. (1996b). Nonlinear continuum theory of dislocations. Int. J. Eng. Sci., 34:339–358.

[13] Bilby B.A., Gardner L.R.T., Smith E. (1958). The relation between dislocation density and stress. Acta Metall. 6, 29–33.

[14] Kröner, E. (1955). Der fundamentale Zusammenhang zwischen Versetzungs- dichte und Spannungsfunktionen. Z. Phys. 142, 463-475.

[15] Cahn R.W. (1949). Recrystallization of single crystals after plastic bending. Journal of the Institute of Metals 76, 121–143.

[16] Gilman J.J. (1955). Structure and polygonization of bent zinc monocrystals. Acta Metall. 3, 277–288.

[17] Hansen N., Huang X., Winther G. (2008). Grain orientation, deformation microstructure and flow stress. Mat. Sci. and Eng. A 494, 61–67.

[18] West C. D., Optical Study of Monocrystal Bent Corundum Rods, Technical Report, ONR Contract N7onr39102.

[19] Hybler J., Greninger Chart, http://www-xray.fzu.cz/xraygroup/www/grchart.html.

[20] Kaluza M., Le K.C. (2011). On torsion of a single crystal rod. Int. J. Plasticity. 27, 460–469.

[21] Kochmann D.M., Le K.C. (2008). Dislocation pile-ups in bicrystals within continuum dislocation theory. Int. J. Plasticity. 24, 2125–2147.

[22] Kochmann D.M., Le K.C. (2009a). Plastic deformation of bicrystals within continuum dislocation theory. J. Math. Mech. Solids 14, 540–563.

[23] Kochmann D.M., Le K.C. (2009b). A continuum model for initiation and evolution of deformation twinning. J. Mech. Phys. Solids 57, 987–1002.

[24] Kuhlmann-Wilsdorf D. (2001). Q: Dislocation structures - how far from equilibrium? A: very close indeed. Mater. Sci. Eng. A 315, 211–216.

[25] Le K.C. (1999). Vibrations of shells and rods, Springer, Berlin.

[26] Le K.C., Sembiring P. (2008). Analytical solution of the plane constrained shear problem for single crystals within continuum dislocation theory. Arch. Appl. Mech. 78, 587–597.

[27] Le K.C., Sembiring P. (2008). Plane constrained shear of single crystal strip with two active slip systems. J. Mech. Phys. Solids 56, 2541–2554.

[28] Le K.C., Sembiring P. (2009).Plane constrained uniaxial extension of a single crystal strip. Int. J. Plasticity 25, 1950–1969.

[29] Le K.C., Nguyen Q.S. (2011). Polygonization as low energy dislocation structure. Continuum Mech. Thermodyn. 22, 291–298.

[30] Mura T. (1987). Micromechanics of defects in solids. Kluwer Academic Publishers, Oxford.

[31] Nye J.F. (1953). Some geometrical relations in dislocated crystals. Acta Metall. 1, 153–162.

[32] Read W.T., Shockley W. (1950). Dislocation models of crystal grain boundaries. Phys. Rev. 78, 275–289.

[33] Read W.T. (1957). Dislocation theory of plastic bending. Acta Metall. 5, 83–88.

[34] Evans, J.T., (1995). Bending produced by dislocations in a beam, International Journal of Engineering Science 33, 1321–1329.

[35] Lubliner, J., (1990). Plasticity theory. Macmillan, New York.

[36] Sedov, L.I., (1966). Some problems of designing new models of continuous medium. In: 11th International Congress of Applied Mechanics, pp. 23–41. Springer, Berlin.

[37] Wang, W., Huang, Y., Hsia, K.J., Hu, K.X., Chandra, A., (2003). A study of microbend test by strain gradient plasticity, Int. J. Plasticity 19, 365–382.

[38] Berdichevsky, V.L., Le, K.C., (2002). Theory of charge nucleation in two dimensions. Physical Review E 66(2), 026129.

Bibliography

[39] Gurtin, M. (2004). A gradient theory of small-deformation isotropic plasticity that account for the burgers vector and for dissipation due to plastic spin. J. Mech. Phys. Solids, 52:1379–1406.

[40] Bilby, B.A., Gardner, L.R.T., Stroh, A.N., (1957). Continuous distributions of dislocations and the theory of plasticity, in: Extrait des actes du IXe congrès international de mécanique appliquée, pp. 35–44.

[41] Brünig, M., (1999). Numerical simulation of the large elastic-plastic deformation behavior of hydrostatic stress-sensitive solids. International Journal of Plasticity 15(11), 1237–1264.

[42] Carstensen, C., Hackl, K., Mielke, A., (2002). Non-convex potentials and microstructures in finite strain plasticity. Proceedings of the Royal Society of London. Series A: Mathematical, Physical and Engineering Sciences 458(2018), 299–317.

[43] Christian, J.W., Mahajan, S., (1995). Deformation twinning. Progress in materials science 39(1), 1-157.

[44] Engels, P., Ma, A., Hartmaier, A., (2012). Continuum simulation of the evolution of dislocation densities during nanoindentation. International Journal of Plasticity 38, 159-169.

[45] Fukuda, Y., Oh-ishi, K., Furukawa, M., Horita, Z., Langdon, T.G., (2006). Influence of crystal orientation on ECAP of aluminum single crystals. Materials Science and Engineering A 420(1), 79-86.

[46] Gurtin, M.E., (1981). An Introduction to Continuum Mechanics. Academic Press, New York.

[47] Abbaschian, R., Abbaschian, L., Reed-Hill, R. E. (2009). Physical Metallurgy Principles. Cengage Learning.

[48] Hansen, N., Kuhlmann-Wilsdorf, D., (1986). Low energy dislocation structures due to unidirectional deformation at low temperatures. Materials Science and Engineering 81, 141-161.

[49] Hansen, N., (2004). Hall-Petch relation and boundary strengthening. Scripta Materialia 51(8), 801-806.

[50] Harren, S.V., Deve, H.E., Asaro, R.J., (1988). Shear band formation in plane strain compression. Acta Metallurgica 36(9), 2435-2480.

[51] Hughes, D.A., Hansen, N., (1997). High angle boundaries formed by grain subdivision mechanisms. Acta Materialia 45(9), 3871-3886.

[52] Jia, D., Ramesh, K.T., Ma, E., (2003). Effects of nanocrystalline and ultrafine grain sizes on constitutive behavior and shear bands in iron. Acta Materialia 51(12), 3495-3509.

[53] Jiang, B., Weng, G.J., (2004). A generalized self-consistent polycrystal model for the yield strength of nanocrystalline materials. Journal of the Mechanics and Physics of Solids 52(5), 1125-1149.

[54] Kondo, K. (1952). On the geometrical and physical foundations of the theory of yielding. In Proceedings of the 2nd Japan Congress on Applied Mechanics, 41–47, Tokyo.

[55] Kröner, E., (1992). Mikrostrukturmechanik. GAMM-Mitteilungen 15, 104–119.

[56] Kröner, E. (1958). Kontinuumstheorie der Versetzungen und Eigenspannungen. Springer,Berlin.

[57] Kuhlmann-Wilsdorf, D. (1989). Theory of plastic deformation:-properties of low energy dislocation structures. Materials Science and Engineering A113, 1-41.

[58] Kuhlmann-Wilsdorf, D., Hansen, N., (1991). Geometrically necessary, incidental and subgrain boundaries. Scripta Metallurgica et Materialia 25(7), 1557-1562.

[59] Kysar, J.W., Saito, Y., Oztop, M.S, Lee, D., Huh, W.T., (2010). Experimental lower bounds on geometrically necessary dislocation density. Int. J. Plasticity 26, 1097-1123.

[60] Laird, C., Charsley, P., Mughrabi, H., (1986). Low energy dislocation structures produced by cyclic deformation. Materials Science and Engineering 81, 433-450.

[61] Hull, D., Bacon, D. J., (2011). Introduction to dislocations. Elsevier.

[62] Lee, J.C., Seok, H.K., Suh, J.Y., (2002). Microstructural evolutions of the Al strip prepared by cold rolling and continuous equal channel angular pressing. Acta Mate-

Bibliography

rialia 50(16), 4005-4019.

[63] Lee, M.G., Lim, H., Adams, B.L., Hirth, J.P., Wagoner, R.H., (2010). A dislocation density-based single crystal constitutive equation. International Journal of Plasticity 26, 925-938.

[64] Lim, H., Lee, M.G., Kim, J.H., Adams, B.L., Wagoner, R.H., (2011). Simulation of polycrystal deformation with grain and grain boundary effects. International Journal of Plasticity 27, 1328-1354.

[65] Mayeur, J. R., McDowell, D. L., (2014). A comparison of Gurtin type and micropolar theories of generalized single crystal plasticity. International Journal of Plasticity 57, 29-51.

[66] Öztop, M.S., Niordson, C.F., Kysar, J.W., (2013). Length-scale effect due to periodic variation of geometrically necessary dislocation densities. International Journal of Plasticity 41, 189-201.

[67] Ortiz, M., Repetto, E.A., (1999). Nonconvex energy minimization and dislocation structures in ductile single crystals. J. Mech. Phys. Solids 47, 397–462.

[68] Ortiz, M., Repetto, E.A., Stainier, L., (2000). A theory of subgrain dislocation structures. J. Mech. Phys. Solids 48, 2077–2114.

[69] Sakai, G., Horita, Z., Langdon, T.G., (2005). Grain refinement and superplasticity in an aluminum alloy processed by high-pressure torsion. Materials Science and Engineering A393(1), 344-351.

[70] Sedov, L.I., (1965). Mathematical methods of constructing models of continuum media. Usp. Matem. Nauk. 20, 123–182.

[71] Segal, V.M., (1995). Materials processing by simple shear. Materials Science and Engineering A197(2), 157-164.

[72] Segal, V.M., (1999). Equal channel angular extrusion: from macromechanics to structure formation. Materials Science and Engineering A271(1), 322-333.

[73] Tome, C.N., Lebensohn, R.A., Kocks, U.F., (1991). A model for texture development dominated by deformation twinning: application to zirconium alloys. Acta Metallurgica et Materialia 39(11), 2667-2680.

[74] M.D. Uchic, P.A. Shade, D.M. Dimiduk , (2009). Plasticity of Micrometer-Scale Single Crystals in Compression. Annu. Rev. Mater. Res. 39, 361–386.

[75] Valiev, R.Z., Islamgaliev, R.K., Alexandrov, I.V., (2000). Bulk nanostructured materials from severe plastic deformation. Progress in Materials Science 45(2), 103-189.

[76] Valiev, R.Z., Langdon, T.G., (2006). Principles of equal-channel angular pressing as a processing tool for grain refinement. Progress in Materials Science 51(7), 881-981.

[77] Valiev, R.Z., Islamgaliev, R.K., Alexandrov I.V., (1999). Bulk nanostructured materials from severe plastic deformation. Progress in Materials Science 45, 103-189.

[78] Vorhauer, A., Pippan, R., (2004). On the homogeneity of deformation by high pressure torsion. Scripta Materialia 51(9), 921-925.

[79] Zhu, X., Dai, S., Xiang, Y., (2013). Numerical simulation of dynamics of dislocation arrays and long-range stress fields of nonplanar dislocation arrays. International Journal of Plasticity, 43, 85-100.

[80] Zhu, X., Xiang, Y., (2014). Continuum framework for dislocation structure, energy and dynamics of dislocation arrays and low angle grain boundaries. Journal of the Mechanics and Physics of Solids, 69, 175-194.

[81] Xiao, H., Bruhns, I. O., Meyers, I. A., (1997). Logarithmic strain, logarithmic spin and logarithmic rate. Acta Mechanica 124, 89–105.

[82] Iwahashi, Y., Wang, J., Horita, Z., Nemoto, M., Langdon, T.G., (1996). Principle of equal-channel angular pressing for the processing of ultra-fine grained materials. Scripta Materialia 35, 143–146.

[83] Burgers, J. M. (1939). Some considerations on the fields of stress connected with dislocations in a regular crystal lattice. Kon. Nederl. Akad. v. Wet. Vol, 42:293–325.

Curriculum vitae

PERSONAL INFORMATION

First Name   :   Binh Duong

Last Name   :   Nguyen

Date of Birth   :   22.01.1986

Place of Birth   :   Dak Lak, Vietnam

Nationality   :   Vietnamese

EDUCATION

Ph.D. Candidate – Chair of Mechanics-Material Theory (2012 – Present)

Ruhr-University Bochum, Germany

Master of Science – Computational Engineering (2009 – 2011)

Vietnamese-German University, Vietnam in cooperation with Ruhr-University Bochum, Germany

Bachelor of Engineering – Engineering Mechanics (2004 – 2009)

Ho Chi Minh University of Technology, Vietnam

Higher Diploma In Software Engineering (2008 – 2010)

Aptech India, Vietnam

PUBLICATIONS

"*Formation of grain boundaries in ductile single crystals at finite plastic deformations*", International Journal of Plasticity (03/2015); 69:134-151.

"*On bending of single crystal beam with continuously distributed dislocations*", International Journal of Plasticity (03/2013) ; 48:152-167.

"*Polygonization: theory and comparison with experiments*", International Journal of Engineering Science (10/2012); 59:211-218.

"*Simulating the 2D contact problems by radial point interpolation method using nodal integration*", In Proceedings of Scientific Conference at Ho Chi Minh University of Technology (2009)

CONFERENCE PRESENTATIONS

GAMM 86th Annual Scientific Conference – Lecce, Italy, 2015

"*Formation of the microstructure in the plates under compression*"

GAMM 85th Annual Scientific Conference – Erlangen-Nürnberg, Germany, 2014

"*Shear banding of single crystal beam with continuously distributed dislocations under compression*"

GAMM 84th Annual Scientific Conference – Novi Sad, Serbia, 2013

"*On bending of single crystal beam with continuously distributed dislocations*"

Scientific Conference at Ho Chi Minh University of Technology – Ho Chi Minh, Vietnam, 2009

"*Simulating the 2D contact problems by radial point interpolation method using nodal integration*"